# A MODIFIED NAMBU-JONA-LASINIO MODEL AND ITS APPLICATION TO THE QUARK MATTER

by

QING SUN

A dissertation submitted to the Graduate Faculty in Physics
in partial fulfillment of the requirements for the degree of
Doctor of Philosophy, The City University of New York

2007

This manuscript has been read and accepted for the Graduate Faculty in Physics in satisfaction of the dissertation requirement for the degree of Doctor of Philosophy.

| | |
|---|---|
| | Professor Carl Shakin |
| 11/17/2005 | |
| Date | Chair of Examining Committee |
| | Professor Sultan Catto |
| 11/17/2005 | |
| Date | Executive Officer |

Professor Carl Shakin

Professor Kai Shum

Professor Xiangdong Li

Professor Ming-Kung Liou

Professor Peter Lesser

Professor Victor Franco

Supervision Committee

THE CITY UNIVERSITY OF NEW YORK

ABSTRACT

# A REVISED NAMBU-JONA-LASINIO MODEL AND ITS APPLICATION TO THE QUARK MATTERS

by QING SUN

Advisor: Dr. Carl Shakin, Distinguished Professor

The NJL model has been effectively applied to investigate the chiral symmetry breaking and other related phenomena on the quark model. We extended the regular NJL with a covariant lorentz-vector model of confinement, and made a trial to build a nonlocal NJL model. By using this noval model, we suggest to use temperature-dependent and density-dependent coupling constants. Some calculations are made to compare with QCD and lattice QCD results. These result shows our generalized NJL model demostrates better agreement with the corresponding QCD results.

# ACKNOWLEDGMENTS

The compilation of this document is a conclusion of my five years PHD education of Physics. I came to this unknown nation to study five years ago. So at first I want to thank those people who helped me and accustomed me to the life of this land. Thank you those generous americans.

Most important, I would like to thank my advisor, Carl Shakin, for his encouragement, interest, and patience. Personally, I would like to thank him for sharing his knowledge which has enriched my study in Physics. I hope he would been proud of this.

I also want to thank my colleagers. Among them, Mr. Li Hu gives me the most generous help. He provides me invaluable insight of the physics. Mr. He Bin and Mr. Wang Huangsheng are also in the list. We worked together and shared the joys of the solving of problems.

Other than mentioned above there are many people to help me in live and studies. I simply listed their name below: Professor Louis Celenza, Professor Liu Ming-kung, Ms. Laura Incampo, Ms. Suzan White and so on.

In conclusion I would like to thank a few people without whom, I would not have complete this. I would like to thank my parents who brought me into this world and always provided me the supports on my way of study. I would like to thank my wife He Juan, with whom I married during the period of my PHD education and whom I left right after our marriage. She always selflessly supports me and listens to me, makes me peaceful to continue my studies.

# Contents

# List of Figures

# List of Tables

# Chapter 1

# Introduction

## 1.1 the Nambu–Jona-Lasinio Model

The Nambu–Jona-Lasinio (NJL) model has been extensively studied for several decades [12, 23, 22]. It was originally proposed as a model explaining the nucleon mass in terms of the self-energy of some primary fermion field which is through the same mechanism as the appearance of the energy gap in the BCS superconductivity theory. Now the model has been widely adapted to investigate the chiral symmetry breaking and the related phenomena on the quark model. The model is an effective Lagrangian of relativitistic fermions interacting through local fermion coupling. The assertion is that this model might serve as a suitable approximation to the Quantum Chromodynamics (QCD) in the low-energy and long-wavelength limit. It assumes that, gluon degree of freedom can be frozen into effective pointlike interactions between quarks.

Comparing to the Quantum Chromodynamics (QCD) theory, the NJL theory conserves the symmetries of quantum fields but also provides people a simpler form in mathematics which is tractable. NJL model successfully shows the symmetries also the breaking of those symmetries, which is the key feature that QCD is distinguished. Other features of QCD, like the Goldstone modes and the results of current algebra

such as Goldgerger-Treiman and Gell-Mann-Oakes-Renner relations, can also be explicitly derived in NJL model. One of the most important symmetries is the chiral symmetry, which is essential to the understanding of the lightest hadrons. The spontaneous breakdown of chiral symmetry is now widely believed in the real world. Other than QCD and NJL theory, it has also been certified by lattice calculation.

It is not saying the NJL has no shortcomings. One of shortcomings is, it is a model that can not be renormalized. A regularization scheme is needed, which defines the length scale for the theory. In mathematics it can be expressed as a cutoff on the quark momenta. It is naturally to do so since this model is an effective theory and people would expect that it will be effective only in some certain scales. A second shorcoming is that, the NJL model is never confining since a local interaction does not confine quarks. In the most applications we applies NJL model only to the properties for which the confinement is not essential: the strength of quark pair condensation $\ll \bar{\psi}\psi \gg$, the pion mass $M_\pi$, the pion decay constant $f_\pi$ and so on. In the description of properties related to baryons, it will be needy to extend the standard NJL model with confinements.

In this chapter, we are attempting to make a brief description of the plain NJL model. This is the platform that our furture investigation will base on. After the description of the NJL model, we will give a description of this thesis, including the topics and arrangement.

## 1.2 The SU(3) NJL Model

We start from a description of the $SU(3)$ NJL model since in this thesis we have most of our discussions based on it. As mentioned above the NJL model came from an approximation to the QCD theory. So first of all, we can look at the symmetries of QCD.

In the case of three quark flavors, the quark fields consist of $u-$, $d-$ and $s-$quarks. Apart from the local $SU(3)_{color}$ gauge symmetry, QCD with massless quarks in invariant under global chiral transformations, i.e. under the group

$$U(3)_L \otimes U(3)_R = SU(3)_L \otimes SU(3)_R \otimes U(1)_V \otimes U(1)_A \tag{1.2.1}$$

The chiral flavour group $SU(3)_L \otimes SU(3)_R$ transforms the left- and right-handed quark fields $\psi_{L,R} = \frac{1}{2}(1+\gamma_5)\psi$ according to $\psi_{L,R} \rightarrow exp(i\frac{\vec{\lambda}\cdot\vec{\alpha}_{L,R}}{2})\psi_{L,R}$ where $\vec{\lambda}$ is the set of $SU(3)_{flavour}$ matrices and $\vec{\alpha}_{L,R}$ are arbitrary phases. The $U(1)_V$ group generates the phase transformations $\psi \rightarrow e^{i\alpha_V}\psi$. The conserved current related to this symmetry is the baryon current $\bar{\psi}\lambda_\mu\psi$.

The axial $U(1)_A$ symmetry, i.e. invarant under $\psi \rightarrow e^{i\lambda_5\alpha_A}\psi$ is known to be broken in nature and probably broken in QCD by instanton effects. The remaining global symmetry in the chiral limit with $m_0 \rightarrow 0$ is then $SU(3)_L \otimes SU(3)_R \otimes U(1)_V$.

The $SU(3)$ NJL model starts from above symmetries and assuming that in the low-energy and long-wavelength limit, gluon degrees of freedom are frozen and absorbed into local effective interaction between quarks. The Lagrangian is

$$\mathcal{L} = \bar{q}(i\partial\!\!\!/ - m^0)q + \mathcal{L}_{int} \tag{1.2.2}$$

where the $\lambda^i (i = 0, \cdots, 8)$ are the Gell-Mann matrices, with $\lambda^0 = \sqrt{2/3}\,\mathbf{1}$, $m^0 = \mathrm{diag}\,(m_u^0, m_d^0, m_s^0)$ is a matrix of current quark masses. Here we use $q$ instead of $\psi$ to note the quark field. The $\mathcal{L}_{int}$ is the interaction part which is

$$\mathcal{L}_{int} = \mathcal{L}_{int}^{(4)} + \mathcal{L}_{int}^{(6)} \tag{1.2.3}$$

consisting of a local four-point interaction $\mathcal{L}_{int}^{(4)}$ and a $U(1)_A$-breaking term $\mathcal{L}_{int}^{(6)}$ which is minimally a six-point vertex. The interaction $\mathcal{L}_{int}^{(6)}$ is constructed such that it

simulates $U(1)_A$-breaking instanton effects. Just like in QCD theory we can introduce the 't Hooft determinant interaction

$$\mathcal{L}_{int}^{(6)} = \frac{G_D}{2}\{\det[\bar{q}(1+\gamma_5)q] + \det[\bar{q}(1-\gamma_5)q]\} \tag{1.2.4}$$

The $\mathcal{L}_{int}^{(4)}$ should satisfy chiral $U(3)_L \otimes U(3)_R$ symmetry and symmetry under $SU(3)_{color}$ and $PCT$. It can be shown that

$$\begin{aligned}\mathcal{L}_{int}^{(4)} = \quad & \frac{G_S}{2}\sum_{i=0}^{8}[(\bar{q}\lambda^i q)^2 + (\bar{q}i\gamma_5\lambda^i q)^2] \\ & -\frac{G_V}{2}\sum_{i=0}^{8}[(\bar{q}\lambda^i\gamma_\mu q)^2 + (\bar{q}\lambda^i\gamma_5\gamma_\mu q)^2] \\ & +\mathcal{L}_{other}^{(4)}\end{aligned} \tag{1.2.5}$$

Where $\mathcal{L}_{other}^{(4)}$ includes other color singlet terms and the color octet terms.

Our researches will be based on the $SU(3)$ NJL model listed above. Here we have listed the result of NJL model in general. For more detals about the NJL model, you may refer to [23] and [12].

## 1.3 Thesis Topics

At finite density and temperature, many applications have been made of the NJL model in the study of light meson spectra, decay constants, and mixing angles. In this thesis we will report to extend our model to include a description of deconfinement at finite density and finite temperature.

### 1.3.1 Finite Temperature

There has been a great deal of interest in understanding the properties of quantum chromodynamics (QCD) for a finite value of the chemical potential and for finite temperature. Studies have been made of the restoration of chiral symmetry in matter and at finite temperature. The phenomenon of deconfinement is also of great interest, with studies of the temperature dependence of the confining interaction reported recently.

The NJL model is then a model of interests for the corresponding calculations. In this thesis, the temperature-dependent feature of NJL is given. It successfully describes the restoration of the chiral symmetry with the increasing temperature. Also the deconfinement of light mesons is studied.

### 1.3.2 Finite Density

There has been extensive application of the NJL model in the study of matter at high density, with particular interest in diquark condensation and color superconductivity [32, 33, 34, 35]. These studies find application in the study of neutron stars. The NJL model is the model of choice, since the study of the properties of matter at finite density in lattice simulations of QCD is only in an early stage of development. A problem in these studies is associated with the introduction of a chemical potential, which makes the Euclidean-space fermion determinant complex [41, 42, 43, 44, 45, 46].

The use of the NJL model in the hadronic phase of matter is limited, since the standard version of the model does not contain a model of confinement [12, 23, 22]. It is clearly of value to extend the NJL model so that one can study the full range of densities of interest at this point in time. We are encouraged in this program by recent results, obtained in lattice simulations of QCD with dynamical quarks, that provide information on the temperature dependence of the confining interaction [14].

It is generally believed that the presence of matter will play a role similar to that of finite temperature, with deconfinement taking place at some finite density, which might be several times that of nuclear matter.

### 1.3.3 Quark-gluon Plasma

At extremely high density and temperature, the confining feature of quarks and the spontaneous breakdown of chiral symmetry might be distroyed. Actually, the lattice calculation has shown that at zero baryon density these features are both distroyed at the same temperature. A new phase of matter, quark-gluon plasma has then been suggested. It is of interest to obtain insight into the lattice results in the NJL model, that describes the restoration of chiral symmetry with increasing temperature. In this thesis we will report our calculations of quark-gluon plasma.

## 1.4 Thesis Structure

In this thesis we want to report our studies with our modified NJL model. In chapter 2, we describe the our extended NJL model with confinement. In chapter 3, a nonlocal NJL model is given. We will also include the descriptions of some basic physics quantities in these two chapters, since these two chapters are the preparation of the discussions in the followed chapters.

In chapter 4, we focus our investigation on finite temperature. Two cases are covered, in which the first is the chiral symmetry restoration, and another is the excitations of quark-gluon plasma.

In the chapter 5 we will study the deconfinement at finite matter density. This discussion is parallel to the finite temperature case that we have in chapter 3.

In the last chapter we focus on the dense matters. We will first discuss the quark

and nucleon self-energy. Then the quark propagation in the quark-gluon plasma is studied.

# Chapter 2

# The NJL Model with Confinement

## 2.1 Models of Confinement

In recent years we have developed a generalized Nambu–Jona-Lasinio (NJL) model that incorporates a covariant model of confinement [21, 20, 18, 17, 16]. The Lagrangian of the model is

$$\begin{aligned}\mathcal{L} = \quad & \bar{q}(i\partial\!\!\!/ - m^0)q + \frac{G_S}{2}\sum_{i=0}^{8}[(\bar{q}\lambda^i q)^2 + (\bar{q}i\gamma_5\lambda^i q)^2] \\ & -\frac{G_V}{2}\sum_{i=0}^{8}[(\bar{q}\lambda^i\gamma_\mu q)^2 + (\bar{q}\lambda^i\gamma_5\gamma_\mu q)^2] \\ & +\frac{G_D}{2}\{\det[\bar{q}(1+\gamma_5)q] + \det[\bar{q}(1-\gamma_5)q]\} \\ & +\mathcal{L}_{conf}\,, \end{aligned} \tag{2.1.1}$$

where the $\lambda^i (i = 0, \cdots, 8)$ are the Gell-Mann matrices, with $\lambda^0 = \sqrt{2/3}\,\mathbf{1}$, $m^0 = \mathrm{diag}\,(m_u^0, m_d^0, m_s^0)$ is a matrix of current quark masses and $\mathcal{L}_{conf}$ denotes our model of confinement.

There are several models of confinement in use. One approach is particularly suited to Euclidean-space calculations of hadron properties. In that case one constructs a model

of the quark propagator by solving the Schwinger-Dyson equation. By appropriate choice of the interaction one can construct a propagator that has no on-mass-shell poles when the propagator is continued into Minkowski space. Such calculations have recently been reviewed by Roberts and Schmidt [52]. In the past, we have performed calculations of the quark and gluon propagators in Euclidean space and in Minkowski space. These calculations give rise to propagators which did not have on-mass-shell poles [53, 54, 55, 56]. However, for our studies of meson spectra, which included descriptions of radial excitations, we found it useful to work in Minkowski space.

The construction of our covariant confinement model has been described in a number of works [21, 20, 18, 17, 16]. In all our work we have made use of Lorentz-vector confinement, so that the Lagrangian of our model exhibits chiral symmetry. For Euclidean-space calculations we may write

$$\mathcal{L}_{conf} = \int d^4y \overline{q}(x)\gamma^\mu q(x) V^C(x-y)\overline{q}(y)\gamma_\mu q(x) \tag{2.1.2}$$

where in momentum-space, $V^C$ describes four-momentum transfer. However, for the Minkowski-space calculations, we found it useful to neglect the energy transfer by the confining field in the meson rest frame. We begin with the form $V^C(r) = \kappa r \exp[-\mu r]$ and obtain the momentum-space potential via Fourier transformation. Thus,

$$V^C(\vec{k}-\vec{k}\,') = -8\pi\kappa\left[\frac{1}{[(\vec{k}-\vec{k}\,')^2+\mu^2]^2} - \frac{4\mu^2}{[(\vec{k}-\vec{k}\,')^2+\mu^2]^3}\right], \tag{2.1.3}$$

with the matrix form

$$\overline{V}^{\,C}(\vec{k}-\vec{k}\,') = \gamma^\mu(1) V^C(\vec{k}-\vec{k}\,')\gamma_\mu(2)\,, \tag{2.1.4}$$

appropriate to Lorentz-vector confinement. We may write a covariant version of

$V^C(\vec{k}-\vec{k}')$ by introducing the four-vectors

$$\hat{k}^\mu = k^\mu - \frac{(k\cdot P)P^\mu}{P^2}\,, \tag{2.1.5}$$

and

$$\hat{k}'^\mu = k'^\mu - \frac{(k'\cdot P)P^\mu}{P^2}\,. \tag{2.1.6}$$

Thus, we have

$$V^C(\hat{k}-\hat{k}') = -8\pi\kappa\left[\frac{1}{[-(\hat{k}-\hat{k}')^2+\mu^2]^2} - \frac{4\mu^2}{[-(\hat{k}-\hat{k}')^2+\mu^2]^3}\right]. \tag{2.1.7}$$

Originally, the parameter $\mu = 0.010$ GeV was introduced to simplify our momentum-space calculations. However, in the light of the following discussion, we can remark that $\mu$ may be interpreted as describing screening effects as they affect the confining potential [14]. In our work, we found that the use of $\kappa = 0.055$ GeV$^2$ gave very good results for meson spectra.

The potential $V^C(r) = \kappa r\exp[-\mu r]$ has a maximum at $r = 1/\mu$, at which point the value is $V_{max} = \kappa/\mu e = 2.023$ GeV. If we consider pseudoscalar mesons, which have $L = 0$, the continuum of the model starts at $E_{cont} = m_1 + m_2 + V_{max}$, so that for $m_1 = m_2 = m_u = m_d = 0.364$ GeV, $E_{cont} = 2.751$ GeV. It is also worth noting that the potential goes to zero for very large r. Thus, there are scattering states whose lowest energy would be $m_1 + m_2$. However, barrier penetration plays no role in our work. The bound states in the interior of the potential do not communicate with these scattering states to any significant degree. It is not difficult to construct a computer program that picks out the bound states from all the states found upon diagonalizing the random-phase-approximation Hamiltonian.

Bound states in the confining field may be found by solving the equation for the

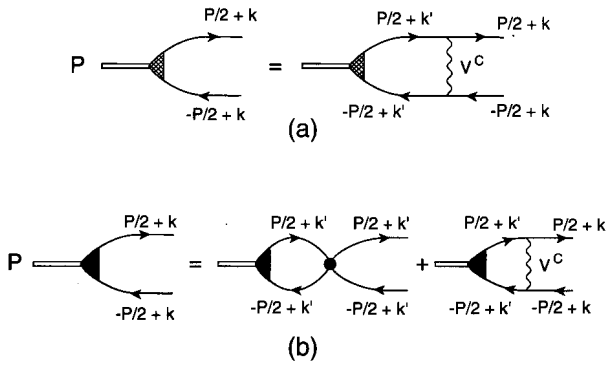


Figure 2.1: a) Bound states in the confining field (wavy line) may be found by solving the equation for the vertex shown in this figure, b) Effects of both the confining field and the short-range NJL interaction (filled circle) are included when solving for the vertex shown in this figure.

mesonic vertex function shown in Fig. 2.1a. Inclusion of the short-range NJL interaction leads to an equation for the vertex shown in Fig. 2.1b. We will return to a consideration of Fig. 2.1b when we discuss our covariant RPA formalism in Section 4.3.3.

## 2.2 Covariant Lorentz-vector Model of Confinement

Next, we provide a review of the important features of the model. As a first step, we introduce a vertex function for the confining interaction. [See Fig. 2.1b.] For example, the vertex useful in the study of pseudoscalar mesons satisfies an equation of the form [21]

$$\begin{aligned}\overline{\Gamma}_{5,ab}(P,k) &= \gamma_5 - i\int\frac{d^4k'}{(2\pi)^4}\,[\gamma^\mu S_a(P/2+k') \\ &\quad \times\overline{\Gamma}_{5,ab}(P,k')S_b(-P/2+k')\gamma_\mu]V^C(\vec{k}-\vec{k}')\,,\end{aligned} \tag{2.2.1}$$

where $S_a(P/2+k') = [\not{P}/2 + \not{k}' - m_a + i\eta]^{-1}$. Here, $m_a$ and $m_b$ are the constituent quark masses. We consider the form $V^C(r) = \kappa r \exp[-\mu r]$ and obtain the Fourier transform as Eq. (2.1.3), which is used in Eq. (2.2.1). We then define Eq. (2.1.7), which reduces to $V^C(\vec{k}-\vec{k}')$ of Eq. (2.1.3) in the meson rest frame, where $\vec{P}=0$.

It is also useful to define scalar functions $\Gamma^{+-}_{5,ab}(P,k)$ and $\Gamma^{-+}_{5,ab}(P,k)$ [21]. We introduce

$$\Lambda_a^{(+)}(\vec{k}) = \frac{\not{k}_a + m_a}{2m_a} \tag{2.2.2}$$

and

$$\Lambda_a^{(-)}(-\vec{k}) = \frac{\widetilde{\not{k}}_a + m_a}{2m_a}\,, \tag{2.2.3}$$

where $k^\mu = [E_a(\vec{k}), \vec{k}]$ and $\widetilde{k}^\mu = [-E_a(\vec{k}), \vec{k}]$, and define

$$\Lambda_a^{(+)}(\vec{k})\overline{\Gamma}_{5,ab}(P,k)\Lambda_b^{(-)}(-\vec{k}) = \Gamma^{+-}_{5,ab}(P,k)\Lambda_a^{(+)}(\vec{k})\gamma_5\Lambda_b^{(-)}(-\vec{k})\,, \tag{2.2.4}$$

and

$$\Lambda_a^{(-)}(-\vec{k})\overline{\Gamma}_{5,ab}(P,k)\Lambda_b^{(+)}(\vec{k}) = \Gamma^{-+}_{5,ab}(P,k)\Lambda_a^{(-)}(-\vec{k})\gamma_5\Lambda_b^{(+)}(\vec{k})\,. \tag{2.2.5}$$

We have obtained equations for $\Gamma_5^{+-}(P,k)$ and $\Gamma_5^{-+}(P,k)$. For example, with $m_a = m_b$, we have

$$\Gamma_5^{+-}(P^0,|\vec{k}|) = 1 - \int\frac{d^3k'}{(2\pi)^3}\left[\frac{m^2 - 2E(\vec{k})E(\vec{k}')}{E(\vec{k})E(\vec{k}')}\right]\frac{\Gamma_5^{+-}(P^0,|\vec{k}'|)V^C(\vec{k}-\vec{k}')}{P^0 - 2E(\vec{k}')}\,. \tag{2.2.6}$$

Note that $\Gamma_5^{+-}(P^0,|\vec{k}'|) = 0$, when $P^0 = 2E(\vec{k}')$, so that one need not introduce a small quantity, $i\epsilon$, in the denominator on the right-hand side of Eq. (2.2.6). (Alternatively, we may note that $\Gamma_5^{+-}(P^0,|\vec{k}|) = 0$ when the quark and antiquark in Fig. 4.6 are on mass shell.) The confinement vertex functions defined in our work may be

used to calculate vacuum polarization functions which are real functions. The unitarity cut, that would otherwise be present, is eliminated by the vertex functions which vanish when both the quark and antiquark go on mass shell [16, 17, 18, 19, 20, 21].

We have presented Eq. (2.2.6), since we wish to stress that for the study of light mesons the constituent quark mass, $m$, is of the order of $|\vec{k}|$, so that $|\vec{k}|/m$ is not small. Therefore, the term in the square bracket on the right-hand side of Eq. (2.2.6), which would be equal to $-1$ in the nonrelativistic limit, provides quite important relativistic corrections to the form given in Eq. (2.1.7).

In Fig. 2.1a we show the homogeneous equation for the confining vertex. The solution of the homogeneous equation allows us to construct the wave functions bound in the confining field. For example, we may define

$$\psi_i^{(+)}(k) = \frac{\Gamma_5^{+-}(P_i^0, k)}{P_i^0 - 2E(\vec{k})} \tag{2.2.7}$$

and

$$\psi_i^{(-)}(k) = -\frac{\Gamma_5^{-+}(-P_i^0, k)}{P_i^0 + 2E(\vec{k})}\,, \tag{2.2.8}$$

which we may term the "large" and "small" components of the wave function of the bound state with energy $P_i^0$. In Fig. 2.1b we show the equation for the vertex function that includes both the effects of the short-range NJL interaction and the confining interaction.

## 2.3 Density and Temperature Dependence of the Confining Field

In part, our study has been stimulated by the results presented in Ref. [14] for the temperature-dependent potential, $V(r)$, in the case dynamical quarks are present. We reproduce some of the results of that work in Fig. 2.2. There, the filled symbols represent the results for $T/T_c = 0.68, 0.80, 0.88$ and $0.94$ when dynamical quarks are present. This figure represents definite evidence of "string breaking", since the force between the quarks appears to approach zero for $r > 1$ fm. This is not evidence for deconfinement, which is found for $T = T_c$. Rather, it represents the creation of a second $\bar{q}q$ pair, so that one has two mesons after string breaking. Some clear evidence for string breaking at zero temperature and finite density is reported in Ref. [28].

In order to study deconfinement in our generalized NJL model, we need to specify the interquark potential at finite density. We start with our model that was described in Section 2.1. In that case we had $V^C(r) = \kappa r \exp[-\mu r]$. For the model we study in this work, we write

$$V^C(r,\rho) = \kappa r \exp[-\mu(\rho) r] \tag{2.3.1}$$

and put

$$\mu(\rho) = \frac{\mu_0}{1 - \left(\frac{\rho}{\rho_C}\right)^2}\,, \tag{2.3.2}$$

with $\rho_C = 2.25\rho_{NM}$ and $\mu_0 = 0.010$ GeV. With this modification our results for meson spectra in the vacuum are unchanged. Other forms than that given in Eqs. (2.3.1) and (2.3.2) may be used. However, in our work we limit our analysis to the model presented in these equations. The corresponding potentials for our model of

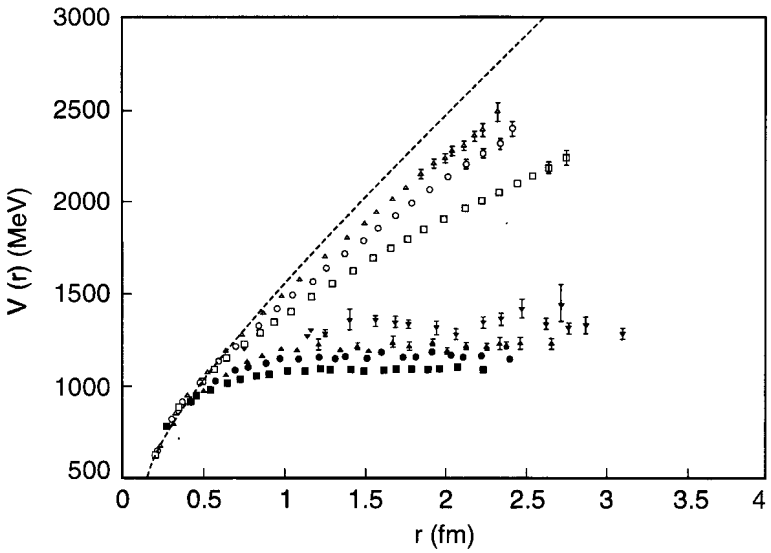


Figure 2.2: A comparison of quenched (open symbols) and unquenched results (filled symbols) for the interquark potential at finite temperature [14]. The dotted line is the zero temperature quenched potential. Here, the symbols for $T = 0.80T_c$ [open triangle], $T = 0.88T_c$ [open circle], $T = 0.94T_c$ [open square], represent the quenched results. The results with dynamical fermions are given at $T = 0.68T_c$ [solid downward-pointing triangle], $T = 0.80T_c$ [solid upward-pointing triangle], $T = 0.88T_c$ [solid circle], and $T = 0.94T_c$ [solid square].

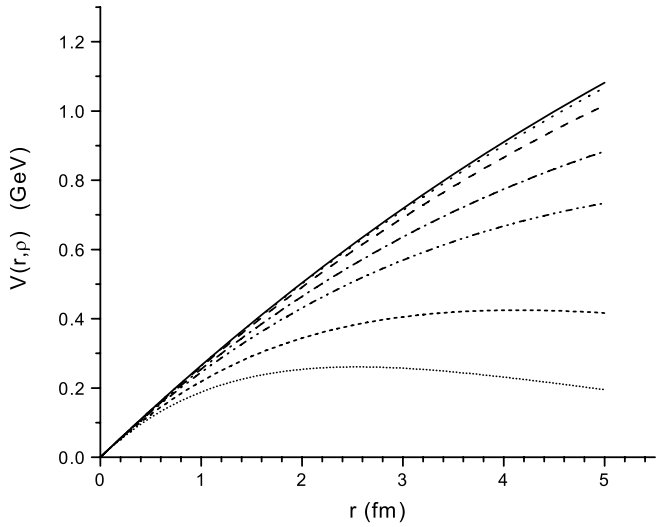


Figure 2.3: Values of $V(r,\rho)$ are shown, where $V(r,\rho) = \kappa r \exp[-\mu(\rho)r]$ and $\mu(\rho) = \mu_0/[1-(\rho/\rho_C)^2]$. Here $\rho_C = 2.25\rho_{NM}$ and $\mu_0 = 0.010$ GeV. The values of $\rho/\rho_{NM}$ are 0.0 [solid line], 0.50 [dotted line], 1.0 [dashed line], 1.50 [dashed-dotted line]. 1.75 [dashed-dotted-dotted line], 2.0 [short-dashed line], and 2.1 [small dotted line].

Lorentz-vector confinement are shown in Fig. 2.3 for several values of $\rho/\rho_{NM}$.

Similar calculations can be applied to the case of temeperature-dependent confinement. We introduced a temperature-dependent confining potential, whose form was motivated by recent lattice simulations of QCD in which the temperature dependence of the confining interaction was calculated with dynamical quarks [14]. (See Fig. 2.2.) In order to include such effects, we modified the form of our confining interaction, $V^C(r) = \kappa r \exp[-\mu r]$, by replacing $\mu$ by

$$\mu(T) = \frac{\mu_0}{\left[1 - 0.7\left(\frac{T}{T_c}\right)^2\right]}, \tag{2.3.3}$$

with $\mu_0 = 0.010$ GeV. The maximum value of $V^C(r,T)$ is then

$$V^C_{max}(T) \;=\; \frac{\kappa}{\mu(T)e}, \tag{2.3.4}$$

$$= \frac{\kappa\,[1-0.7(T/T_c)^2]}{\mu_0 e}\,, \tag{2.3.5}$$

with $r_{max} = 1/\mu(T)$. To better represent the qualitative features of the results shown in Fig. 2.2, we can use $V^C(r,T) = \kappa r \exp[-\mu(T)r]$ for $r \leq r_{max}$ and $V^C(r,T) = V^C_{max}(T)$ for $r > r_{max}$. We also note that we use Lorentz-vector confinement and carry out all our calculations in momentum-space. The value of $\kappa$ used in our work is 0.055 GeV$^2$. For more details please refer to Chapter 4.3. Here we will not go into this case in any more details.

## 2.4 Calculation of Constituent Quark Mass Values

In this section we will show our calculation of the density dependence of the constituent quark masses of the up (or down) and strange quarks. The role of confinement in the calculation of the constituent mass was studied in an earlier work in which calculations were made in Euclidean space [47]. The results were similar to those obtained in Minkowski-space calculations in which confinement was neglected and it is the latter calculations which we discuss here.

The equations for the quark masses in the SU(3)-flavor NJL model are [23]

$$m_u = m_u^0 - 2G_S\langle\bar{u}u\rangle - G_D\langle\bar{d}d\rangle\langle\bar{s}s\rangle\,, \tag{2.4.1}$$

$$m_d = m_d^0 - 2G_S\langle\bar{d}d\rangle - G_D\langle\bar{u}u\rangle\langle\bar{s}s\rangle\,, \tag{2.4.2}$$

$$m_s = m_s^0 - 2G_S\langle\bar{s}s\rangle - G_D\langle\bar{u}u\rangle\langle\bar{d}d\rangle\,, \tag{2.4.3}$$

where $\langle\bar{u}u\rangle, \langle\bar{d}d\rangle$ and $\langle\bar{s}s\rangle$ are the quark vacuum condensates. These equations are depicted in Fig. 2.4a, where the last term represents the 't Hooft interaction. For

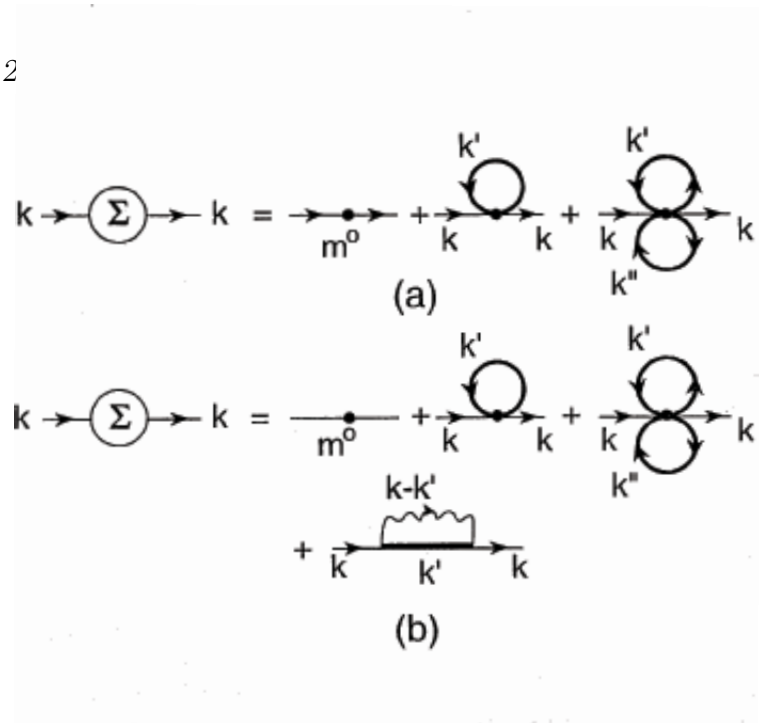


Figure 2.4: a)A diagrammatic representation of the equation for the self-energy for a quark of momentum $k$. The first term on the right is the contribution of the current quark mass $m^0$. The second term corresponds to the term proportional to $G_S$ in Eqs. (2.4.2)–(2.5.6) and the last term represents the 't Hooft interaction. b)The self-energy equation in the presence of a confining interaction (wavy line.) Without the 't Hooft interaction, we have a representation of SU(2)-flavor model studied in Ref. [75]. (See Eqs. (2.15) and (2.16).)

example,

$$\langle \bar{u}u \rangle = -4N_c i \int \frac{d^4k}{(2\pi)^4} \, \frac{m_u}{k^2 - m_u^2 + i\epsilon} \, . \tag{2.4.4}$$

If this integral is evaluated in a Minkowski-space calculation, a cutoff is used such that $|\vec{k}| \leq \Lambda_3$. Thus,

$$\langle \bar{u}u \rangle = -4N_c \int^{\Lambda_3} \frac{d^3k}{(2\pi)^3} \, \frac{m_u}{2E_u(\vec{k})} \, , \tag{2.4.5}$$

etc. Here $E_u(\vec{k}) = \left[\vec{k}^2 + m_u^2\right]^{1/2}$.

For studies at finite density, we consider the presence of two ideal Fermi gases of up and down quarks with Fermi momentum $k_F$. We also take $m_u^0 = m_d^0$ and obtain the

density-dependent equations, with $\langle\bar{u}u\rangle_\rho = \langle\bar{d}d\rangle_\rho$,

$$m_u(\rho) = m_u^0 - 2G_S\langle\bar{u}u\rangle_\rho - G_D\langle\bar{d}d\rangle_\rho\langle\bar{s}s\rangle_\rho\,, \tag{2.4.6}$$

$$m_s(\rho) = m_s^0 - 2G_S\langle\bar{s}s\rangle_\rho - G_D\langle\bar{u}u\rangle_\rho\langle\bar{d}d\rangle_\rho\,. \tag{2.4.7}$$

Equation 2.4.5 is now replaced by

$$\langle\bar{u}u\rangle_\rho = -4N_c\left[\int_0^{\Lambda_3}\frac{d^3k}{(2\pi)^3}\,\frac{m_u(\rho)}{2E_u(\vec{k})} - \int_0^{k_F}\frac{d^3k}{(2\pi)^3}\,\frac{m_u(\rho)}{2E_u(\vec{k})}\right]\,, \tag{2.4.8}$$

with $E_u(\vec{k}) = \left[\vec{k}^2 + m_u^2(\rho)\right]^{1/2}$. On the other hand, since we do not consider a background of strange matter, we have

$$\langle\bar{s}s\rangle_\rho = -4N_c\int_0^{\Lambda_3}\frac{d^3k}{(2\pi)^3}\,\frac{m_s(\rho)}{2E_s(\vec{k})}\,, \tag{2.4.9}$$

with $E_s(\vec{k}) = \left[\vec{k}^2 + m_s^2(\rho)\right]^{1/2}$.

We may argue that, with respect to our mean-field analysis, the Fermi gases of up and down quarks yield contributions to the scalar density that are similar to what would be obtained if the quarks are organized into nucleons. One part of the argument is based upon the well-known model-independent relation for the density dependence of the condensate [48]

$$\frac{\langle\bar{q}q\rangle_\rho}{\langle\bar{q}q\rangle_0} = \left(1 - \frac{\sigma_N\rho}{f_\pi^2 m_\pi^2} + \cdots\right)\,, \tag{2.4.10}$$

where $\sigma_N$ is the pion-nucleon sigma term and $\rho$ is the density of the matter. If we take $f_\pi = 0.0942$ GeV, $m_\pi = 0.138$ GeV, $\rho_{NM} = (0.109\,\text{GeV})^3$ and $\sigma_N = 0.050$ GeV, we find a reduction of the condensate in nuclear matter of 38%, which is consistent with relativistic models of nuclear matter [49, 50].

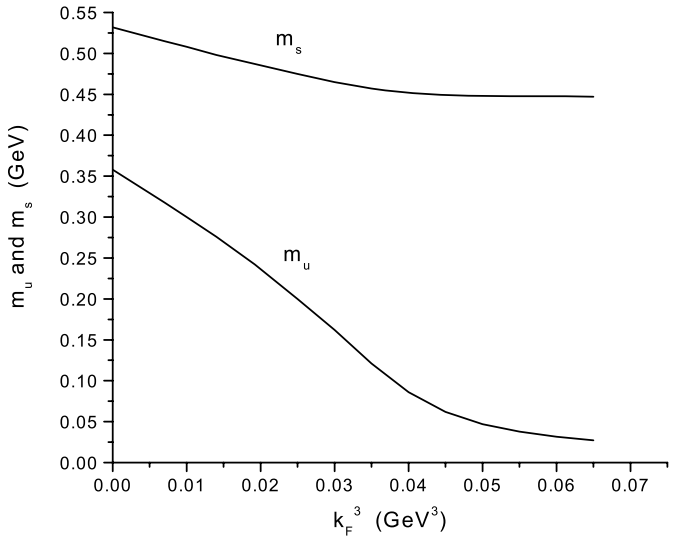


Figure 2.5: The solution of Eqs. (2.4.6) and (2.4.7) for the density-dependent constituent quark masses, $m_u(\rho) = m_d(\rho)$ and $m_s(\rho)$ are shown. Here $G_S = 9.00$ GeV$^{-2}$, $G_D = -240.0$ GeV$^{-5}$, $\Lambda_3 = 0.631$ GeV, $m_u^0 = 0.0055$ GeV and $m_s^0 = 0.130$ GeV.

We now consider the corresponding relation for a quark gas of up and down quarks,

$$\frac{\langle \bar{q}q \rangle_\rho}{\langle \bar{q}q \rangle_0} = \left( 1 - \frac{\sigma_q \rho_q}{f_\pi^2 m_\pi^2} + \cdots \right) , \tag{2.4.11}$$

where $\rho_q$ is the density of quarks ($\rho_q = 3\rho$) and $\sigma_q$ is a "quark sigma term". We have shown in earlier work [51] that $\sigma_q$ is in the range of 15-17 MeV, so that Eqs. (2.4.10) and (2.4.11) imply that quite similar mean fields are generated by the quark gas and by nuclear matter.

In Table 2.1 and in Fig. 2.5, we show the results obtained when Eqs. (2.4.8) and (2.4.9) are solved with $G_S = 9.00$ GeV$^{-2}$, $G_D = -240$ GeV$^{-5}$, $\Lambda_3 = 0.631$ GeV, $m_u^0 = 0.0055$ GeV and $m_s^0 = 0.130$ GeV. We note that the dependence of $m_u(\rho)$ on density is approximately linear for $\rho/\rho_{NM} \leq 2$, with a 32% reduction in the value of $m_u(\rho)$ when $\rho/\rho_{NM} = 1$. Another point to note is that $m_s(\rho)$ is density-dependent

| $k_F^3$ ( GeV$^3$) | $\rho/\rho_{NM}$ | $m_u(\rho)$ [GeV] | $m_s(\rho)$ [GeV] |
|---|---|---|---|
| 0.00 | 0.00 | 0.358 | 0.532 |
| 0.007 | 0.364 | 0.318 | 0.515 |
| 0.010 | 0.521 | 0.300 | 0.508 |
| 0.0140 | 0.729 | 0.276 | 0.498 |
| 0.0192 | 1.00 | 0.242 | 0.487 |
| 0.025 | 1.302 | 0.200 | 0.475 |
| 0.030 | 1.562 | 0.162 | 0.465 |
| 0.035 | 1.823 | 0.121 | 0.457 |
| 0.040 | 2.083 | 0.0860 | 0.452 |
| 0.045 | 2.343 | 0.0618 | 0.449 |
| 0.050 | 2.604 | 0.0470 | 0.448 |
| 0.055 | 2.864 | 0.0378 | 0.448 |
| 0.060 | 3.125 | 0.0316 | 0.448 |
| 0.065 | 3.385 | 0.0272 | 0.447 |

Table 2.1: Values of $m_u(\rho)$ and $m_s(\rho)$ obtained from the solution of Eqs. (2.4.6) and (2.4.7) are given for various values of the ratio $\rho/\rho_{NM}$. (Here, $k_F^3 = 0.0192$ GeV$^3$ for nuclear matter, $m_u^0 = 0.0055$ GeV, $m_s^0 = 0.130$ GeV, $\Lambda_3 = 0.631$ GeV, $G_S = 9.00$ GeV$^{-2}$, $G_D = -240.0$ GeV$^{-5}$.)

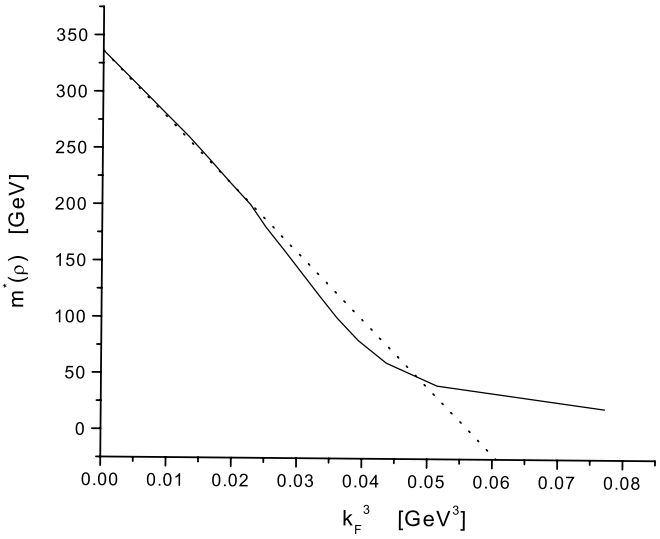


Figure 2.6: The solution of Eq. (2.4.12) for $m_u(\rho)$ is shown. Here $G_S = 10.15$ GeV$^{-2}$, $m_u^0 = 0.0055$ GeV and $\Lambda_3 = 0.631$ GeV. (See Table V of Ref. [12].) The dashed line is a linear approximation to the result which we use for $\rho \leq 2\rho_{NM}$. (Nuclear matter density corresponds to $k_F^3 = 0.0192$ GeV$^3$.

for finite values of $G_D$, since the $\langle \bar{s}s \rangle$ condensate is modified by the coupling to the up and down quark condensates via the 't Hooft interaction [12, 23, 22]. This coupling becomes less important as the up and down quark condensates are reduced at increasing density. [See Fig. 2.5.]

We have also considered the solution for the SU(2) version of the above equations

$$m_u(\rho) = m_u^0 - 2G_S \langle \bar{u}u \rangle_\rho \,, \tag{2.4.12}$$

and have used the parameters specified in the Klevansky review article [12], $G_S = 10.15$ GeV$^{-2}$, $m_u^0 = 0.0055$ GeV and $\Lambda_3 = 0.631$ GeV. The results for $m_u(\rho)$ are similar to that seen in Fig. 2.6, except that $m_u(0) = 0.336$ GeV. [See Fig. 2.6.] In this case, $m_u(\rho)$ is reduced by about 32% when $\rho = \rho_{NM}$.

For the case of temperature-dependent constituent quark mass calculation, the cal-

culation is similar. We will have a detailed discuss in Section 4.3.2.

## 2.5 The Quark Self-energy

Here are some reviews of the calculation of the quark self-energy in the local SU(3)-flavor NJL model. One of our jobs is to add a confinement interaction, as was done in an earlier study of the quark self-energy [75]. We consider the generalization to a model with nonlocal short-range and 't Hooft interactions. The Lagrangian of the model we have used is

$$\begin{aligned}\mathcal{L} = \quad & \bar{q}(i\partial\!\!\!/ - m^0)q + \frac{G_S}{2}\sum_{i=0}^{8}[(\bar{q}\lambda^i q)^2 + (\bar{q}i\gamma_5\lambda^i q)^2] \\ & + \frac{G_D}{2}\{\det[\bar{q}(1+\gamma_5)q] + \det[\bar{q}(1-\gamma_5)q]\}\,. \end{aligned} \tag{2.5.1}$$

Here $m^0$ is the matrix of quark current masses, $m^0 = \mathrm{diag}\,(m_u^0, m_d^0, m_s^0)$ and the $\lambda^i (i = 1, \cdots, 8)$ are the Gell-Mann matrices. Further, $\lambda_0 = \sqrt{2/3}\,\mathbb{1}$, with $\mathbb{1}$being the unit matrix in the flavor space.

The quark propagator is written as

$$iS(k) = \frac{i}{\not{k} - \Sigma(k) + i\epsilon}\,, \tag{2.5.2}$$

with

$$\Sigma(k) = A(k^2) + B(k^2)\not{k}\,. \tag{2.5.3}$$

We may define

$$M_u(k^2) = \frac{A_u(k^2)}{1 - B_u(k^2)}\,, \tag{2.5.4}$$

and

$$Z_u(k^2) = \frac{1}{1 - B_u(k^2)}\,, \tag{2.5.5}$$

with similar definitions for $M_d(k^2), M_s(k^2), Z_d(k^2)$ and $Z_s(k^2)$.

In the absence of a confinement model, we have $B(k^2) = 0, A_u(k^2) = A_d(k^2) = m_u$ and $A_s(k^2) = m_s$, where $m_u$ and and $m_s$ are constants. (Here, we have take $m_u^0 = m_d^0$.) In this case we have Eqs. (2.4.1 - 2.4.3)[23]. The up quark vacuum condensate is given by

$$\begin{aligned} \langle \bar{u}u \rangle &= -N_c i \int \frac{d^4k}{(2\pi)^4}\, \mathtt{Tr} \frac{C(k^2)}{\not{k} - m_u + i\epsilon}\,, & (2.5.6) \\ &= -4N_c i \int \frac{d^4k}{(2\pi)^4}\, \frac{m_u C(k^2)}{k^2 - m_u^2 + i\epsilon}\,. & (2.5.7) \end{aligned}$$

Here, $C(k^2)$ is a function needed to regulate the integral. In this work we will use the Pauli-Villars procedure and evaluate the integral in Euclidean space, as was done in Ref. [75]. In the general case we may write

$$\langle \bar{u}u \rangle = -4N_c i \int \frac{d^4k}{(2\pi)^4}\, \frac{Z_u(k^2) M_u(k^2) C(k^2)}{k^2 - M_u^2(k^2) + i\epsilon}\,, \tag{2.5.8}$$

where $Z_u(k^2)$ and $M_u^2(k^2)$ were defined in Eqs. (2.5.4) and (2.5.5).

In Ref. [75] we obtained the following coupled equations in the case of the SU(2)-flavor model

$$A(k^2) = i \int \frac{d^4k'}{(2\pi)^4}\, \frac{[-4V^c(k-k') + 4N_c n_f G_S] A(k'^2)}{k'^2[1 - B(k'^2)]^2 - A^2(k'^2) + i\epsilon}\,, \tag{2.5.9}$$

$$k^2 B(k^2) = i \int \frac{d^4k'}{(2\pi)^4}\, \frac{2(k \cdot k')[1 - B(k'^2)] V^c(k-k')}{k'^2[1 - B(k'^2)]^2 - A^2(k'^2) + i\epsilon}\,. \tag{2.5.10}$$

where $V^c$ is the Lorentz-vector confinement we introduced in this chapter. These equations were solved after passing to Euclidean space and including a Pauli-Villars

regulator of the form

$$C(k_E^2) = \frac{2\Lambda^4}{[k_E^2 + A^2(k_E^2) + \Lambda^2][k_E^2 + A^2(k_E^2) + 2\Lambda^2]} \tag{2.5.11}$$

in Euclidean space. Note that the form

$$\widetilde{C}(k_E^2) = \frac{2\Lambda^4}{[k_E^2\,(1 - B(k_E^2))^2 + A^2(k_E^2) + \Lambda^2][k_E^2\,(1 - B(k_E^2))^2 + A^2(k_E^2) + 2\Lambda^2]} \tag{2.5.12}$$

may also be used. (In Eqs. (2.5.9) and (2.5.10) $V^c$ appears with a sign opposite to that given in Ref. [75], since, in that work, we used a negative value of $\kappa$. For the present work we use a positive value of $\kappa$ to be consistent with all of our other publications.)

## 2.6 Discussion

As we have done in this chapter, we modified the Nambu–Jona-Lasinio model with a Lorentz-vector confinement. This noval model is capable to apply to either density-dependent or temperature-dependent situations.

But as mentioned in Klevansky's paper [12], this model has the shortcoming that the local interaction does not confine quarks. We need further extend our model to a nonlocal one. This will be done in next chapter.

# Chapter 3

# A Nonlocal NJL Model

## 3.1 History

In recent years there has been strong interest in the study of quark matter at high densities, using the NJL model and related models. In particular, one finds color superconductivity under certain conditions and it has been suggested that some compact stars might be made of superconducting quark matter [32, 35, 65, 66, 33, 67, 68]. It is our belief that in such studies one should use a model which reproduces, as well as possible, know features of QCD. In this chapter we wish to generalize the SU(3)-flavor version of the NJL model to be consistent with the type of momentum-dependent quark masses found in lattice simulations of QCD [69]. For example, in Figs. 3.1 and 3.2 we show some of the results obtained in Ref. [69]. It may be seen from these figures that, in Euclidean space, the quark mass goes over to the current mass for Euclidean momentum $k \gtrsim 2$ GeV. On the other hand, the NJL model, in the standard analysis [12], gives rise to a constant value for the constituent quark mass. As we will see, the form of the nonlocality used here is different from that used in Refs. [65, 70, 71, 72, 73, 74]. For example, in reference [70] the $q\bar{q}$ vertex is modified by a form factor which depends on the relative momentum of the quark and

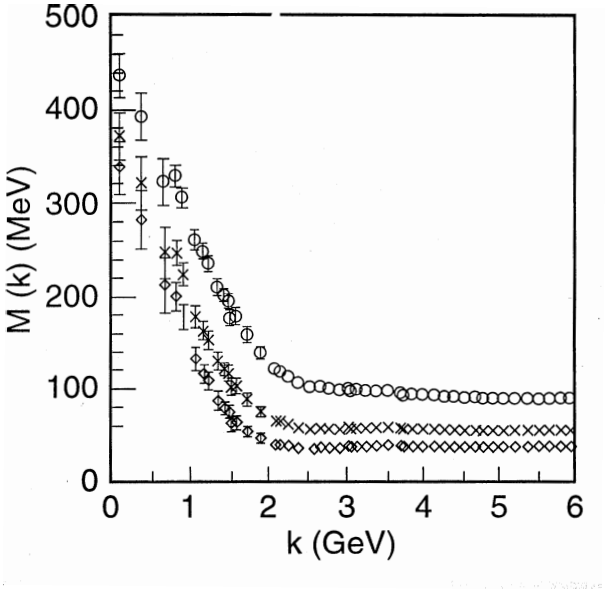


Figure 3.1: Quark mass values obtained in Ref. [69] for various current quark masses: $m^0 = 91$ MeV [ circles], $m^0 = 54$ MeV [crosses] and $m^0 = 35$ MeV [diamonds].

antiquark, while, in another scheme, a form factor is associated with each quark line appearing in a diagram. In the latter procedure no further regularization is needed. However, for the problem considered in our work, the nonlocal models that appear in the literature are of limited applicability, since, in the limit of zero current quark mass, the quark self-energy is proportional to the form factors used to define the nonlocality [70].

## 3.2 A Nonlocal NJL Model

A diect consideration is to introduce a regulator and a nonlocal quark interaction. We stress that the procedure used here differs from any that appears in the literature. In this section we describe the procedures we use to create a nonlocal version of our generalized NJL model. In this case, it is useful to start from a term involving the

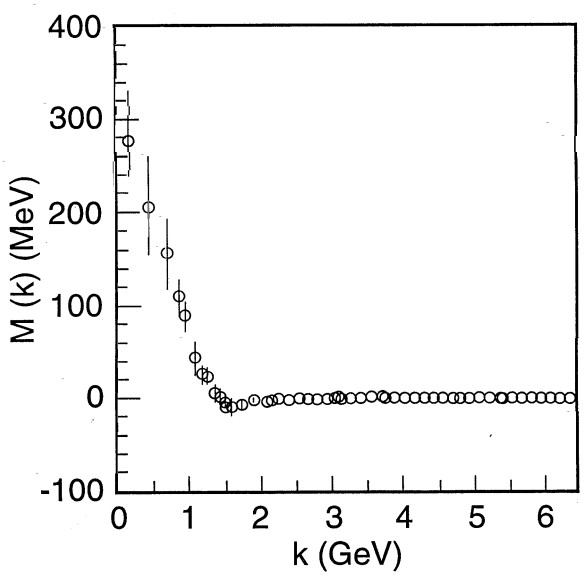


Figure 3.2: Quark mass values obtained in Ref. [69] using an extrapolation of the current quark mass to zero. (The small dip at $k \sim 1.6$ GeV is not statistically significant [69].

interaction of two currents. We replace the second term of Eq. (2.5.1) by a nonlocal form

$$
\begin{aligned}
G_S j^\mu(x)\Gamma(x,y)j_\mu(y) &= \frac{G_S}{2}\sum_{i=0}^{8}\bar{q}(x)\lambda^i\gamma^\mu f(x)q(x)\bar{q}(y)\lambda^i\gamma^\mu f(y)q(y) && (3.2.1)\\
&= \frac{G_S}{2}\sum_{i=0}^{8}\{[\bar{q}(x)\lambda^i f(x)q(y)\bar{q}(y)\lambda^i f(y)q(x)] && (3.2.2)\\
&\qquad + [\bar{q}(x)\lambda^i i\gamma_5 f(x)q(y)\bar{q}(y)\lambda^i i\gamma_5 f(y)q(x)]\}\\
&\quad + \cdots ,
\end{aligned}
$$

where we have used a separable form for $\Gamma(x,y) = f(x)f(y)$ and have performed a Fierz rearrangement to pass from Eq. (3.2.1) to Eq. (3.2.3). We have not written the vector and axial-vector interaction that arise in the Fierz transformation. (See Appendix B of Ref. [12].)

A related modification may be made for the 't Hooft interaction. It is useful, however,

to describe these modifications as they affect momentum-space calculations. With reference to Fig 3.3, we replace $G_S$ by $f(k_2-k_3)G_Sf(k_1-k_4)$. In the evaluation of the second term of Fig. 3.2 we need $G_S(k-k')=f(k-k')G_Sf(k-k')$ and choose to write

$$\begin{aligned} G_S(k-k') &= \exp[-(k-k')^{2n}/2\beta]G_S\exp[-(k-k')^{2n}/2\beta] \\ &= G_S\exp[-(k-k')^{2n}/\beta]\,. \end{aligned} \tag{3.2.3}$$

In this work we take $n=4$ and $\beta=20$ GeV$^8$. In Fig. 3.4 we exhibit the function $F(k^2)=\exp[-k^{2n}/\beta]$. It is clear that many other functions may be chosen.

We now rewrite Eqs. (2.5.9) and (2.5.10) for the up, down and strange quarks. For example, for the SU(3)-flavor case

$$A_u(k^2) = m_u^0 + i\int\frac{d^4k'}{(2\pi)^4}\,\frac{[-4V^c(k-k')+8N_cG_S(k-k')]A_u(k'^2)}{k'^2[1-B_u(k'^2)]^2-A_u^2(k'^2)+i\epsilon} \tag{3.2.4}$$

,

$$k^2B_u(k^2) = i\int\frac{d^4k'}{(2\pi)^4}\,\frac{2(k\cdot k')[1-B_u(k'^2)]V^c(k-k')}{k'^2[1-B_u(k'^2)]^2-A_u^2(k'^2)+i\epsilon}\,, \tag{3.2.5}$$

with similar equations for $A_d(k^2), B_d(k^2)$, etc. Again, these equations are solved after passing to Euclidean space and introducing regulator functions: $C_u(k^2)$, $C_d(k^2)$ and $C_s(k^2)$. In Euclidean space we write

$$C_u(k^2)=\frac{2\Lambda^4}{[k^2+A_u^2(k^2)+\Lambda^2][k^2+A_u^2(k^2)+2\Lambda^2]}\,, \tag{3.2.6}$$

etc. Note that without the 't Hooft interaction the equations for the up, down and strange quarks are uncoupled.

Our treatment of the 't Hooft interaction is based upon a generalization of the last term in Eqs. (2.4.1)-(2.4.3). With reference to the third term on the right in Fig.

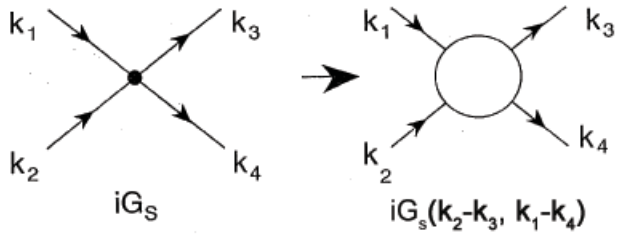


Figure 3.3: The figure indicates the replacement of the local quark interaction, $iG_S$, by the nonlocal (separable) term, $iG_S(k_2 - k_3, k_1 - k_4) = iG_S f(k_2 - k_3) f(k_1 - k_4)$. The distinction between our separable model and that of Ref. [70], for example, is that in Ref. [70] the alternative replacement $iG_S \longrightarrow iG_S(k_2 + k_4, k_1 + k_3) = iG_S f(k_2 + k_4) f(k_1 + k_3)$ was used.

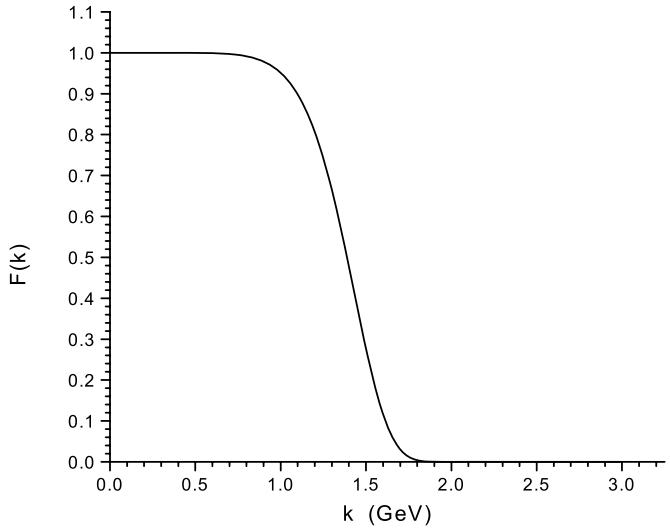


Figure 3.4: The correlation function $F(k) = \exp[-k^{2n}/\beta]$ is shown for $n = 4$ and $\beta = 20$ GeV$^8$.

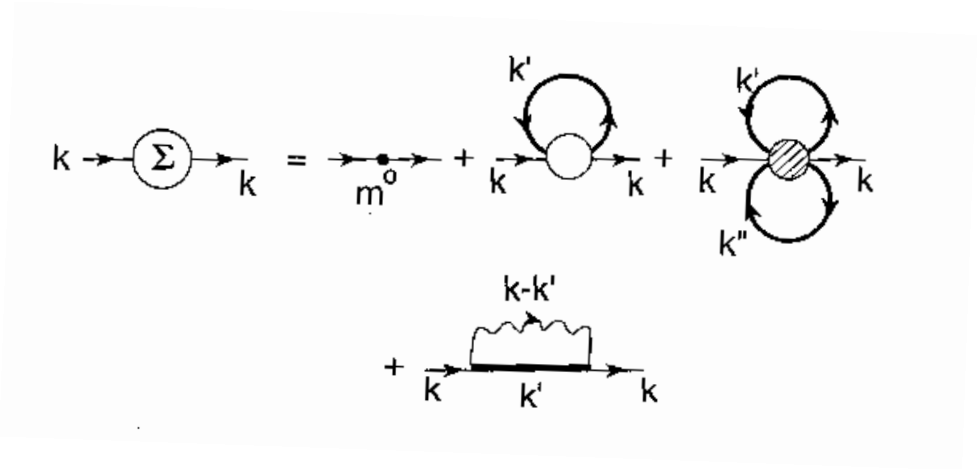


Figure 3.5: The quark self-energy equation is depicted, with nonlocal terms replacing $G_S$ and $G_D$. [See Fig. 3.3]

3.5, we introduce a correlation between the quark of momentum $k$ and the quark of momentum $k'$. We also include a correlation between the quark of momentum $k$ and that of momentum $k''$. (Therefore, our procedure does not introduce a correlation between the two quarks in the separate condensates. At this stage of the development of our model that seems to be a reasonable approximation and avoids having to define a three-quark correlation function, $f(k-k', k'-k'', k-k'')$.) For example, we generalize the term $-G_D\langle\bar{d}d\rangle\langle\bar{s}s\rangle$ to obtain the contribution to $A_u(k)$:

$$A_u^t(k) = -G_D\left[-4N_c i\int\frac{d^4k'}{(2\pi)^4}\,\frac{C_d(k'^2)Z_u(k'^2)M_u(k'^2)f^2(k-k')}{k'^2[1-B_u(k'^2)]^2 - A_u^2(k'^2)}\right] \qquad (3.2.7)$$
$$\times\left[-4N_c i\int\frac{d^4k''}{(2\pi)^4}\,\frac{C_s(k''^2)Z_s(k''^2)M_s(k''^2)f^2(k-k'')}{k''^2[1-B_s(k''^2)]^2 - A_s^2(k''^2)}\right]$$

in Minkowski space. This expression is then evaluated in Euclidean space and added to the right-hand side of Eq. (3.2.4). In a similar fashion, we calculate $A_d^t(k)$ and $A_s^t(k)$.

## 3.3 Some Numerical Results

### 3.3.1 Condensates and Constituent Mass Values

There is a good deal of flexibility in choosing the regulators $C_u(k^2)$, $C_d(k^2)$, and $C_s(k^2)$. Also, various forms could be chosen for the correlation functions, $f(k-k')$. Previously, in our Minkowski-space studies of the $\eta$ mesons we used $G_S = 11.84\ \mathrm{GeV}^{-2}$ and $G_D \simeq -200\ \mathrm{GeV}^{-5}$ [21]. However, in that work we used a Gaussian regulator in Minkowski space so that a direct comparison with the present study can not be made. On the other hand, we do not expect to find radically different parameters, if the constituent masses in the two calculations are similar. For example, in our earlier work, in which $m_u$ and $m_s$ were parameters, we used $m_u = 0.364$ GeV, which can be compared to the value of $M_u(0)$ calculated here. We have also used either $m_s = 0.565$ GeV [16, 17, 18, 19, 20] or $m_s = 0.585$ GeV [21], values which may be compared to $M_s(0)$.

To proceed, we take $\Lambda = 1.0$ GeV, $G_S = 13.30\ \mathrm{GeV}^{-2}$, $\kappa = 0.055\ \mathrm{GeV}^2$, $m_u^0 = 0.0055$ GeV, $m_s^0 = 0.130$ GeV, $\mu = 0.010$ GeV and $\beta = 20.0\ \mathrm{GeV}^8$. We then consider values of $G_D = 0$, $G_D = -20G_S$, $G_D = -30G_S$ and $G_D = -40G_S$. The results of our calculations are given in Table 3.3.1. Recall that the function $F(k)$ does not appear in our expression for the condensates. The calculation of the condensates includes the Pauli-Villars regulators, $C_u(k^2)$, $C_d(k^2)$ and $C_s(k^2)$, however. [See Eqs. (2.5.6)-(2.5.8).] In our calculation of the properties of the $\eta$ mesons [21] we had $-G_D/G_S \simeq 15-18$, since we used $G_D$ values in the range $-180\ \mathrm{GeV}^{-5} \leq G_S \leq -220\ \mathrm{GeV}^{-5}$ in that work.

In order to specify a value of $G_D$ for this work, we note that a calculation based upon chiral perturbation theory yields $\langle \bar{s}s \rangle / \langle \bar{u}u \rangle = 1.689$ [76]. Inspection of Table 3.3.1 suggests that the values of $G_D$, other than $G_D = 0$, given in Table 3.3.1 are

| $G_D$ [ GeV$^{-5}$] | 0.0 | -266.0 | -399.0 | -532.0 |
|---|---|---|---|---|
| $M_u(0)$ [GeV] | 0.334 | 0.377 | 0.396 | 0.416 |
| $M_s(0)$ [GeV] | 0.538 | 0.555 | 0.564 | 0.575 |
| $\langle\bar{u}u\rangle^{\frac{1}{3}}$ [GeV] | -0.207 | -0.215 | -0.217 | -0.220 |
| $\langle\bar{s}s\rangle^{\frac{1}{3}}$ [GeV] | -0.2605 | -0.261 | -0.261 | -0.261 |
| $\frac{\langle\bar{s}s\rangle}{\langle\bar{u}u\rangle}$ | 2.00 | 1.80 | 1.73 | 1.68 |
| $A_u(0)$ [GeV] | 0.447 | 0.481 | 0.496 | 0.512 |
| $B_u(0)$ | -0.335 | -0.276 | -0.253 | -0.233 |
| $A_s(0)$ [GeV] | 0.614 | 0.628 | 0.636 | 0.645 |
| $B_s(0)$ | -0.139 | -0.131 | -0.127 | -0.122 |

Table 3.1: Calculated values for the condensates and for $A(0), B(0),$ and $M(0)$ are given for the up and strange quarks for four values of $G_D$. The parameters $m_u^0 = 0.0055$ GeV, $m_s^0 = 0.130$ GeV, $\kappa = 0.055$ GeV$^2$, $\beta = 20$ GeV$^8$, $\mu = 0.010$ GeV, $\Lambda = 1.0$ GeV, $G_S = 13.30$ GeV$^{-2}$ were used. The values of $\kappa$ and $\mu$ were fixed in earlier work [21, 16, 17, 18, 19, 20]. Values of $\langle\bar{u}u\rangle \simeq \langle\bar{d}d\rangle \simeq -(0.240 \pm 0.025 \text{ GeV})^3$ have been suggested [80], so we see that our calculated values are at, or near, the lower limit for that quantity.

acceptable. For $G_D = -266$ GeV$^{-5}$ we have $M_u(0) = 0.377$ GeV and $M_s(0) = 0.555$ GeV, which are reasonably close to the phenomenological parameters $m_u = 0.364$ GeV and $m_s = 0.565$ GeV used in our earlier work [16, 17, 18, 19, 20].

It is worth noting that, in standard application of the SU(3)-flavor NJL model, one finds $\langle\bar{s}s\rangle/\langle\bar{u}u\rangle \sim 1.1$ [12], so that the results shown in Table 3.3.1 are encouraging, given that the value for $\langle\bar{s}s\rangle/\langle\bar{u}u\rangle$ obtained using chiral perturbation theory is about 1.7 [76], as noted above.

### 3.3.2 Momentum Dependence of the Constituent Quark Masses

In Fig. 3.6 we show $M_u(k)$, where $k$ is the magnitude of the Euclidean momentum. The dashed line exhibits the result without the confining interaction ($\kappa = 0$). It is interesting to see that inclusion of confinement improves the shape of the curve when we compare our results to the lattice results shown in Figs. 3.1 and 3.2. We note

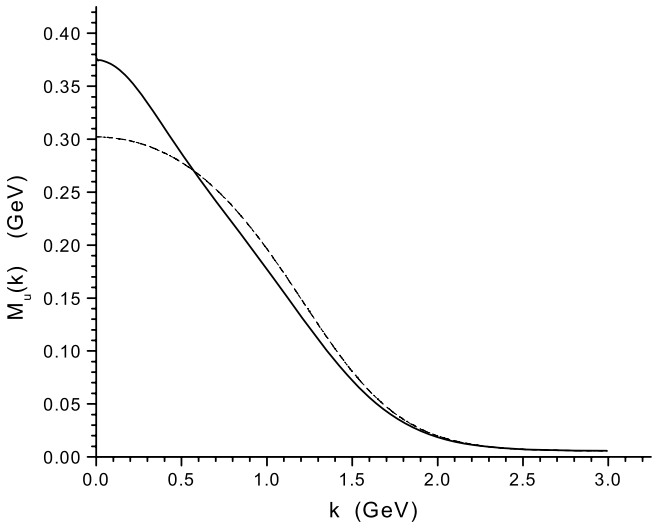


Figure 3.6: Values of $M_u(k)$ are shown for the parameters $m_u^0 = 0.0055$ GeV, $m_s^0 = 0.130$ GeV, $\kappa = 0.055$ GeV$^2$, $\mu = 0.010$ GeV, $\Lambda = 1.0$ GeV, $\beta = 20$ GeV$^8$, $G_S = 13.3$ GeV$^{-2}$, and $G_D = -266$ GeV$^{-5}$. The dashed line shows the result without confinement ($\kappa = 0$).

that $M_u(k)$ goes over to $m_u^0 = 0.0055$ GeV for large $k$. In Fig. 3.7 we show $B_u(k)$. (Recall that $Z_u(k) = [1 - B_u(k)]^{-1}$.) We remark that $B_u(k) = 0$ when $\kappa = 0$. In Figs. 3.8 and 3.9 we show $M_s(k)$ and $B_s(k)$, respectively. As expected, we find that $M_s(k)$ goes over to $m_s^0 = 0.130$ GeV when $k$ is large.

## 3.4 Density Dependence

As stated earlier, the behavior of the NJL model for finite values of the baryon density is an extensively explored topic [12, 77, 78], with particular recent emphasis on color superconductivity [32, 35, 65, 66, 33, 67, 68]. In this section we explore the behavior of our model at finite baryon density. (It should be noted that the nature of the phase transition describing chiral symmetry restoration at finite density is quite model dependent. For example, the inclusion of current quark masses can change a

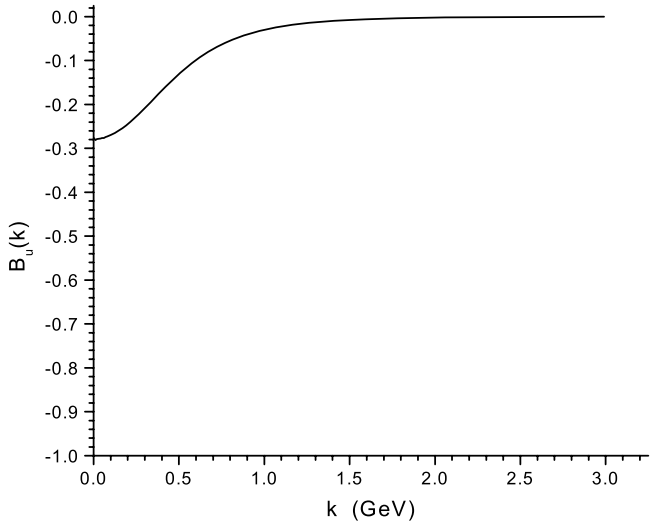


Figure 3.7: Values of $B_u(k)$ are shown. (See caption to Fig. 3.6.)

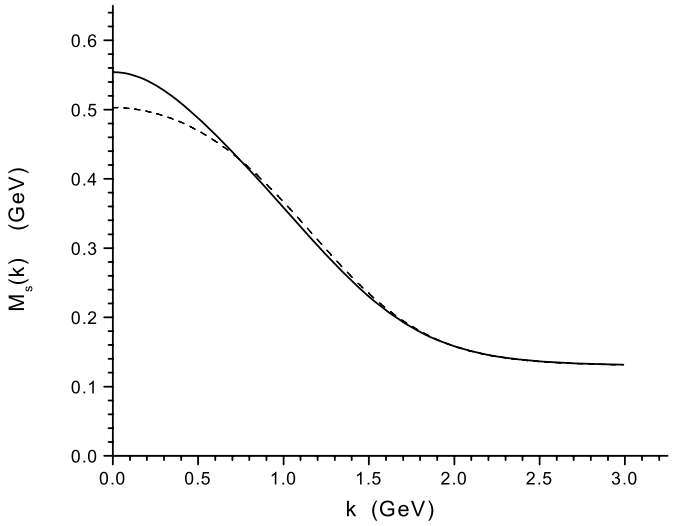


Figure 3.8: Values of $M_s(k)$ are shown. (See caption to Fig. 3.6.)

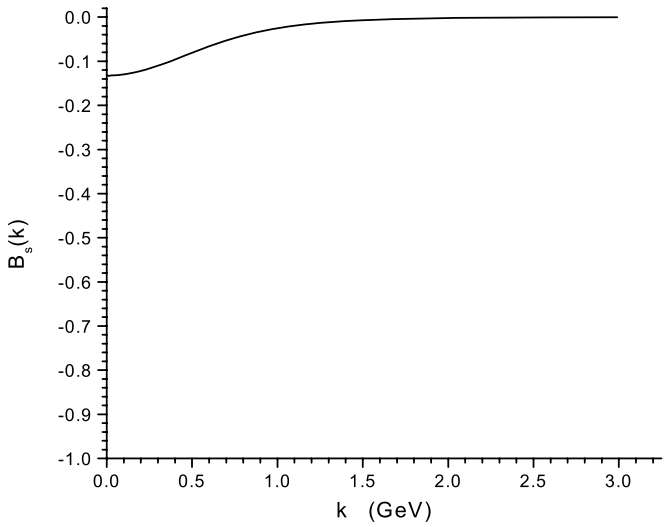


Figure 3.9: Values of $B_s(k)$ are shown. (See caption to Fig. 3.6.)

strong first-order transition to a smooth second-order transition [78].)

A comprehensive study of the thermodynamics of the three-flavor NJL model has been reported in Ref. [79]. There it is found that the up, down and strange quark masses are essentially constant up to the density where a first-order phase transition appears. At that point, the up and down quark masses drop from a value of about 380 MeV to about 30 MeV. That behavior differs from the behavior expected at low density. For example, we have the well-known relation Eq. (2.4.10) between the value of the condensate and the baryon density of nuclear matter, where $\sigma_N$ is the pion-nucleon sigma term. This relation is valid to first-order in the density. It may be derived, in the case of nuclear matter, by writing

$$\langle\bar{q}q\rangle_\rho = \langle\bar{q}q\rangle_0 + \langle N|\bar{q}q|N\rangle\rho_B \tag{3.4.1}$$

and making use of the definition of the pion-nucleon sigma term, $\sigma_N$, and the Gell-Mann–Oakes–Renner relation. If we put $\sigma_N = 0.045$ GeV, we have $\langle\bar{q}q\rangle_\rho/\langle\bar{q}q\rangle_0 =$

$1 - 0.273\rho_B$, where $\rho_B$ is in GeV$^3$ units. For nuclear matter $\rho_B =$( 0.109 GeV)$^3$, so we see that the condensate is reduced by about 35%, if we evaluate Eq. (2.4.10) at nuclear matter density. We can check whether the density dependence given by Eq. (2.4.10) is reproduced in our model, since it should not matter whether the scalar density of the background matter is generated by quarks in nucleons or by the presence of free quarks. In the former case, we may write, for the baryon density,

$$\rho_B = 4\int^{k_F} \frac{d^3k}{(2\pi)^3} \tag{3.4.2}$$

where the factor of 4 is arises from the product of the spin and isospin factors. In the case of quarks, we have

$$\rho_B = 4N_c\left(\frac{1}{3}\right)\int^{k_F} \frac{d^3k}{(2\pi)^3} \tag{3.4.3}$$

where, in this case, the factor of 4 again arises from the spin and isospin factor. (Both up and down quarks are present in equal numbers.) The color factor, $N_c = 3$, is cancelled by the baryon number of 1/3 of each quark.

We need to modify the equations for the quark self-energy to take into account the presence of the Fermi seas of up and down quarks whose Fermi momentum is $k_F$. We take one Fermi sea to be composed of on-mass-shell up quarks with constituent mass $M_u(0)$. The following term is then added to the equation for $A_u(k)$.

$$A_u^{(\rho)}(k) = -(2G_S)N_c 2\int^{k_F} \frac{d^3k'}{(2\pi)^3}\,\frac{M_u(0)}{E_u(k)} f^2(k-k') \tag{3.4.4}$$

where $E_u(k) = \left[\vec{k}^2 + M_u^2(0)\right]^{\frac{1}{2}}$. The second factor of 2 in Eq. (3.4.4) reflects the spin degeneracy. We note that $M_u(0)$ is density-dependent and could be written as $M_u(0,\rho)$ in keeping with the labelling of Fig. 3.10, where $M_u(k,\rho)$ is used. Also, if $f(k-k') = 1$, $A_u^{(\rho)}(k)$ would then represent $-2G_S\,\rho_S$, where $\rho_S$ is the scalar density

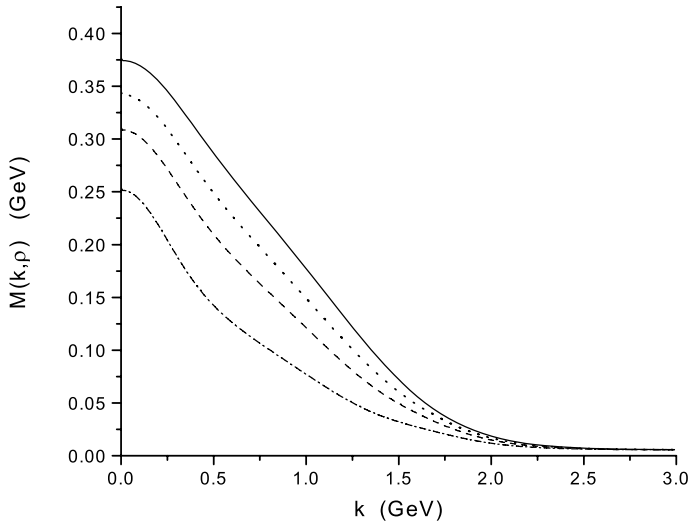


Figure 3.10: The values of $M(k,\rho)$ are shown for $\rho/\rho_{NM} = 0.26$ [dotted line], $\rho/\rho_{NM} = 0.52$ [dashed line], and $\rho/\rho_{NM} = 0.78$ [dash-dot line].

associated with the up-quark Fermi sea.

In Fig. 3.10 we show $M(k,\rho)$ calculated for four values of $\rho$ and in Fig. 3.11 we show $M(0)$ as a function of $k_F^3$. Since the quarks in the Fermi sea are taken to be on-mass-shell, we would, in principle, require $M_u(k,\rho)$ in Minkowski space. However, since $k_F = 0.268$ GeV for the case of nuclear matter, only a very modest extrapolation of the curves shown in Fig. 3.10 is needed for the densities considered in this work. In Fig. 3.12 we show the value of the up quark condensate as a function of $k_F^3$. (Note that $k_F^3 = 19.2 \times 10^{-3}$ GeV$^3$ represents the density of nuclear matter.) It is seen that, for small values of the density, the density dependence of the condensate reproduces what is expected from Eq. (2.4.10). (If we extrapolate the curve using a linear approximation, the condensate is reduced by about 30% at nuclear matter density.)

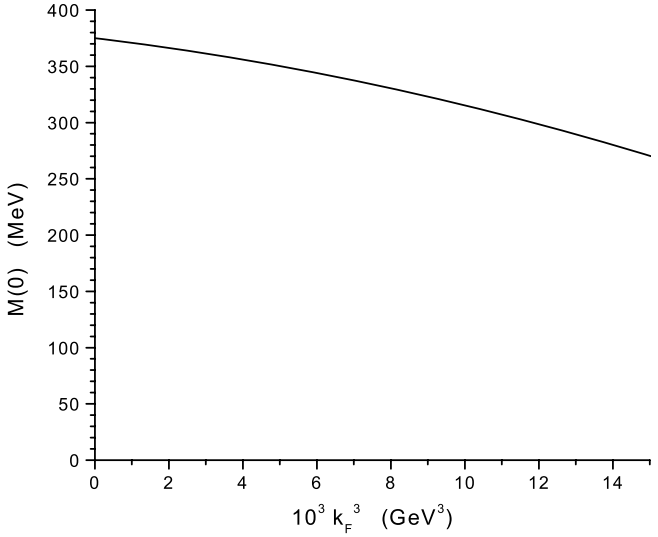


Figure 3.11: Values of $M(0)$ are shown as a function of $k_F^3$. Note that $\rho_B = (2/3\pi^2)k_F^3$.

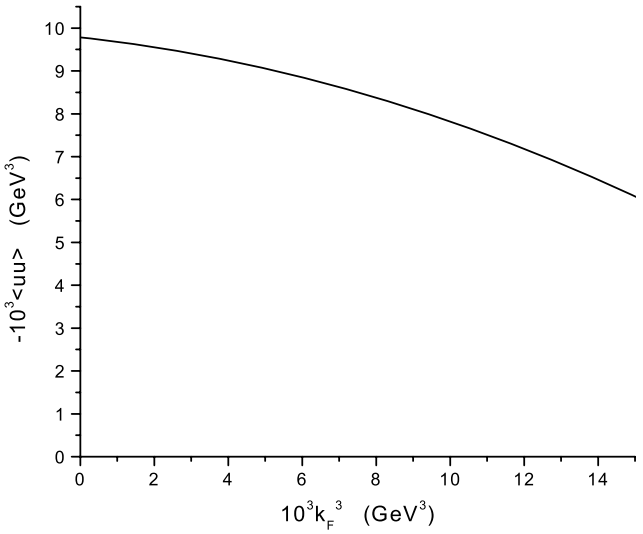


Figure 3.12: The values of the up quark condensate are given as a function of $k_F^3$. Note that $\rho_B = (2/3\pi^2)k_F^3$.

## 3.5 Discussion

We have remarked earlier in this work that the large values of the condensate ratio $\langle\bar{s}s\rangle/\langle\bar{u}u\rangle$ seen in Table 3.3.1 play a role in obtaining a good fit to the mixing angles of the $\eta(947)$ and $\eta\prime(958)$ mesons [16]. To understand this remark we note that the effective singlet-octet coupling constants for pseudoscalar states are [22]

$$G_{00}^{P} = G_S - \frac{2}{3}(\alpha+\beta+\gamma)\frac{G_D}{2}\,, \tag{3.5.1}$$

$$G_{88}^{P} = G_S - \frac{1}{3}(\gamma-2\alpha-2\beta)\frac{G_D}{2}\,, \tag{3.5.2}$$

and

$$G_{08}^{P} = -\frac{\sqrt{2}}{6}(2\gamma-\alpha-\beta)\frac{G_D}{2}\,, \tag{3.5.3}$$

where $\alpha = \langle\bar{u}u\rangle$, $\beta = \langle\bar{d}d\rangle$ and $\gamma = \langle\bar{s}s\rangle$. We take $\alpha = \beta$, so that

$$G_{08}^{P} = -\frac{\sqrt{2}}{3}(\gamma-\alpha)\frac{G_D}{2}\,. \tag{3.5.4}$$

If $\gamma = 1.7\alpha$, the result for $G_{08}^{P}$ is six times larger than when $\gamma = 1.1\alpha$.

In addition to the effects of $G_{08}^{P}$, singlet-octet mixing is induced by the quantity [16]

$$E_{08}(k) = \frac{2\sqrt{2}}{3}[E_u(k) - E_s(k)]\,, \tag{3.5.5}$$

where $E_u(k) = \left[\vec{k}^2 + m_u^2\right]^{\frac{1}{2}}$, etc. It is found that, since $G_{08}^{P}$ and $E_{08}(k)$ tend to cancel in our formalism, the significant singlet-octet mixing generated by $E_{08}(k)$ is reduced by the values of $G_{08}^{P}$ obtained for the larger value of the ratio $\langle\bar{s}s\rangle/\langle\bar{u}u\rangle$, with the result that we reproduce the values of the mixing angles found in other studies that make use of experimental data to obtain values for the mixing angles [16].

In our earlier work, which was carried out in Minkowski space, the values of $m_u = m_d$ and $m_s$ were taken as parameters. Inspection of our figures which exhibit values of $M_u(k)$ and $M_s(k)$ suggests that an extrapolation into Minkowski space may be made if $k^2$ is not too large. The fact that $M_u(0)$ and $M_s(0)$ are close to our phenomenological parameters for $G_D = -266$ GeV$^{-5}$ is encouraging and suggests that some support for our choice of quark mass parameters may be found in our Euclidean-space analysis.

The full consequences of separating the specification of the nonlocality of the quark interaction from the choice of the regulator of the theory should be explored more fully. Although that feature of our model introduces greater flexibility, that comes with the disadvantage of having to introduce other parameters in the model. We have made only limited variation of the form of the nonlocality and the regulator. For further applications it may be of interest to explore a more comprehensive parameter variation. It is also necessary to extend the calculations reported in Figs. 3.10–3.12 to larger values of the density than those considered here. That step will require more complex methods for solving our nonlinear equations for the self-energy than the simple iteration scheme we have used thus far.

Our work may be compared to that of Alkofer, Watson and Weigel [81] who have solved the Schwinger-Dyson equation using a gluon propagator whose low-momentum behavior is enhanced by a Gaussian function. (That modification requires the introduction of two phenomenological parameters [82].) The behavior found for $A(k)$ and $B(k)$ in Euclidean space is similar to that obtained in this work. (See Fig. 1 of Ref. [81].) Those authors also solve the Bethe-Salpeter equation to obtain the properties of various $q\bar{q}$ mesons with generally satisfactory results. It is of interest to note that the Minkowski space solution for $A(k)$ and $B(k)$ is such that the quark can go on-mass-shell. That feature may be related to our work [21, 16, 17, 18, 19, 20] in which we use on-mass-shell quarks with masses $m_u = m_d = 0.364$ GeV and $m_s = 0.565$ GeV (or 0.585 GeV [18]) when solving the Bethe-Salpeter equation in our study of

$q\bar{q}$ mesons.

# Chapter 4

# Finite Temperature

## 4.1 Temperature-dependent NJL Model

We have studied a generalized version of the Nambu–Jona-Lasinio (NJL) model which includes a covariant model of Lorentz-vector confinement [16, 17, 18, 19, 20]. Extensive applications have been made in the study of light mesons, with particularly satisfactory results for the properties of the $\eta(547)$, $\eta'(958)$ and their radial excitations [21]. Since the modifications of the confining potential at finite temperature have recently been obtained in lattice simulations of QCD [14, 25, 26, 27, 28, 29] (see Fig. 2.2), we became interested in introducing that feature in our generalized NJL model, whose Lagrangian is as Eq. (2.1.1) which we have introduced in chapter 2.

There are three important temperature-dependent features of our model. Temperature-dependent constituent quark masses were calculated using the equation [12]

$$m(T) = m^0 + 2G_S(T)N_c\frac{m(T)}{\pi^2}\int_0^\Lambda dp\frac{P^2}{E_p}\tanh(\frac{1}{2}\beta E_p)\,. \tag{4.1.1}$$

Here, $m^0$ is the current quark mass, $G_S(T)$ is a temperature-dependent coupling

constant introduced in our model [11]

$$G_S(T) = G_S \left[1 - 0.17 \left(\frac{T}{T_c}\right)\right] , \tag{4.1.2}$$

$N_c = 3$ is the number of colors, $\beta = 1/T$ and $E_p = [\vec{p}^{\,2} + m^2(T)]^{1/2}$. Further, $\Lambda = 0.631$ GeV is a cutoff such that $|\vec{p}| \leq \Lambda$. Results obtained for the up (or down) and strange quark masses are given in Fig. 4.1. In calculating the constituent mass values we have neglected the confining interaction. That interaction was taken into account in our earlier Euclidean-space calculation of the quark self-energy [13], which also included the effects related to 't Hooft interaction. We found that, to a good approximation, we could neglect the confining and 't Hooft interactions, if we modified the value of the NJL coupling constant, $G_S$, and we adopt that approach when using Eq. (4.1.1).

In addition to the temperature dependence of the coupling constant and constituent mass values, we also introduced a temperature-dependent confining potential, whose form was motivated by recent lattice simulations of QCD in which the temperature dependence of the confining interaction was calculated with dynamical quarks [14]. (See Fig. 2.2.) In order to include such effects, we modified the form of our confining interaction, $V^C(r) = \kappa r \exp[-\mu r]$, by replacing $\mu$ by

$$\mu(T) = \frac{\mu_0}{\left[1 - 0.7 \left(\frac{T}{T_c}\right)^2\right]} , \tag{4.1.3}$$

with $\mu_0 = 0.010$ GeV. The maximum value of $V^C(r, T)$ is then

$$V^C_{max}(T) = \frac{\kappa}{\mu(T) e} , \tag{4.1.4}$$

$$= \frac{\kappa \left[1 - 0.7 (T/T_c)^2\right]}{\mu_0 e} , \tag{4.1.5}$$

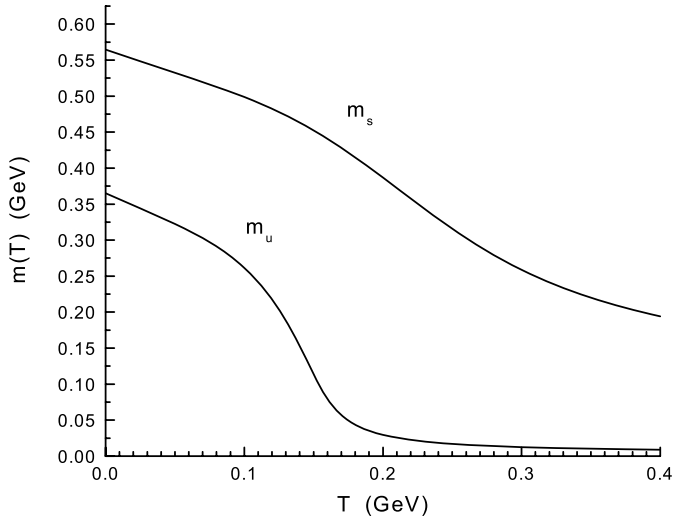


Figure 4.1: Temperature-dependent constituent mass values, $m_u(T)$ and $m_s(T)$, calculated in a mean-field approximation [12] are shown. [See Eq. (4.1.1)]. Here $m_u^0 = 0.0055$ GeV, $m_s^0 = 0.120$ GeV, and $G(T) = 5.691[1 - 0.17(T/T_c)]$ GeV$^2$, if we use Klevansky's notation [12]. (The value of $G$ used in our work is defined such that it is twice the value of $G$ used in Ref. [12].)

with $r_{max} = 1/\mu(T)$. To better represent the qualitative features of the results shown in Fig. 2.2, we can use $V^C(r,T) = \kappa r \exp[-\mu(T)r]$ for $r \leq r_{max}$ and $V^C(r,T) = V^C_{max}(T)$ for $r > r_{max}$. We also note that we use Lorentz-vector confinement and carry out all our calculations in momentum-space. The value of $\kappa$ used in our work is 0.055 GeV$^2$.

## 4.2 A Brief Justification

Here we provide a justification for our noval model of temperature-dependent coupling constant. We make reference to Fig. 1.3 of Ref. [39]. That figure shows the behavior of the ratio $\epsilon/T^4$ and $3P/T^4$ for the pure gauge sector of QCD. Here $\epsilon$ is the energy density and $P$ is the pressure. Ideal gas behavior implies $\epsilon = 3P$. The values of $\epsilon/T^4$ and $3P/T^4$ are compared to the value $\epsilon_{SB}/T^4 = 8\pi^2/15$ for an ideal gluon gas. It may be seen from the figure that at $T = 3T_c$ there are still significant differences from the ideal gluon gas result. Deviations from ideal gas behavior become progressively smaller with increasing $T/T_c$ and could be considered to be relatively unimportant for $T/T_c > 5$.

To provide evidence for temperature-dependent coupling constants, we discuss the calculation of hadronic current correlators in the deconfined phase. The basic polarization functions that are calculated in the NJL model are shown in Fig. 4.2. We will consider calculations of such functions in the frame where $\vec{P} = 0$. In our earlier work, calculations were made after a confinement vertex was included. That vertex is represented by the filled triangular region in Fig. 4.2. However, we here consider calculations for $T \geq 1.2T_c$ where confinement may be neglected. We will, however, use the temperature-dependent mass values shown in Fig. 4.1.

The procedure we adopt is based upon the real-time finite-temperature formalism, in which the imaginary part of the polarization function may be calculated. Then, the

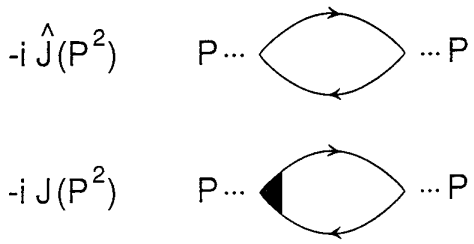


Figure 4.2: The upper figure represents the basic polarization diagram of the NJL model in which the lines represent a constituent quark and a constituent antiquark. The lower figure shows a confinement vertex [filled triangular region] used in our earlier work. For the present work we neglect confinement for $T \geq 1.2T_c$, with $T_c = 170$ MeV.

real part of the function is obtained using a dispersion relation. The result we need for this work has been already given in the work of Kobes and Semenoff [40]. (In Ref. [40] the quark momentum is $k$ and the antiquark momentum is $k - P$. We will adopt that notation in this dissertation for ease of reference to the results presented in Ref. [40].) With reference to Eq. (5.4) of Ref. [40], we write the imaginary part of the scalar polarization function as

$$\begin{aligned} \mathrm{Im}\, J^S(P^2,T) = \frac{1}{2}(2N_c)\beta_S\,\epsilon(p^0)\int\frac{d^3k}{(2\pi)^3}\,e^{-\vec{k}^{\,2}/\alpha^2}\left(\frac{2\pi}{2E_1(k)2E_2(k)}\right) \\ \{(1-n_1(k)-n_2(k))\delta(p^0-E_1(k)-E_2(k)) \\ -(n_1(k)-n_2(k))\delta(p^0+E_1(k)-E_2(k)) \\ -(n_2(k)-n_1(k))\delta(p^0-E_1(k)+E_2(k)) \\ -(1-n_1(k)-n_2(k))\delta(p^0+E_1(k)+E_2(k))\}\,. \end{aligned} \tag{4.2.1}$$

Here, $E_1(k) = [\vec{k}^{\,2} + m_1^2(T)]^{1/2}$. Relative to Eq. (5.4) of Ref. [40], we have changed the sign, removed a factor of $g^2$ and have included a statistical factor of $2N_c$, where the factor of 2 arises from the flavor trace. In addition, we have included a Gaussian regulator, $\exp[-\vec{k}^{\,2}/\alpha^2]$, with $\alpha = 0.605$ GeV, which is the same as that used in most of our applications of the NJL model in the calculation of meson properties. We also

note that

$$n_1(k) = \frac{1}{e^{\beta E_1(k)} + 1}\,, \tag{4.2.2}$$

and

$$n_2(k) = \frac{1}{e^{\beta E_2(k)} + 1}\,. \tag{4.2.3}$$

For the calculation of the imaginary part of the polarization function, we may put $k^2 = m_1^2(T)$ and $(k-p)^2 = m_2^2(T)$, since in that calculation the quark and antiquark are on-mass-shell. We will first remark upon the calculation of scalar correlators [40]. In that case, the factor $\beta_S$ in Eq. (4.2.1) arises from a trace involving Dirac matrices, such that

$$\begin{aligned} \beta_S &= -\mathrm{Tr}[(\not{k} + m_1)(\not{k} - \not{P} + m_2)] & (4.2.4)\\ &= 2P^2 - 2(m_1 + m_2)^2\,, & (4.2.5) \end{aligned}$$

where $m_1$ and $m_2$ depend upon temperature. In the frame where $\vec{P} = 0$, and in the case $m_1 = m_2$, we have $\beta_S = 2P_0^2(1 - 4m^2/P_0^2)$. For the scalar case, with $m_1 = m_2$, we find

$$\mathrm{Im}\, J^S(P^2, T) = \frac{N_c P_0^2}{4\pi}\left(1 - \frac{4m^2}{P_0^2}\right)^{3/2} e^{-\vec{k}^{\,2}/\alpha^2}[1 - 2n_1(k)]\,, \tag{4.2.6}$$

where

$$\vec{k}^{\,2} = \frac{P_0^2}{4} - m^2(T)\,. \tag{4.2.7}$$

We may evaluate Eq. (2.2.4) for $m(T) = m_u(T) = m_d(T)$ and define $\mathrm{Im}\, J_u^S(P^2, T)$. Then we put $m(T) = m_s(T)$, we define $\mathrm{Im}\, J_s^S(P^2, T)$. These two functions are needed

for a calculation of the scalar-isoscalar correlator. The real parts of the functions $J_u^S(P^2,T)$ and $J_s^S(P^2,T)$ may be obtained using a dispersion relation, as noted earlier.

For pseudoscalar mesons, we replace $\beta_S$ by

$$\begin{aligned}\beta_P &= -\mathrm{Tr}[i\gamma_5(\not{k}+m_1)i\gamma_5(\not{k}-\not{P}+m_2)] &(4.2.8)\\ &= 2P^2-2(m_1-m_2)^2\,, &(4.2.9)\end{aligned}$$

which for $m_1=m_2$ is $\beta_P = 2P_0^2$ in the frame where $\vec{P}=0$. We find, for the $\pi$ mesons,

$$\mathrm{Im}\,J^P(P^2,T) = \frac{N_c P_0^2}{4\pi}\left(1-\frac{4m(T)^2}{P_0^2}\right)^{1/2} e^{-\vec{k}^{\,2}/\alpha^2}[1-2n_1(k)]\,, \qquad (4.2.10)$$

where $\vec{k}^{\,2} = P_0^2/4 - m_u^2(T)$, as above. Thus, we see that, relative to the scalar case, the phase space factor has an exponent of $1/2$ corresponding to a $s$-wave amplitude, rather than the $p$-wave amplitude of scalar mesons. For the scalars, the exponent of the phase-space factor is $3/2$, as seen in Eq. (4.2.6).

For a study of vector mesons we consider

$$\beta_{\mu\nu}^V = \mathrm{Tr}[\gamma_\mu(\not{k}+m_1)\gamma_\nu(\not{k}-\not{P}+m_2)]\,, \qquad (4.2.11)$$

and calculate

$$g^{\mu\nu}\beta_{\mu\nu}^V = 4[P^2-m_1^2-m_2^2+4m_1m_2]\,, \qquad (4.2.12)$$

which, in the equal-mass case, is equal to $4P_0^2+8m^2(T)$, when $m_1=m_2$ and $\vec{P}=0$. Note that for the elevated temperatures considered in this work $m_u(T)=m_d(T)$ is quite small, so that $4P_0^2+8m_u^2(T)$ can be approximated by $4P_0^2$ when we consider the $\rho$ meson.

We now consider the calculation of temperature-dependent hadronic current correla-

tion functions. The general form of the correlator is a transform of a time-ordered product of currents,

$$C(P^2,T) = i\int d^4x e^{\,ip\cdot x} << \mathrm{T}(j(x)j(0) >> , \tag{4.2.13}$$

where the double bracket is a reminder that we are considering the finite temperature case.

For the study of pseudoscalar states, we may consider currents of the form $j_{P,i}(x) = \bar{q}(x)i\gamma_5\lambda^i q(x)$, where, in the case of the $\pi$ mesons, $i = 1, 2$, and 3. For the study of pseudoscalar-isoscalar mesons, we again introduce $j_{P,i}(x) = \bar{q}(x)\lambda^i q(x)$, but here $i = 0$ for the flavor-singlet current and $i = 8$ for the flavor-octet current.

In the case of the $\pi$ mesons, the correlator may be expressed in terms of the basic vacuum polarization function of the NJL model, $J_P(P^2,T)$. Thus,

$$C_\pi(P^2,T) = J_P(P^2,T)\frac{1}{1 - G_\pi(T)J_P(P^2,T)} , \tag{4.2.14}$$

where $G_\pi(T)$ is the coupling constant appropriate for our study of the $\pi$ mesons. We have found $G_\pi(0) = 13.49$ GeV$^{-2}$ by fitting the pion mass in a calculation made at $T = 0$, with $m_u = m_d = 0.364$ GeV.

The calculation of the correlator for pseudoscalar-isoscalar states is more complex, since there are both flavor-singlet and flavor-octet states to consider. We may define polarization functions for $u$, $d$ and $s$ quarks: $J_u(P^2,T)$, $J_d(P^2,T)$ and $J_s(P^2,T)$. In terms of these polarization functions we may then define

$$J_{00}(P^2,T) = \frac{2}{3}[J_u(P^2,T) + J_d(P^2,T) + J_s(P^2,T)] , \tag{4.2.15}$$

$$J_{08}(P^2,T) = \frac{\sqrt{2}}{3}[J_u(P^2,T) + J_d(P^2,T) - 2J_s(P^2,T)] , \tag{4.2.16}$$

and

$$J_{88}(P^2,T) = \frac{1}{3}[J_u(P^2,T) + J_d(P^2,T) + 4J_s(P^2,T)]\,. \tag{4.2.17}$$

We also introduce the matrices

$$J(P^2,T) = \begin{bmatrix} J_{00}(P^2,T) & J_{08}(P^2,T) \\ J_{80}(P^2,T) & J_{88}(P^2,T) \end{bmatrix}, \tag{4.2.18}$$

$$G(T) = \begin{bmatrix} G_{00}(T) & G_{08}(T) \\ G_{80}(T) & G_{88}(T) \end{bmatrix}, \tag{4.2.19}$$

and

$$C(P^2,T) = \begin{bmatrix} C_{00}(P^2,T) & C_{08}(P^2,T) \\ C_{80}(P^2,T) & C_{88}(P^2,T) \end{bmatrix}. \tag{4.2.20}$$

We then write the matrix relation

$$C(P^2,T) = J(P^2,T)[1 - G(T)J(P^2,T)]^{-1}\,. \tag{4.2.21}$$

The use of our energy-dependent coupling constants is meant to be consistent with the approach to asymptotic freedom at high temperature. In order to understand this feature in our model, we can calculate the correlator with *constant* values of $G_{00}$, $G_{88}$ and $G_{08}$ and also with $G_{00}(T) = G_{00}[1 - 0.17\,T/T_c]$, etc. (In this work we use $G_{00} = 8.09$ GeV$^{-2}$, $G_{88} = 13.02$ GeV$^{-2}$ and $G_{08} = -0.4953$ GeV$^{-2}$.)

We now consider the values of $\mathrm{Im}\,C_{88}(P^2)$ for $T/T_c = 4.0$. In Fig. 4.3 we show the values of $\mathrm{Im}\,C_{88}(P^2)$ calculated in our model with temperature-dependent coupling parameters as a dashed line. The dotted line shows the values of the correlator for

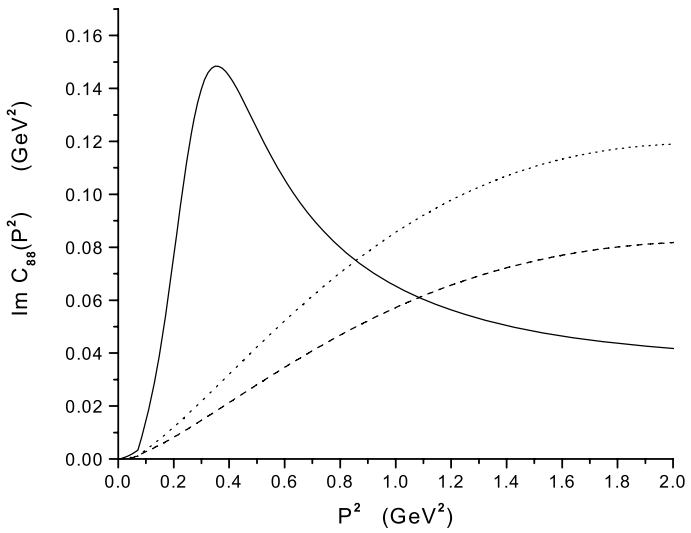


Figure 4.3: The imaginary part of the correlator $C_{88}(P^2)$ is shown for $T/T_c = 4.0$. The dashed line is the result for the temperature-dependent coupling parameters of our model, while the solid line represents the results for coupling parameters kept at their $T = 0$ values. The dotted line shows the values of the correlator when the coupling parameters are set equal to zero.

$G_{00} = G_{88} = G_{08} = 0$, while the solid line shows the values when the coupling parameters are kept at their values at $T = 0$. We see that we have resonant behavior in the case the parameters are temperature independent.

In Fig. 4.4 we show similar results for $T/T_c = 5.88$. Here the temperature-dependent coupling constants are equal to zero, so that the lines corresponding to the dashed and dotted lines of Fig. 4.3 coincide. The solid line again shows resonant behavior at a value of $T/T_c$ where we expect only weak interactions associated with asymptotic freedom. We conclude that the model with constant values of the coupling parameters yields unacceptable results, while our model, which has temperature-dependent coupling parameters, behaves as one may expect, when the results of lattice simulations of QCD thermodynamics are taken into account.

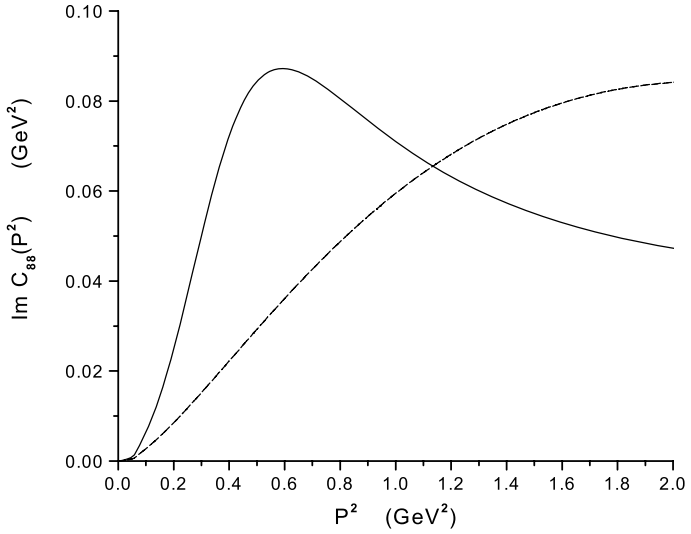


Figure 4.4: The imaginary part of the correlator $C_{88}(P^2)$ is shown for $T/T_c = 5.88$. [See caption to Fig. 4.3.] Here the dashed and dotted lines of Fig. 4.3 coincide.

## 4.3 Chiral Symmetry Restoration

### 4.3.1 Covariant Lorentz-vector Model of Confinement

We have see in Section 2.1 the Lorentz-vector confinement. In order to motivate our treatment of the temperature dependence of the confining interaction for Lorentz-vector confinement, we have presented some results obtained with dynamical quarks (filled symbols) in Fig. 2.2. The fact that the potential becomes (approximately) constant for $r > 1$ fm is ascribed to "string breaking" in the presence of dynamical quarks. (Note that, upon string breaking, the force between the infinitely massive quark and antiquark vanishes.)

For our calculations we have used $\mu = 0.010$ GeV and $\kappa = 0.055$ GeV$^2$ in the past. In order to introduce temperature dependence in our model, we replace $V^C(r) = \kappa r \exp[-\mu r]$ by $V^C(r,T) = \kappa r \exp[-\mu(T) r]$, with $\mu(T)$ defined as 4.1.3. Values of $V^C(r,T)$ for various values of the ratio $T/T_c$ are given in Fig. 4.5. We remark that, while $V^C(r) \to 0$ for large $r$, the bound-state solutions found for $V^C(r)$ are largely unaffected, since barrier penetration effects are extremely small in our model. The maximum value of the potential is $V^C_{max} = \kappa/\mu e$ with the corresponding value of $r_{max} = 1/\mu$. Thus, in the study of the bound states, our model is essentially equivalent to one with $V^C(r) = \kappa r \exp[-\mu r]$ for $r < r_{max}$ and $V^C(r) = V^C_{max}$ for $r > r_{max}$. The same remarks pertain, if we replace $\mu$ by $\mu(T)$ of Eq. (4.1.3). With that replacement, we have Eq. 4.1.5. We note that $V_{max}$ is finite at $T = T_c$ , a result that is in general accord with what is found in lattice calculations of the interquark potential for massive quarks.

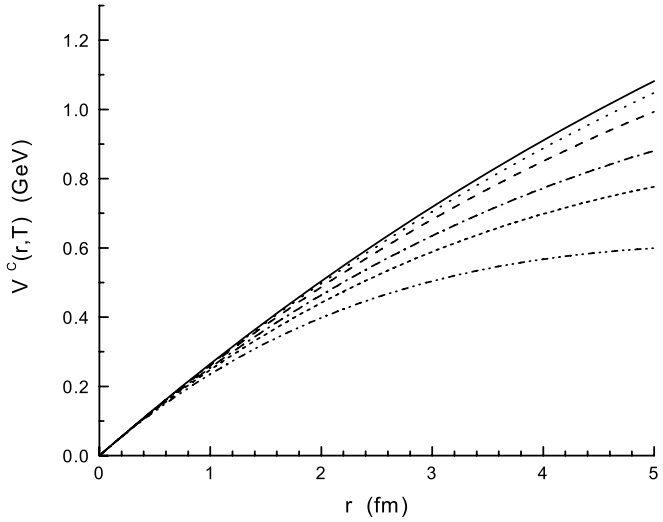


Figure 4.5: The potential $V^C(r,T)$ is shown for $T/T_c = 0$ [solid line], $T/T_c = 0.4$ [dotted line], $T/T_c = 0.6$ [dashed line], $T/T_c = 0.8$ [dash-dot line], $T/T_c = 0.9$ [short dashes], $T/T_c = 1.0$ [dash-dot-dot line]. Here, $V^C(r,T) = \kappa r \exp[-\mu(T)r]$, with $\mu(T) = 0.01\text{GeV}/[1 - 0.7(T/T_c)^2]$.

### 4.3.2 Calculation of Constituent Quark Masses

In an earlier work we carried out a Euclidean-space calculation of the up, down, and strange constituent quark masses taking into account the 't Hooft interaction and our confining interaction [31]. The 't Hooft interaction plays only a minor role in the coupling of the equations for the constituent masses. If we neglect the confining interaction and the 't Hooft interaction in the mean field calculation of the constituent masses, we can compensate for their absence by making a modest change in the value of $G_S$. [See Eq. (2.1.1).] For the calculations of this work we calculate the meson masses using the formalism presented in the Klevansky review [12]. (Note that our value of $G_S$ is twice the value of $G$ used in that review.) The relevant equation is Eq.

(5.38) of Ref. [12]. Here, we put $\mu = 0$ and write

$$m(T) = m^0 + 4GN_C \frac{m(T)}{\pi^2} \int_0^\Lambda dp \frac{p^2}{E_p} \tanh(\frac{1}{2}\beta E_p)\,, \tag{4.3.1}$$

where $\Lambda = 0.631$ GeV is a cutoff for the momentum integral, $\beta = 1/T$ and $E_p = [\vec{p}^2 + m^2(T)]^{1/2}$. In our calculations we replace $G$ by $G_S(T)/2$ and solve the equation (4.1.1) with $G_S(T) = 11.38[1 - 0.17\,T/T_c]$ GeV, $m_u^0 = 0.0055$ GeV and $m_s^0 = 0.120$ GeV. Thus, we see that $G_S(T)$ is reduced from the value $G_S(0)$ by 17% when $T = T_c$. The results obtained in this manner for $m_u(T)$ and $m_s(T)$ are shown in Fig. 4.1. Here, the temperature dependence we have introduced for $G_S(T)$ serves to provide a somewhat more rapid restoration of chiral symmetry than that which is found for a constant value of $G_S$. That feature and the temperature dependence of the confining field leads to the deconfinement of the light mesons considered here at $T = T_c$. (See Section 4.3.4.)

### 4.3.3 Random Phase Approximation Calculations For Meson Masses

The analysis of the diagrams of Fig. 2.1b gives rise to a set of equations for various vertex functions. These equations are of the form of relativistic random-phase-approximation equations. The derivation of these equations for pseudoscalar mesons is given in Ref. [21], where we discuss the equations for pionic, kaonic and eta mesons. The equations for the eta mesons are the most complicated, since we consider singlet-octet mixing as well as pseudoscalar–axial-vector mixing. In that case there are eight vertex functions to consider, $\Gamma^{+-}_{P,0}$, $\Gamma^{+-}_{A,0}$, $\Gamma^{+-}_{P,8}$, $\Gamma^{+-}_{A,8}$, $\Gamma^{-+}_{P,0}$, $\Gamma^{-+}_{A,0}$, $\Gamma^{-+}_{P,8}$, $\Gamma^{-+}_{A,8}$, where $P$ refers to the $\gamma_5$ vertex and $A$ refers to the $\gamma_0\gamma_5$ vertex, which mixes with the $\gamma_5$ vertex. Corresponding to the eight vertex functions one may define eight wave function amplitudes [21].

The simplest example of our RPA calculations is that of the $a_0$ mesons, where there are only two vertex functions $\Gamma_S^{+-}$ and $\Gamma_S^{-+}$ to be calculated [19]. Associated with $\Gamma_S^{+-}$ and $\Gamma_S^{-+}$ are two wave functions $\phi_S^+$ and $\phi_S^-$, which are the large and small components respectively. In vacuum one has coupled equations for these wave functions.

$$2E_u(k)\phi^+(k) + \int dk' \, [H_C(k,k') + H_{NJL}(k,k')]\phi^+(k') + \int dk' \, H_{NJL}(k,k')\phi^-(k') = P^0\phi^+(k)\,, \tag{4.3.2}$$

$$-2E_u(k)\phi^-(k) - \int dk' \, [H_C(k,k') + H_{NJL}(k,k')]\phi^-(k') - \int dk' \, H_{NJL}(k,k')\phi^+(k') = P^0\phi^-(k)\,, \tag{4.3.3}$$

where $E_u(k) = [\vec{k}^{\,2} + m_u^2]^{1/2}$,

$$H_C(k,k') = -\frac{1}{(2\pi)^2}\frac{[2V_0^C(k,k')k^2k'^2 + m_u^2 kk' V_1^C(k,k')]}{E_u(k)E_u(k')}\,, \tag{4.3.4}$$

and

$$H_{NJL} = \frac{8N_c}{(2\pi)^2}\frac{k^2k'^2 G_{a_0} e^{-k^2/2\alpha^2} e^{-k'^2/2\alpha^2}}{E_u(k)E_u(k')}\,. \tag{4.3.5}$$

In Eq. (4.3.5), $G_{a_0}$ is the effective coupling constant for the $a_0$ mesons, which depends upon the values of $G_S$, $G_D$ and the vacuum condensates. These relations for the various coupling constants, $G_{a_0}$, $G_\pi$, $G_K$, $G_{f_0}$, $G_{K_0^*}$, etc. may be found in Ref. [22]. In Eq. (4.3.4) we have introduced

$$V_l^C(k,k') = \int_{-1}^{1} dx \, P_l(x) V^C(\vec{k} - \vec{k}')\,. \tag{4.3.6}$$

Here, $x = \cos\theta$ and $P_l(x)$ is a Legendre function. The terms $\exp[-k^2/2\alpha^2]$ and $\exp[-k'^2/2\alpha^2]$ are regulators with $\alpha = 0.605$ GeV.

In order to solve these equations at finite temperature, we replace $m_u$, $G_{a_0}$ and $\mu_0$ by $m_u(T)$, $G_{a_0}(T)$ and $\mu(T)$. The values of $m(T)$ are given in Fig. 4.1, and we recall that $\mu(T) = \mu_0/[1 - 0.7(T/T_c)^2]$. In the RPA, the solutions of Eqs. (4.3.3) and (4.3.4) come in pairs. For a state of energy $P_i^0$ there is another state with energy $-P_i^0$. Since the RPA Hamiltonian is not Hermitian, it is possible to obtain imaginary values for the energy. That is a signal of the instability of the ground state of the theory and requires that the problem be reformulated to obtain a stable ground state. This problem does not arise in the calculations reported in this work. In particular, the use of the temperature-dependent values of $G_\pi(T)$ avoids the appearance of pion condensation in the formalism.

### 4.3.4 Results of Numerical Calculations of Meson Masses

As noted earlier, the RPA equations for the $a_0$ mesons are given in Ref. [19] and those for the $\pi$, $K$ and $\eta$ mesons are given in Ref. [21]. The equations needed in the study of the $f_0$ mesons are to be found in Ref. [20], while the RPA equations for the study of the $K_0^*$ mesons are to be found in the Appendix of Ref. [18]. In Figs. 4.6-4.10 we present our results for the $\pi$, $K$, $a_0$, $f_0$ and $K_0^*$ mesons. The values of the coupling constants used are given in the figure captions. The reduction of the number of bound states with increasing temperature can be understood by noting that for the $\pi$ and $a_0$ mesons the continuum of the model lies above $V_{max}(T) + 2m_u(T)$, while for the $K$ and $K_0^*$ mesons the continuum lies above $V_{max}(T) + m_u(T) + m_s(T)$. The situation is more complex in the case of the $f_0$ mesons which contain both $s\bar{s}$, $u\bar{u}$ and $d\bar{d}$ components. The bound states lie below the $s\bar{s}$ continuum which begins at $V_{max}(T) + 2m_s(T)$. However, we note that the absence of bound states at $T = T_c$ for all the mesons considered here is due to the reduction of the value of the confining potential and of the constituent quark masses.

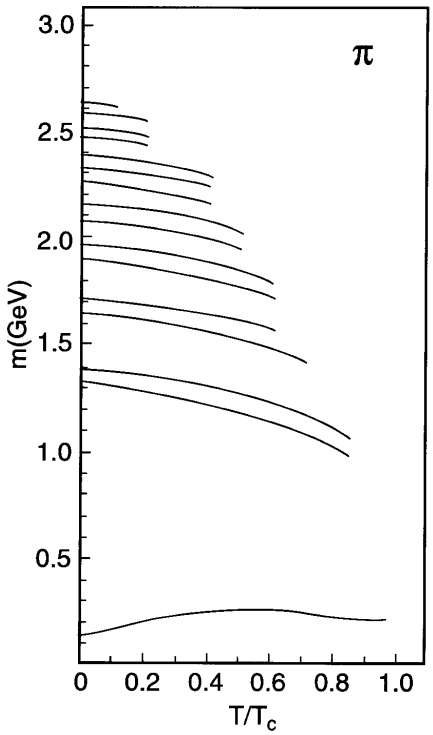


Figure 4.6: The mass values of the pionic states calculated in this work with $G_\pi(T) = 13.49[1 - 0.17\,T/T_c]$ GeV, $G_V(T) = 11.46[1 - 0.17\,T/T_c]$ GeV, and the quark mass values given in Fig. 4.1. The value of the pion mass is 0.223 GeV at $T/T_c = 0.90$, where $m_u(T) = 0.102$ GeV and $m_s(T) = 0.449$ GeV. The pion is bound up to $T/T_c = 0.94$, but is absent beyond that value.

It is of interest to note that the mass values of the $a_0$ and $f_0$ mesons tend toward degeneracy with the pion as $T \to T_c$. However, the mesons disassociate before a greater degeneracy is achieved. That is in contrast to the results obtained in the SU(2) formalism considered by Hatsuda and Kunihiro [22]. Since these authors do not include a model of the confinement-deconfinement transition, they are able to see the approximate degeneracy of the sigma meson and the pion with increasing temperature. It is also worth noting that in the SU(3) formalism the sigma meson is replaced by the $f_0(980)$ as the chiral partner of the pion.

In order to demonstrate the interplay of chiral symmetry restoration and dissolution of our meson states, we have performed calculations in which the quark masses are

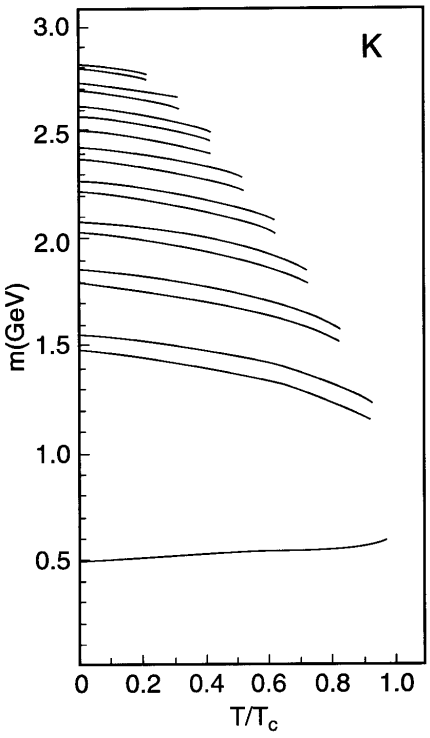


Figure 4.7: Mass values of kaonic states calculated with $G_K(T) = 13.07[1-0.17\,T/T_c]$ GeV, $G_V(T) = 11.46[1 - 0.17\,T/T_c]$ GeV, and the quark mass values given in Fig. 4.1. The value of the kaon mass is 0.598 GeV at $T/T_c = 0.95$, where $m_u(T) = 0.075$ GeV and $m_s(T) = 0.439$ GeV.

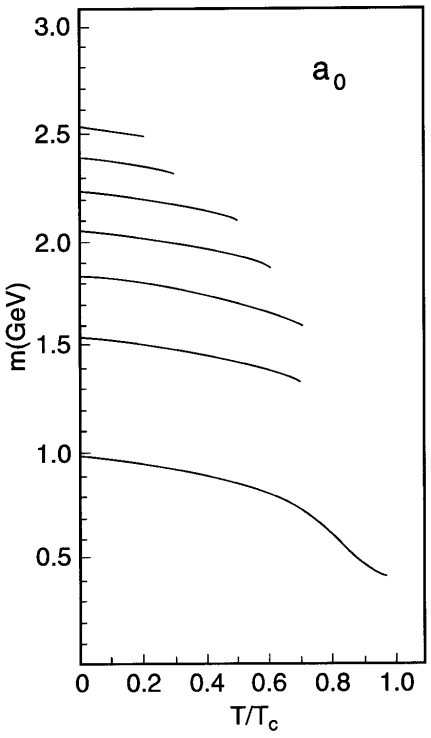


Figure 4.8: Mass values for the $a_0$ mesons calculated with $G_{a_0}(T) = 13.1[1-0.17\,T/T_c]$ GeV, and the quark mass values given in Fig. 4.1. The value of the $a_0$ mass at $T/T_c = 0.95$ is 0.416 GeV.

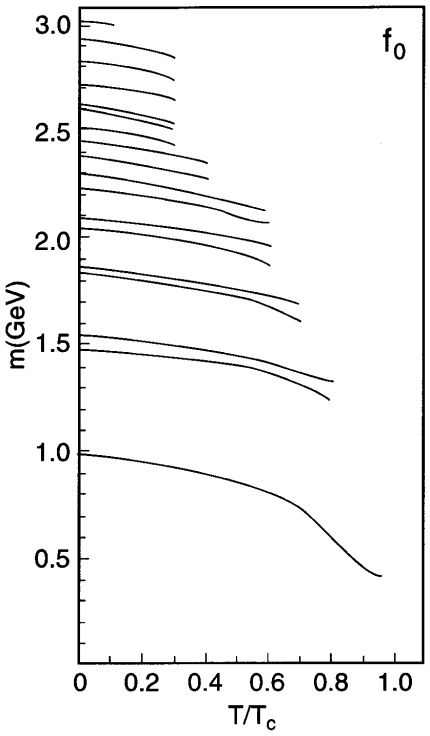


Figure 4.9: Mass values of the $f_0$ mesons calculated with $G_{00}(T) = 14.25[1-0.17\,T/T_c]$ GeV, $G_{88}(T) = 10.65[1 - 0.17\,T/T_c]$ GeV, $G_{08}(T) = 0.495[1 - 0.17\,T/T_c]$ GeV, and $G_{80}(T) = G_{08}(T)$ in a singlet-octet representation. The quark mass values used are shown in Fig. 4.1. The $f_0$ has a mass of 0.400 GeV at $T/T_c = 0.95$.

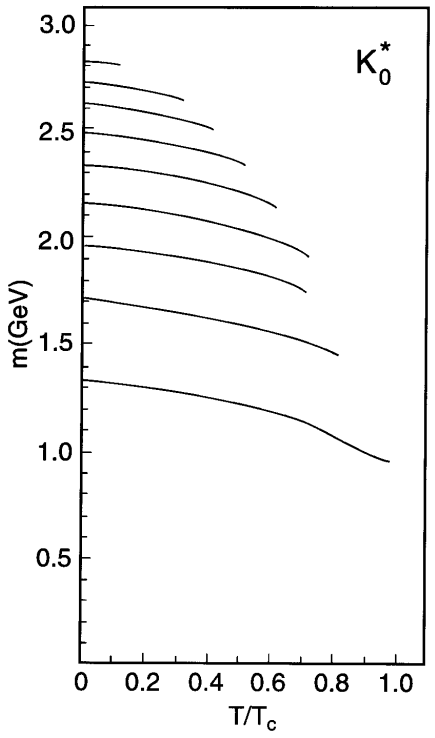


Figure 4.10: Mass values obtained for the $K_0^*$ mesons with $G_{K_0^*}(T) = 10.25[1 - 0.17\,T/T_c]$ GeV, and the quark mass values shown in Fig. 4.1.

unchanged from their value at $T = 0$. For the pion, with $m_u = m_d = 0.364$ GeV and for $T/T_c = 0.95$, we find bound states at 0.530, 1.242 and 1.305 GeV. If we also consider the values of the coupling constants and quark masses fixed at their $T = 0$ values, bound states are found at 0.102, 2.248 and 1.298 GeV when $T/T_c = 0.95$. A similar analysis for the kaon states yields bound states at $T = T_c$ of 0.738, 1.395 and 1.444 GeV, if we put $m_u = 0.364$ GeV and $m_s = 0.565$ GeV. If, in addition, we neglect the temperature dependence of the coupling constants, we have bound kaon states at 0.482, 1.440 and 1.439 GeV.

In the case of the $a_0$ states, putting $m_u = m_d = 0.364$ GeV yields a single state at 0.960 GeV at $T = T_c$, if we neglect the temperature dependence of the coupling constant. If we maintain the temperature dependence of the coupling constant, we find a single state at 1.067 GeV, if the quark masses are kept at their $T = 0$ values.

From this analysis, we see that the reduction of the quark masses with increasing temperature, which represents a partial restoration of chiral symmetry, is an essential feature of our model. In the past, lattice simulations of QCD have indicated that deconfinement and restoration of chiral symmetry take place at the same temperature. Since our Lagrangian contains current quark masses for the up, down and strange quarks, chiral symmetry is not completely restored at the higher temperatures in our model. However, the model does exhibit quite significant reductions of the up and down constituent quark masses for $T \gtrsim T_c$ (See Fig. 4.1), so that deconfinement is here associated with a significant restoration of chiral symmetry.

### 4.3.5 Discussion

In recent years we have seen extensive applications of the NJL model in the study of matter at high density [32, 33, 34, 35, 36]. There is great interest in the diquark condensates and color superconductivity predicted by the NJL model and closely

related models that are based upon instanton dynamics. It is noted by workers in this field that the NJL model does not describe confinement, with the consequence that one can not present a proper description of the hadronic phase that exists at the smaller values of the temperature and density in the QCD phase diagram. Thus, the attitude adopted is that, if one works in the deconfined phase, the NJL model may provide a satisfactory description of the quark interaction. In the present work we have modified the NJL model so that we can describe light mesons and their radial excitations, as well as the confinement-deconfinement transition at $T = T_c$. In an earlier work we studied the confinement-deconfinement transition for finite matter density at $T = 0$ [30]. (A more comprehensive study would include both finite temperature and finite density.) As in the present work, in which we introduced a temperature-dependent coupling constants, we used density-dependent coupling constants in Ref. [30]. If such dependence exists, it would have important consequences for the study of dense matter using the NJL model.

One interesting feature of our results is that both the lowest $a_0$ and $f_0$ states move toward degeneracy with the pion as the temperature is increased. However, the system is deconfined before such degeneracy can be exhibited.

We stress that the restoration of chiral symmetry is intimately connected with the dissolution of our meson states at $T = T_c$. As we saw in the discussion toward the end of Section V, the various mesons studied here still have bound states at $T = T_c$, if only the temperature dependence of the confining field is included in the model.

The behavior of charmonium across the deconfinement transition has recently been studied using lattice simulations of QCD [37]. The authors of Ref. [37] point out that, unlike the case of light mesons, charmonia may exist as bound states even after the deconfinement transition. They state: "Our studies support the sequential pattern for charmonium dissolution obtained from potential model studies, where the broader bound states (the scalar and axial vector channels) dissolve before the pseudoscalar

and vector channels [38]. The pseudoscalar and vector channels are seen to survive as bound states still at $1.25T_c$ and probably dissolve after $1.5T_c$."

## 4.4 Excitations of the Quark-Gluon Plasma

### 4.4.1 A review

Some years ago it was suggested that the quark-gluon plasma was a "confining medium" in the sense that the important excitations should be color singlets [1]. At about the same time, Hatsuda and Kunihiro reported a study of "soft modes" of the quark-gluon plasma [2]. These authors used a SU(2)-flavor version of the Nambu–Jona-Lasinio (NJL) model [3] and considered both finite temperature and density, making use of the Matsubara imaginary-time formalism [4, 5]. (The standard NJL model does not describe confinement, so that the question arises as to the modifications of the results obtained in Ref. [2] if a model of confinement were to be included.) In Ref. [2] it was found that the sigma meson mass, which lies in the continuum of the model, begins to drop in energy with increasing temperature, while the pion energy increases (slowly) with increasing temperature. Eventually, the sigma and pion become degenerate in energy, with the resulting mode increasing in energy with increasing temperature. These results have been confirmed in a very detailed recent study making use of a field-theoretic approach in the calculation of the pseudoscalar and scalar correlation functions at finite temperature [6]. In that work, phenomenological forms for the nonperturbative features of the gluon propagator were introduced and the Schwinger-Dyson and Bethe-Salpeter equations were solved. In many cases, the model of Ref. [6] yields results that are similar to those obtained when using the NJL model. It is of interest to compare the results of our present study with those obtained in Ref. [6] and to note some of the differences between our SU(3)-flavor analysis and the SU(2)-flavor analysis of Ref. [6]. We will return to a discussion of the results obtained in our work and those obtained in Ref. [6] in Section VI.

Recently, we have also seen an extensive effort in the calculation of hadronic correla-

tion functions using lattice simulation of QCD at finite temperature [7, 8, 9]. These calculations make use of the maximum entropy method (MEM) which is reviewed in Ref. [10]. Various peaks are seen in the spectral functions for $T < T_c$ which persist for $T > T_c$. It is only at relatively large values of $T$ that the correlation functions go over to the smooth behavior expected for a weakly interacting system [7, 8, 9].

Although we have introduced a critical temperature for the purposes of our discussion, we should note that the quark masses and vacuum condensates do not go to precisely zero at large temperature, since the current quark mass is always present in the model. Indeed, the presence of a small current mass, $m_u^0 = 0.0055$ GeV, makes for a significant change in the behavior of $m_u(T)$ with increasing temperature. On the other hand, it is useful to introduce a value of $T_c$ of the order of 170 MeV to facilitate the discussion. The significance of that value for the characterization of the constituent mass of the up (or down) quark may be inferred from Fig. 4.1, which exhibits results calculated for $m_u^0 = 0.0055$ GeV and $m_s^0 = 0.120$ GeV.

In section 4.2 we have see the correlator for the $\pi$ mesons. For some purposes it may be useful to also define a $t$ matrix

$$t(P^2, T) = [1 - G(T)J(P^2, T)]^{-1} G(T)\,, \tag{4.4.1}$$

where $t(P^2, T)$ has the structure shown in Eqs. (4.2.19)-(4.2.21). The same resonant structures are seen in both $C(P^2, T)$ and $t(P^2, T)$. For a study of the correlators related to the $\rho$ meson, we introduce conserved vector currents $j_{\mu,i}(x) = \bar{q}(x)\gamma_\mu \lambda_i q(x)$ with $i = 1, 2$ and 3. In this case we define

$$J_\rho^{\mu\nu}(P^2, T) = \left(g^{\,\mu\nu} - \frac{P^{\,\mu} P^{\,\nu}}{P^2}\right) J_\rho(P^2, T) \tag{4.4.2}$$

and

$$C_\rho^{\mu\nu}(P^2,T) = \left(g^{\,\mu\nu} - \frac{P^{\,\mu}P^{\,\nu}}{P^2}\right) C_\rho(P^2,T)\,, \tag{4.4.3}$$

taking into account the fact that the current $j_{\mu,\,i}(x)$ is conserved. We may then use the fact that

$$\begin{aligned} J_\rho(P^2,T) &= \frac{1}{3} g_{\mu\nu} J_\rho^{\mu\nu}(P^2,T) && (4.4.4)\\ &= \frac{2N_c}{3}\left[\frac{P_0^2 + 2m_u^2(T)}{4\pi}\right]\left(1 - \frac{4m_u^2(T)}{P_0^2}\right)^{1/2} e^{-\vec{k}^{\,2}/\alpha^2}[1 - 2n_1(k)] && (4.4.5)\\ &\simeq \frac{2}{3} J_\pi(P^2,T)\,. && (4.4.6) \end{aligned}$$

See Eq. (4.2.7) for the specification of $k = |\vec{k}|$. We then have

$$C_\rho(P^2,T) = J_\rho(P^2,T)\frac{1}{1 - G_V(T) J_\rho(P^2,T)}\,. \tag{4.4.7}$$

### 4.4.2 Results of Numerical Calculations

We begin our presentation with the results we have obtained for scalar-isoscalar excitations. In Fig. 4.11 we show the values of $\mathrm{Im}\, J_{00}(P^2)$ for $T/T_c = 1.2$, 1.6, 2.0, 4.0 and 6.0. Figure 8 exhibits similar results for $\mathrm{Im}\, J_{08}(P^2)$, while Fig. 4.13 exhibits the results obtained for $\mathrm{Im}\, J_{88}(P^2)$. The real parts of these functions are obtained using a dispersion relation. Once we have the real and imaginary parts of these functions, we can calculate the elements of the correlation functions.

In Figs. 4.14-4.16 we show $\mathrm{Im}\, C_{00}(P^2)$, $\mathrm{Im}\, C_{08}(P^2)$ and $\mathrm{Im}\, C_{88}(P^2)$. In the case of $\mathrm{Im}\, C_{00}(P^2)$ we see a sharp peak at 550 MeV. This peak represents the lowest $f_0$ state at that temperature and has as its "parent" the $f_0(980)$ meson. [See Fig. 4.9]

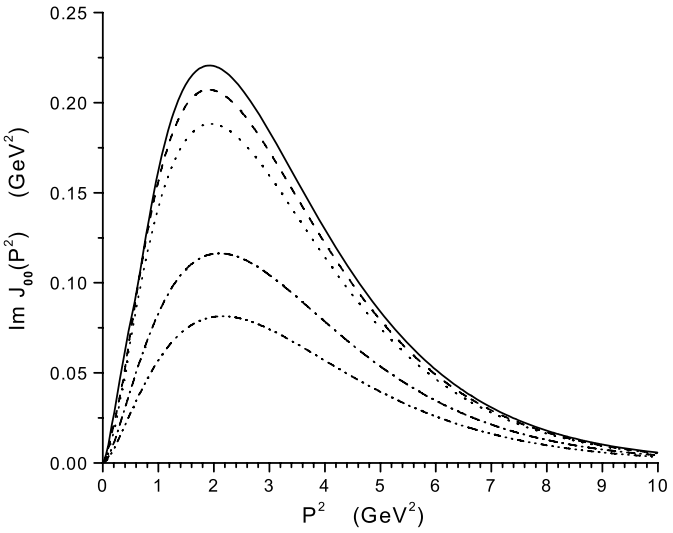


Figure 4.11: Values of $\mathrm{Im}\, J_{00}(P^2)$ are shown. Here, $T/T_c = 1.2$ [solid line], 1.6 [dashed line], 2.0 [dotted line], 4.0 [dashed-dotted line] and 6.0 [dashed-(double) dotted line].

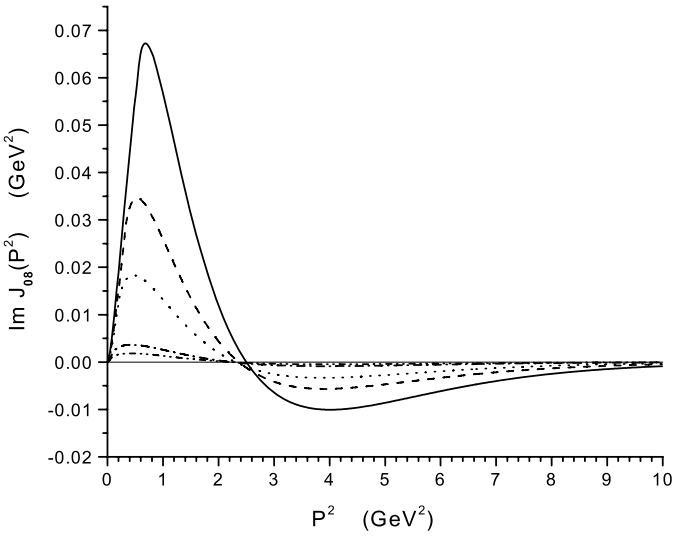


Figure 4.12: Values of $\mathrm{Im}\, J_{08}(P^2)$ are shown. $T/T_c = 1.2$ [solid line], 1.6 [dashed line], 2.0 [dotted line], 4.0 [dashed-dotted line] and 6.0 [dashed-(double) dotted line].

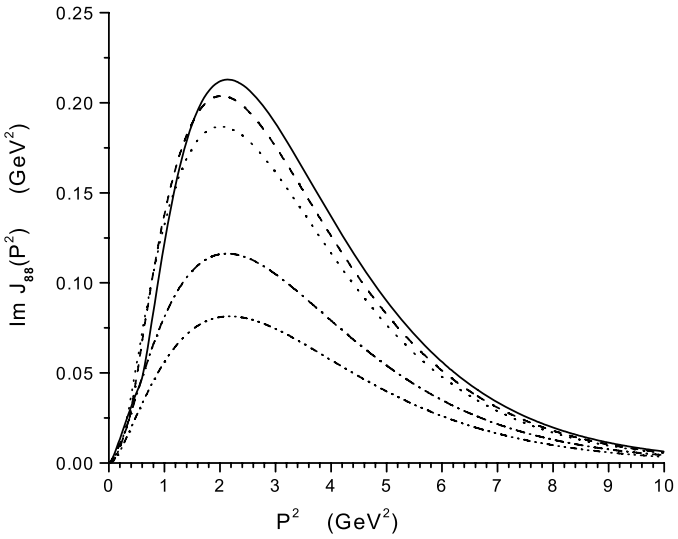


Figure 4.13: Values of $\mathrm{Im}\, J_{88}(P^2)$ are shown. $T/T_c = 1.2$ [solid line], 1.6 [dashed line], 2.0 [dotted line], 4.0 [dashed-dotted line] and 6.0 [dashed-(double) dotted line].

The decay of the state at 550 MeV to two pions will be suppressed since the pionic excitation see in Fig. 4.17 is essentially degenerate with the $f_0$ excitation for $T > T_c$. (Note that in the flavor-SU(3) version of the NJL model the $f_0(980)$ replaces the sigma of the flavor-SU(2) NJL model as the chiral partner of the pion. Thus, it is the state that evolves from the $f_0(980)$ with increasing temperature that becomes degenerate with the pion upon restoration of chiral symmetry.)

The peak seen at about 1100 MeV in Fig. 4.16 is mainly an octet state and is quite prominent in $\mathrm{Im}\, C_{88}(P^2)$. When we calculate the mixing angle for the state at 550 MeV, we find $\theta_1 = 27.7^\circ$ corresponding to the state being about 78% flavor-singlet. A calculation of the mixing angle for the state at 1100 MeV yields $\theta_2 = 17.8^\circ$ which makes the state 95% flavor-octet. These mixing angles appear in the schematic representation

$$|f_0(550)\rangle = \cos\theta_1 \lambda_0 + \sin\theta_1 \lambda_8\,, \tag{4.4.8}$$

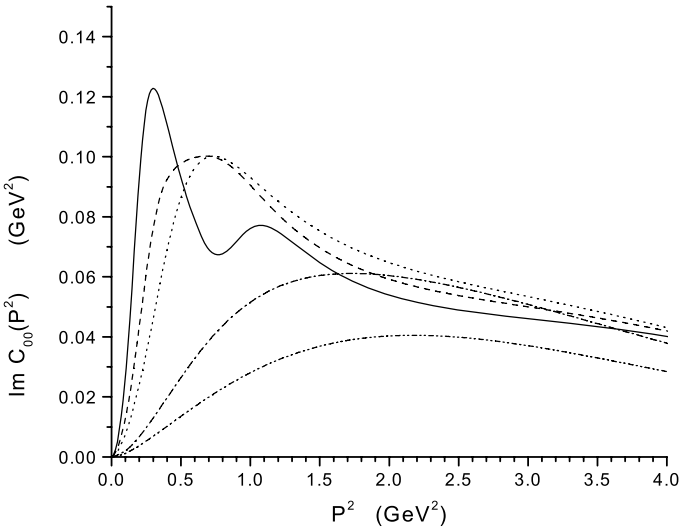


Figure 4.14: Values of $\mathrm{Im}\, C_{00}(P^2)$ are shown. $T/T_c = 1.2$ [solid line], 1.6 [dashed line], 2.0 [dotted line], 4.0 [dashed-dotted line] and 6.0 [dashed-(double) dotted line].

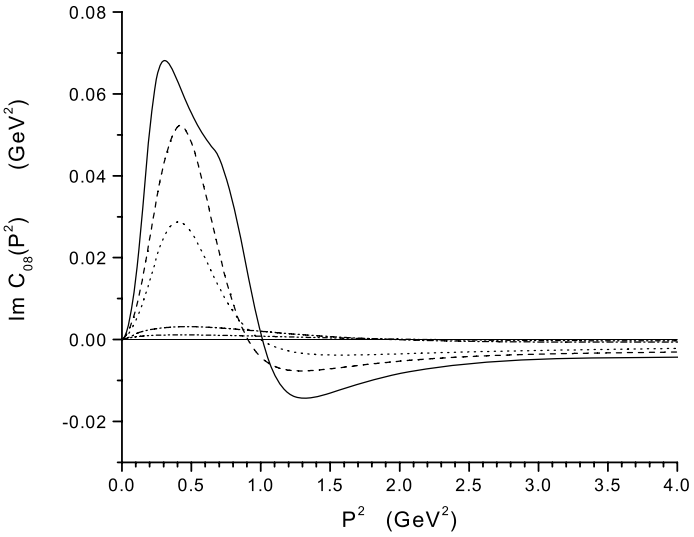


Figure 4.15: Values of $\mathrm{Im}\, C_{08}(P^2)$ are shown. $T/T_c = 1.2$ [solid line], 1.6 [dashed line], 2.0 [dotted line], 4.0 [dashed-dotted line] and 6.0 [dashed-(double) dotted line].

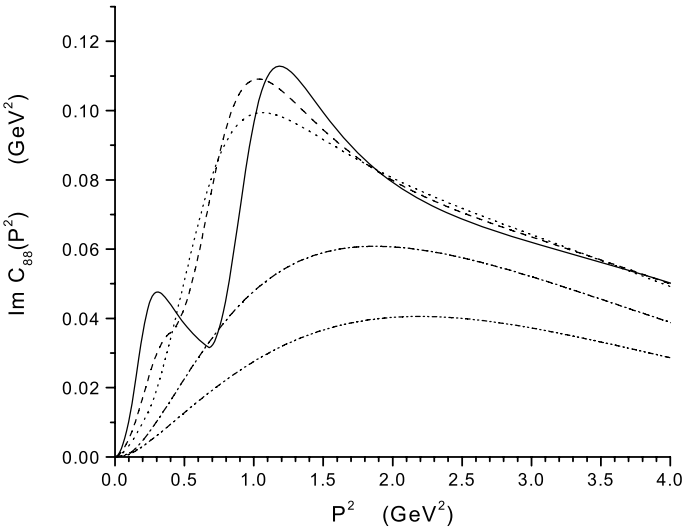


Figure 4.16: Values of $\mathrm{Im}\, C_{88}(P^2)$ are shown. $T/T_c = 1.2$ [solid line], 1.6 [dashed line], 2.0 [dotted line], 4.0 [dashed-dotted line] and 6.0 [dashed-(double) dotted line].

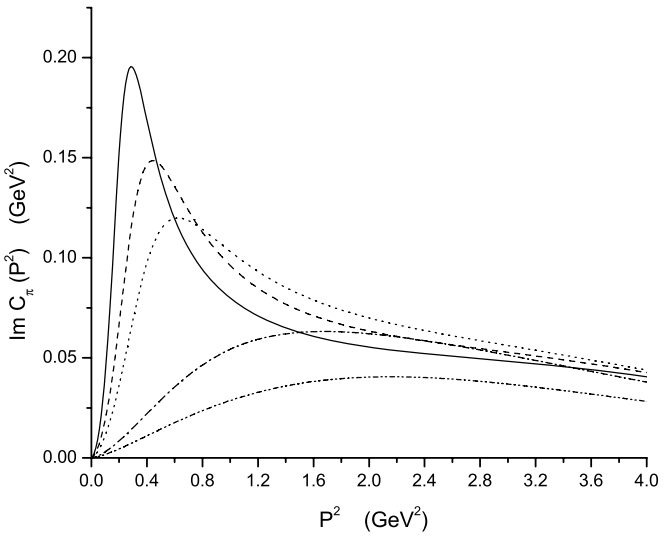


Figure 4.17: Values of $\mathrm{Im}\, C_{\pi}(P^2)$ are shown. $T/T_c = 1.2$ [solid line], 1.6 [dashed line], 2.0 [dotted line], 4.0 [dashed-dotted line] and 6.0 [dashed-(double) dotted line].

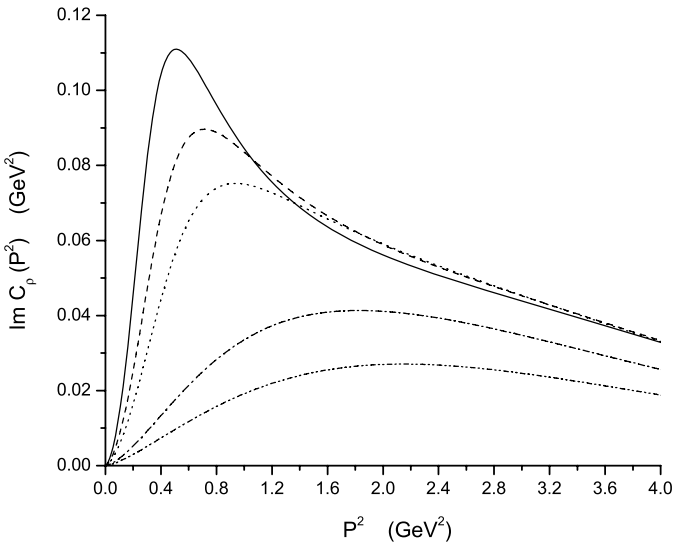


Figure 4.18: Values of $\mathrm{Im}\, C_\rho(P^2)$ are shown. $T/T_c = 1.2$ [solid line], 1.6 [dashed line], 2.0 [dotted line], 4.0 [dashed-dotted line] and 6.0 [dashed-(double) dotted line].

$$|f_0(1100)\rangle = -\sin\theta_2\lambda_0 + \cos\theta_2\lambda_8\,. \tag{4.4.9}$$

It may be seen in Fig. 4.14 that the lowest $f_0$ state moves up in energy and becomes wider when $T = 1.6T_c$, while the state that is at 1100 MeV at $T = 1.2T_c$ moves down in energy at $T = 1.6T_c$. (See Fig. 4.16.) We also see that as the temperature is increased, the states broaden further and the curves eventually become rather featureless.

In Fig. 4.17 we show $\mathrm{Im}\, C_\pi(P^2)$ for the same set of temperatures used to exhibit the properties of the scalar-isoscalar excitations. The curve for $T = 1.2T_c$ [solid line] in Fig. 4.17 has a peak at 547 MeV. With increasing temperature the excitation becomes much broader.

Results for $\mathrm{Im}\, C_\rho(P^2)$ are shown in Fig. 4.18. There is a peak at about 700 MeV that has as a "parent" the $\rho(770)$. Again, we see increased broadening with increasing values of the temperature.

### 4.4.3 Discussion

The formalism we have developed allows for a description of the mass values of various mesons and their radial excitations for the range of temperatures $T < T_c$. Our model also describes the confinement-deconfinement transition at $T = T_c$. When we calculated hadronic current correlators in the real-time formalism we are able to describe the widths of the excitations for $T > T_c$. It is of interest to contrast our results with those obtained using the imaginary-time formalism [4, 6, 22]. The results for the behavior of the sigma and pion masses are similar in the NJL model [4] and the field-theoretic model of Ref. [6]. In Ref. [6] the value of $T_c \simeq 150$ MeV is obtained when the current quark mass is zero. For a finite value of the current quark mass, we may make reference to Fig. 6 of Ref. [6]. There, the sigma mass has a minimum value of approximately 255 MeV at $T = 160$ MeV. At that temperature the pion mass is about 220 MeV. If we consider $T = 1.2T_c = 180$ MeV, we have $m_\pi = m_\sigma = 440$ MeV in Ref. [6]. In our work, we have both $m_{f_0}$ and $m_\pi$ at about 550 MeV when $T = 1.2T_c$. Probably, one of the more significant differences between the imaginary-time formalism used in Refs. [4] and [6] and the real-time formalism used here is the absence of information concerning the widths of the excitations in the imaginary-time formalism. As may be seen in our Figs. 4.11-4.18, the widths of the excitations may play a very important role in understanding the properties of the quark-gluon plasma.

It is believed that measurements of particle ratios obtained in central heavy-ion collisions contain useful information concerning the properties of the quark-gluon plasma. In a recent study, different assumptions concerning the dynamics of the plasma were made and their influence upon predicted particle ratios were obtained [24]. The authors consider calculations based upon both a noninteracting gas model and a chiral SU(3) $\sigma - \omega$ model. They find that "the extracted chemical freeze-out parameters

differ considerably from those obtained in simple noninteracting gas calculations..." when the $\sigma - \omega$ model is used to calculate particle ratios. We believe our model may be useful in performing calculations of the type reported in Ref. [24].

# Chapter 5

# Deconfinement at Finite Matter Density

## 5.1 Pion Condensation

It was suggested many years ago that the ground state of nuclear matter might have an unusual structure due to presence of pionlike excitations [57]. In finite nuclei such effects could imply anomalous behavior in states with $J^\pi = 0^-, 1^+, 2^- \ldots$, etc. However, the nucleon-nucleon interaction is sufficiently repulsive in the relevant channel so that pion condensation does not take place at normal nuclear matter densities. That matter has been discussed in Ref. [58]. A constant $g'$ parametrizes the strength of a nuclear force in the spin-isospin channel that represents short-range correlation effects and exchange effects. (See Eq. (5.11a) of Ref. [58].) The phenomenological value of $g'$, obtained from the study of nuclear excitations, is sufficiently large so that pion condensation does not take place until about three times nuclear matter density. (See Fig. 5.9 of Ref. [58].)

In this chapter we will model the effects that prevent pion condensation by introducing

a density-dependent interaction for the pionic states calculated in the NJL model. We write

$$G_\pi(\rho) = G_\pi(0)[1 - 0.087\rho/\rho_{NM}]\,, \tag{5.1.1}$$

where the second term in Eq. (5.1.1) represents medium effects that reduce the pion self-energy in matter. Here $G_\pi(0)$ is the linear combination of $G_S$ and $G_D$ given on page 269 of Ref. [22],

$$G_\pi = G_S + \frac{G_D}{2}\langle \bar{s}s\rangle\,. \tag{5.1.2}$$

Equation 2.1.1 represents our scheme for parametrizing the nuclear matter effects that prevent pion condensation. In our calculations of pionlike excitations we put $G_\pi(0) = 13.49$ GeV$^{-2}$, and used a constant values of $G_V = 11.46$ GeV$^{-2}$. We may check that our choice of $G_\pi(0)$ is reasonable by using Eq. (5.1.2) with $G_S = 11.84$ GeV$^{-2}$ and $-180$ GeV$^{-5} \leq G_D \leq 240$ GeV$^{-5}$. These values of $G_S$ and $G_D$ were obtained in our extensive study of the eta mesons [21]. Thus, if we take $\langle \bar{s}s\rangle = -(0.258\,\text{GeV})^3$ and $G_D = -190$ GeV$^{-5}$, we find $G_\pi(0) = 13.47$ GeV$^{-2}$. This analysis suggests that, once we fix our parameters in the study of the eta mesons, we can then infer the parameters needed for our study of the pion in vacuum.

For this work, in our study of the kaon, we use $G_K(0) = 13.07$ GeV$^{-2}$ and $G_V = 11.46$ GeV$^{-2}$. Note that [22]

$$G_K(0) = G_S + \frac{G_D}{2}\langle \bar{d}d\rangle_0\,. \tag{5.1.3}$$

If we take $G_S = 11.84$ GeV$^{-2}$, $G_D = -190$ GeV$^{-5}$ and $\langle \bar{u}u\rangle = -(0.240\,\text{GeV})^3$, we find $G_K(0) = 13.15$ GeV$^{-2}$, which is close to the value of $G_K(0) = 13.07$ GeV$^{-2}$ used

in our calculations. In this chapter we have used

$$G_K(\rho) = G_K(0)[1 - 0.087\rho/\rho_{NM}]\,. \tag{5.1.4}$$

In the case of the kaon, about 40% of the assumed density dependence of $G_K(\rho)$ may be attributed to the density dependence of $\langle\bar{u}u\rangle_\rho$ or $\langle\bar{d}d\rangle_\rho$. We may consider the relation

$$G_K(\rho) = G_S(\rho) + \frac{G_D}{2}\langle\bar{d}d\rangle_\rho\,, \tag{5.1.5}$$

and use a somewhat smaller reduction of $G_S(\rho)$ for the kaon than that used for the pion in Eq. (5.1.5), since the reduction of $\langle\bar{u}u\rangle_\rho$ or $\langle\bar{d}d\rangle_\rho$ in matter effectively reduces the interaction strength.

In the absence of $a_0 - f_0$ coupling we have $G_{33}^S = G_{a_0} = G_S - (G_D/2)\langle\bar{s}s\rangle$ [22]. If we again put $G_S = 11.84$ GeV$^{-2}$, $G_D = -190$ GeV$^{-5}$, and $\langle\bar{s}s\rangle = -(0.258\,\text{GeV})^3$, we have $G_{a_0} = 10.21$ GeV$^{-2}$, which places the $a_0(980)$ at 1.13 GeV. However, in the case of the scalar mesons there exist significant contributions to the interaction from processes that describe the scalar meson decay to two-meson channels. An extended discussion of these effects was given in an early work on scalar mesons [59]. In the case of the $f_0(980)$ we presented a discussion of such terms as they affect the energy predicted for the $f_0(980)$ in Ref. [60].

In order to take into account these effects, which are not included in our RPA calculations, we increase the value of the $a_0$ coupling constant to $G_{a_0} = 13.10$ GeV$^{-2}$. That has the effect of moving the $a_0(980)$ mass down to 980 MeV.

We also introduce some density dependence of the interaction to avoid an "$a_0$ condensate", which would otherwise take place at $\rho = 1.75\rho_{NM}$, if we use $m_u(\rho) = m_d(\rho) = 0.0055 + 0.3585(1 - 0.4\rho/\rho_{NM})$. Thus, we use $G_{a_0}(\rho) = G_{a_0}(0)[1 - 0.045\rho/\rho_{NM}]$ when

we allow for the rapid decrease in the value of $m_u(\rho) = m_d(\rho)$ given by the above expression. It is possible that the small reduction of $G_{a_0}(\rho)$ in matter given above has it origin in a somewhat smaller attraction generated at the larger densities by the real part of the polarization operator that describes decay to the two-meson channels [59, 60]. We will provide further details of our treatment of the scalar mesons in Section VIII.

## 5.2 Random Phase Approximation for Mesonic Excitations

In this work we report upon covariant random-phase-approximation (RPA) calculations of meson spectra in vacuum and in dense matter. Before writing the equations of our model, it is worth discussing some properties of RPA calculations made for many-body systems [5, 61]. For example, such calculations have been performed to study excited states of nuclei. In the RPA one usually does not attempt to construct the wave function of the ground state. Rather, one considers amplitudes of particle-hole operators taken between the excited state and the ground state. The dominant amplitude usually involves the creation of a hole in the ground state and the creation of a particle in what are predominantly unoccupied states. Smaller amplitudes are found if one destroys a hole in the ground state and destroys a particle in the predominantly unoccupied states. These smaller amplitudes are only nonzero, if one allows for correlations in the ground state.

Such RPA calculations are particularly important for states that are collective with respect to matrix elements of electromagnetic transition operators, for example. In hadron physics the most "collective state" is the $\pi(138)$. In this case the "large" and "small" components of the wave function, in the sense of the RPA, are comparable

in magnitude and approach equality in magnitude as one approaches the chiral limit, when $m_\pi \to 0$.

Another important feature of RPA calculations is that they may be considered as an investigation of the properties of small oscillations about the ground state. Thus, if one obtains an imaginary energy value for the ground state, one infers that the ground state is unstable. A new ground state must be constructed that will yield real eigenvalues. (Note that imaginary eigenvalues may be obtained, since the RPA Hamiltonian is not Hermitian.)

There is a strong analogy that can be made between the particle-hole RPA calculations described above and the calculation of mesonic excitations. For example, a "hole" in the ground state (the vacuum) is an antiquark, while the particle state is the quark. If we perform relativistic RPA calculations for the pion and its radial excitations, an imaginary energy calculated for the pion is a signal of pion condensation.

Random-phase-approximation equations may be derived using the vertex equation of Fig. 2.1b. The RPA equations for the study of the pion, kaon, and eta mesons were derived in Ref. [21]. In the case of the pion and kaon we include pseudoscalar—axial-vector coupling. The most complex case is that of the eta mesons which, in addition to pseudoscalar—axial-vector coupling, involves singlet-octet coupling in the flavor sector. In Section 4.3.3 we have listed the equations for the simpliest example.

In order to solve those equations in the presence of matter, we replace $m_u$, $G_{a_0}$ and $\mu_0$ by $m_u(\rho)$, $G_{a_0}(\rho)$ and $\mu(\rho)$. (Recall that $\mu(\rho) = \mu_0/[1-(\rho/\rho_C)^2]$.) In our calculation for the $a_0$ states we have taken $m_u(\rho) = m_u^0 + 0.3585\,\mathrm{GeV}\,[1 - 0.4\rho/\rho_{NM}]$ and $G_{a_0}(\rho) = G_{a_0}(0)[1 - 0.045\rho/\rho_{NM}]$, with $m_u^0 = 0.0055$ GeV. As an alternative, the mass values for $m_u(\rho) = m_d(\rho)$ may be taken from Table 2.1.

In our analysis we have neglected the effects of Pauli blocking. Such effects could be calculated for a background of ideal Fermi gases of up and down quarks. However,

in the hadronic phase the quarks are confined to hadrons. We do not know how to calculated Pauli blocking in the confined phase. We suggest that such effects may be small. On the other hand, we have presented an argument in Section II that, with respect to our mean-field analysis, we may use a background of ideal Fermi gases of quarks without making large errors in the hadronic phase. [See Eqs. (2.4.10)-(2.4.11).]

## 5.3 Results of Numerical Calculations

### 5.3.1 Pseudoscalar Mesons

The choice of the parameters in the case of the pion and its radial excitations was discussed in Section V. We use $G_\pi(\rho) = G_\pi(0)[1-0.087\rho/\rho_{NM}]$ and $m_u(\rho) = m_d(\rho) = 0.0055 + 0.3585[1 - 0.4\rho/\rho_{NM}]$ with $G_\pi(0) = 13.49$ GeV$^{-2}$ and $G_V = 11.46$ GeV$^{-2}$. Also, $\mu(\rho) = \mu_0/[1 - (\rho/\rho_C)^2]$ with $\mu_0 = 0.010$ GeV and $\rho_C = 2.25\rho_{NM}$.

The results of our calculations are shown in Fig. 5.1. At $\rho = 0$, the first radial excitation of the pion is found at 1.319 GeV. The large number of states above 1.3 GeV have wave functions that are dominated by either the $\gamma_5$ or $\gamma_0\gamma_5$ vertex. The pion wave function has mainly a $\gamma_5$ vertex structure, with a small admixture of the $\gamma_0\gamma_5$ vertex. (The axial-vector part of the wave function makes a significant contribution in the calculation of the pion decay constant, $f_\pi$.)

It may be seen from the figure, that with the reduction of the value of the constituent mass and of the confining field with increasing values of $\rho/\rho_{NM}$, the radial excitations that appear as bound states become fewer in number. Beyond $\rho/\rho_{NM} = 1.50$ only the nodeless pion wave function is bound and that state is no longer supported beyond $\rho/\rho_{NM} \simeq 1.80$. That represents the beginning of the deconfined phase in the case of the pion for the model introduced in this work.

Somewhat similar behavior is found for the kaon and its radial excitations, as may be

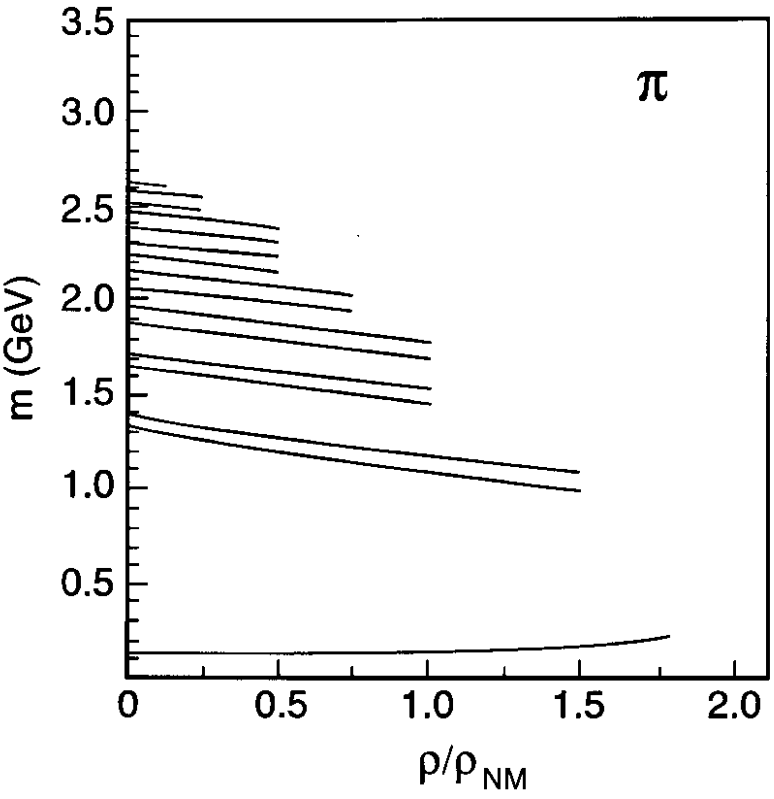


Figure 5.1: The mass values for the pion and its radial excitations are presented as a function of the density of matter. Here, $G_\pi(\rho) = G_\pi(0)[1 - 0.087\rho/\rho_{NM}]$ and $m_u(\rho) = m_d(\rho) = m_u^0 + 0.3585\,\mathrm{GeV}[1 - 0.4\rho/\rho_{NM}]$, with $m_u^0 = 0.0055$ GeV. We use $G_\pi(0) = 13.49\ \mathrm{GeV}^{-2}$, $G_V = 11.46\ \mathrm{GeV}^{-2}$ and $\mu = \mu_0/[1 - (\rho/\rho_C)^2]$, with $\mu_0 = 0.010$ GeV and $\rho_C = 2.25\rho_{NM}$.

seen in Fig. 5.2. Here we have used the mass values given in Table 2.1 and $G_K(\rho) = G_K(0)[1 - 0.087\rho/\rho_{NM}]$ with $G_K(0) = 13.07$ GeV$^{-2}$ and $G_V = 11.46$ GeV$^{-2}$. Again we see only a small increase of the mass of the nodeless state, the pseudo Goldstone boson, as $\rho/\rho_{NM}$ is increased. We again find deconfinement for $\rho/\rho_{NM} > 1.8$. The density dependence of $G_K(\rho)$ is taken to be the same as in the case of the pion. However, in this case, we have noted previously that about 40% of the reduction of $G_K(\rho)$ with increasing density may be ascribed to the density dependence of the up and down quark condensates, $\langle \bar{u}u \rangle_\rho$ and $\langle \bar{d}d \rangle_\rho$. The calculation of the density dependence of the coupling constants in our model is a major undertaking and is beyond the scope of this work.

### 5.3.2 Scalar Mesons

We have recently discussed the properties of the $f_0(980)$, giving particular attention to the role of the polarization diagrams that describe the decay of the $f_0$ mesons to the $\pi\pi$ or $K\bar{K}$ channels [60]. (See Fig. 2 of Ref. [60].) However, when we diagonalize the RPA Hamiltonian we do not take those terms into account. Calculations of such effects are more easily made if we construct a quark-antiquark $T$ matrix. For a single channel example we may write

$$t(p^2) = -\frac{G}{1 - GJ(p^2)}\,, \tag{5.3.1}$$

where $G$ is the appropriate coupling constant for that channel and $J(p^2)$ is the corresponding vacuum polarization operator. In our model $J(p^2)$ is calculated with the confining vertex function that appears in Fig. 2.1a as a crosshatched region. (See Fig. 1 of Ref. [60].) The resulting $J(p^2)$ is a real function, which is singular at the values of $p^2$ for which there is a bound state in the confining field. If we include polarization diagrams that describe coupling to two-meson decay channels, Eq. (5.3.1) is modified

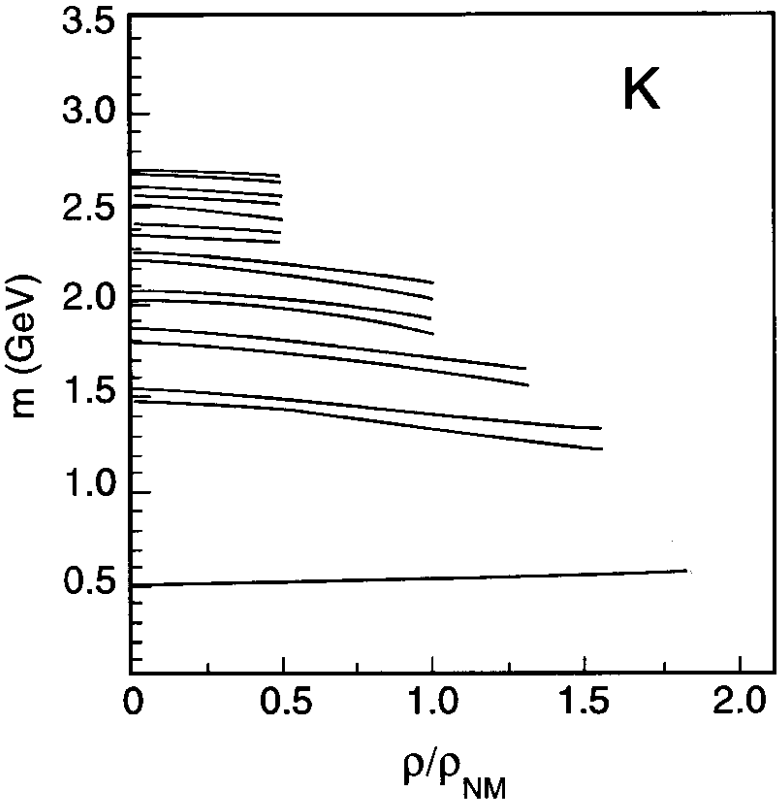


Figure 5.2: Mass values of the $K$ mesons are shown as a function of the density of matter. Here we use $G_K(0) = 13.07$ GeV$^{-2}$, $G_K(\rho) = G_K(0)[1 - 0.087\rho/\rho_{NM}]$, $G_V = 11.46$ GeV$^{-2}$ and $\mu = \mu_0/[1 - (\rho/\rho_C)^2]$, with $\mu_0 = 0.010$ GeV and $\rho_C = 2.25\rho_{NM}$. The mass values given in Table 2.1 are used.

to read

$$t(p^2) = -\frac{G}{1 - G[J(p^2) + \mathrm{Re}K(p^2) + i\mathrm{Im}K(p^2)]}\,. \tag{5.3.2}$$

The calculation of $J(p^2)$ and $K(p^2)$ has been extensively discussed in our earlier work. In the case of the scalar mesons, inclusion of $\mathrm{Re}K(p^2)$ can move the mass of the lowest-energy state down by about 70-100 MeV [59, 60].

In the case of the $a_0(980)$, the use of $G_S$ and $G_D$ determined in our study of the eta mesons places the $a_0(980)$ at 1.13 GeV. In the present work we have increased the coupling constant from $G_{a_0} = 10.21$ GeV$^{-2}$ to $G_{a_0} = 13.10$ GeV$^{-2}$ to move the lowest $a_0$ state down to 980 MeV. That creates a problem of "$a_0$ condensation" which we avoid by taking $G_{a_0}(\rho) = G_{a_0}(0)[1-0.045\rho/\rho_{NM}]$. One may speculate that the effects that increase the effective coupling strength from $G_{a_0} = 10.21$ GeV$^{-2}$ to $G_{a_0} = 13.10$ GeV$^{-2}$ have some density dependence that reduces the induced attraction at the higher densities.

In Fig. 5.3 we show our results for the $a_0$ mesons. There we see deconfinement at about $\rho = 2.0\rho_{NM}$ which is a slightly larger value of the density than that found for the other mesons studied in this work. However, the behavior of the lowest $a_0$ state with increasing density is made somewhat uncertain because of our lack of knowledge of the appropriate form for $G_{a_0}(\rho)$.

For our study of the $f_0$ mesons we work in a singlet-octet representation and use the coupling constants $G^S_{00} = 14.25$ GeV$^{-2}$, $G^S_{88} = 10.65$ GeV$^{-2}$ and $G^S_{08} = G^S_{80} = 0.4953$ GeV$^{-2}$. This choice yields 980 MeV for the mass of the $f_0(980)$. The fact that $G^S_{00} > G^S_{88}$ is a feature of the 't Hooft interaction [12, 23, 22] and leads to the $f_0(980)$ being mainly a singlet state [60]. (For the $\eta(547)$ the behavior of the 't Hooft interaction is such that $G^S_{88} > G^S_{00}$ [22, 60] and, therefore, the $\eta(547)$ is predominantly a flavor octet meson [21].)

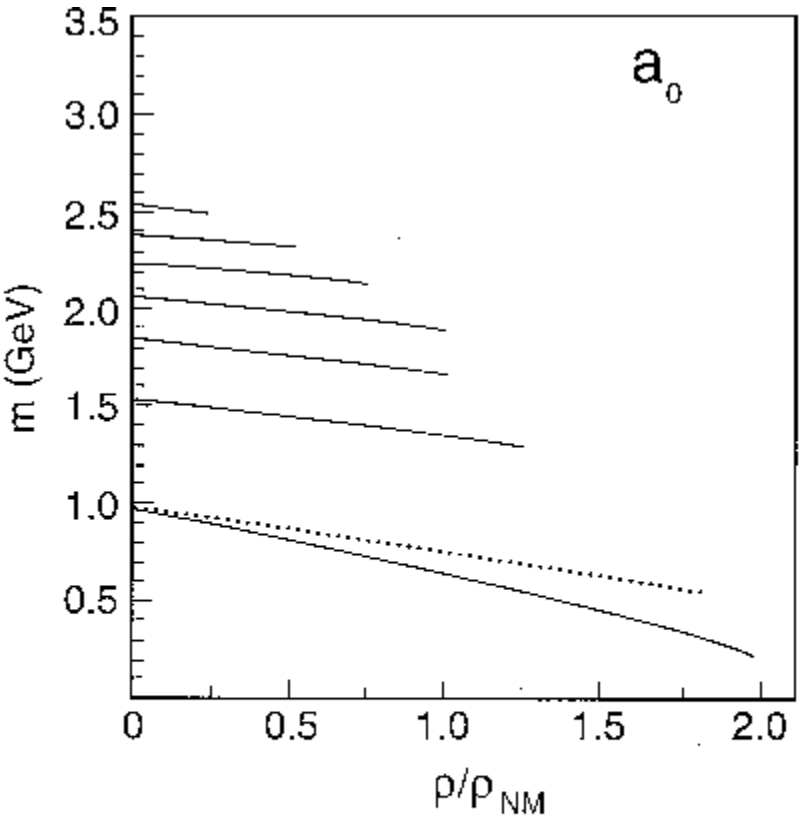


Figure 5.3: Mass values for the $a_0$ mesons are given as a function of the matter density. Here, we have used $G_{a_0}(0) = 13.10\ \mathrm{GeV}^{-2}$ and $G_{a_0}(\rho) = G_{a_0}(0)[1-0.045\rho/\rho_{NM}]$. We have used $m_u = m_u^0 + 0.3585\,\mathrm{GeV}[1-0.4\rho/\rho_{NM}]$ with $m_u^0 = 0.0055$ GeV. The dotted line results, if we put $G_{a_0}(\rho) = G_{a_0}(0)[1-0.087\rho/\rho_{NM}]$ and use the mass values of Table 2.1. The dotted curve is similar to the curve for the $a_0$ mass given in Ref. [19]. The curves representing the masses of the radial excitations are changed very little when we use the second form for $G_{a_0}(\rho)$ given above.

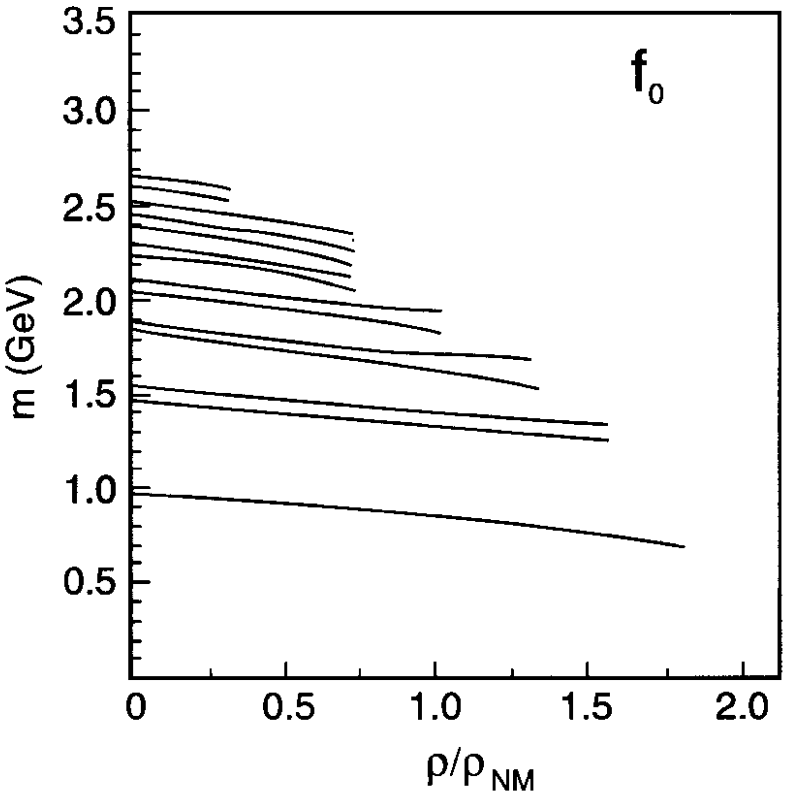


Figure 5.4: The figure shows the mass values of the $f_0$ mesons as a function of density. The mass values for the quarks are taken from Table 2.1. In a singlet-octet representation, we have used the constants $G_{00}^S = 14.25$ GeV$^{-2}$, $G_{08}^S = 0.4953$ GeV$^{-2}$ and $G_{88}^S = 10.65$ GeV$^{-2}$. Deconfinement takes place somewhat above $\rho = 1.8\rho_{NM}$. Here $\mu = \mu_0/[1-(\rho/\rho_C)^2]$ with $\mu_0 = 0.010$ GeV and $\rho_C = 2.25\rho_{NM}$.

In our study of the $f_0$ mesons at finite density we use the mass values of Table 2.1 and do not introduce any density dependence for $G_{00}^S$, $G_{88}^S$ and $G_{08}^S$. The results of our calculation are shown in Fig. 5.4. The mass value only decreases slowly, with a value of 700 MeV for the lowest $f_0$ state at $\rho/\rho_{NM} = 1.82$, where deconfinement sets in. However, if we use the same temperature dependence for $G_{00}^S$, $G_{08}^S$ and $G_{88}^S$ that is used for $G_{a_0}$, the mass values calculated for the lowest $f_0$ and $a_0$ states are quite similar.

In Ref. [60] we provide a discussion of the $T$ matrix for the singlet-octet channels. There the role of $K_{00}^S(p^2)$, $K_{08}^S(p^2)$ and $K_{88}^S(p^2)$ in lowering the energy predicted for

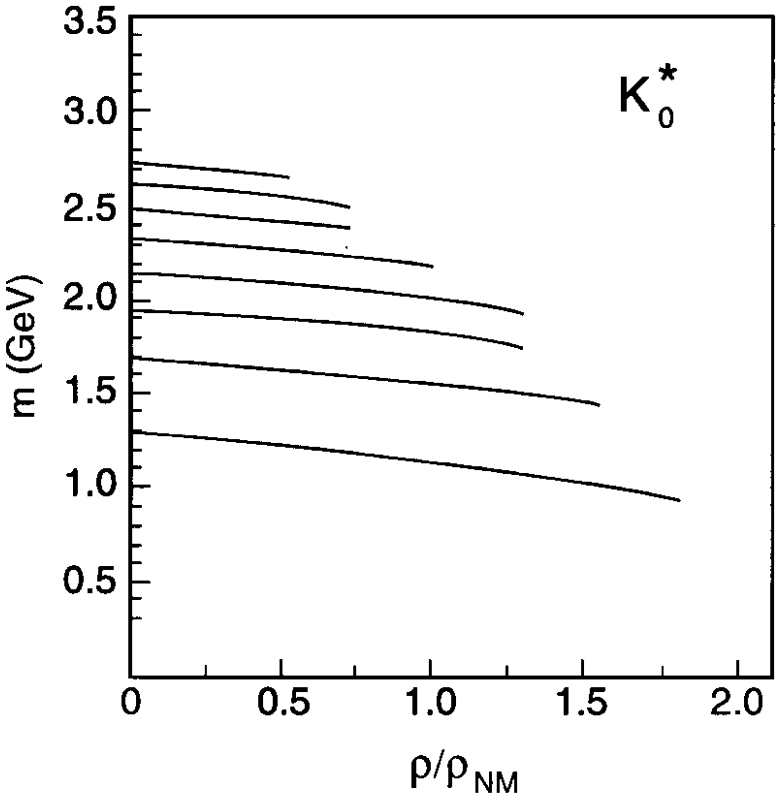


Figure 5.5: The figure shows the mass values obtained for the $K_0^*$ mesons as a function of density. Here we use a constant $G_{K_0^*} = 10.25$ GeV$^{-2}$. Deconfinement takes place somewhat above $\rho = 1.8\rho_{NM}$. The quark mass values were taken from Table 2.1.

the $f_0(980)$ is discussed in some detail.

Our results for the energy levels of the $K_0^*$ mesons are given in Fig. 5.5. In this case we use a constant value for $G_{K_0^*} = 10.25$ GeV$^{-2}$. The results are hardly modified if we allow for a small density dependence of $G_{K_0^*}$. Since the $K_0^*$ mesons contain a strange quark, the density dependence of their energies is not as marked as that of the $a_0$ mesons which only contain up and down quarks in our model. Again we see deconfinement for $\rho > 1.8\rho_{NM}$.

## 5.4 Discussion

We originally chose $\rho_C = 2.25\rho_{NM}$, since the curve in Fig. 2.5 that shows the values of $m_u(\rho)$ seemed to change its behavior at about $k_F^3 = 0.045$ GeV$^3$, which corresponds to $\rho \simeq 2.3\rho_{NM}$. We can attempt to see if that is a reasonable choice by noting that "string breaking" should occur when the energy of the extended string is equal to the energy of the lowest two-meson state that can be formed when the string breaks. Therefore, we may write $V_{max} = m_1 + m_2$, where $m_1 + m_2$ are the masses of the mesons in the final state. We then use $V_{max} = \kappa/\mu(\rho)e$ to find a value $\mu(\rho)$ and obtain $\rho/\rho_C$ from the expression $\mu(\rho) = \mu_0/[1-(\rho/\rho_C)^2]$. We then put $\rho_C = 2.25\rho_{NM}$ and calculate the value of $\rho/\rho_{NM}$ where we might expect string breaking. We consider the final states $\pi\pi$, $\pi K$, $\pi\eta$ and $K\bar{K}$. The corresponding values of $\rho/\rho_{NM}$ are 2.09, 1.86, 1.83, and 1.61 for $\rho_C = 2.25\rho_{NM}$. Note that the $K(495)$ and $K_0^*(1430)$ mesons can break up into the $\pi K$ system, while the $a_0(980)$ is strongly coupled to the $\pi\eta$ channel. The $f_0(980)$ is coupled both to the $\pi\pi$ and $K\bar{K}$ channels. On the whole, the values of $\rho/\rho_{NM}$ calculated above are generally consistent with the value of that quantity that leads to deconfinement in our model. That result tends to suggest that, for light mesons, the density that leads to string breaking may be similar to the density for deconfinement. (In general, however, these processes are distinct and further studies would be needed to see if string breaking and deconfinement are related at finite density.) We may suggest that, if the initial meson is of the same type as the mesons that appear upon string breaking, it becomes reasonable to suggest that the instability of the initial mesons is also felt by the final state mesons, giving rise to the relation of string breaking and deconfinement suggested above for light mesons.

A comprehensive discussion of meson properties at finite temperature and density has been presented by Lutz, Klimt and Weise [62]. Since those authors did not include a model of confinement, they were able to calculate values of the meson masses for

large values of the density. Their Fig. 5.3 shows the calculated masses of the nodeless pion, $f_0$ and $a_0$ mesons for $0 \leq \rho/\rho_{NM} \leq 3.5$. They also give the result for an $f_0'$ excitation. (The $f_0$ and $f_0'$ exhibit singlet-octet mixing.) Compared to our results, their value of the $f_0$ mass falls more rapidly than ours, becoming degenerate with the pion mass at about $\rho/\rho_{NM} = 3$. On the other hand, the mass of the $a_0$ in their work is about 600 MeV at $\rho/\rho_{NM} = 2$. They are able to derive systematic low-density expansions for various quantities which provide important insight into the results obtained in numerical studies. They also show that effects due to finite quasiparticle size are important in stabilizing the density and temperature dependence of the pion mass. The main deficiency of their work is the absence of a model of confinement. Therefore, we believe our work provides a natural extension of the work reported in Ref. [62].

It is worth noting that deconfinement takes place in our model at about $\rho = 1.8\rho_{NM}$, while the confining potential goes to zero at $\rho = \rho_C = 2.25\rho_{NM}$. That suggests that the specific form we have chosen for the density dependence, $\mu(\rho) = \mu_0/[1-(\rho/\rho_C)^2]$, is not particularly important. What is more important is the behavior of our confining potential, $V^C(r,\rho)$, shown in Fig. 2.3. There, we see that the potential still has a substantial magnitude at $\rho = 1.75\rho_{NM}$ and $\rho = 2.10\rho_{NM}$.

Since the analysis of Ref. [62] is made in the absence of a model of confinement, many analytic results can be obtained for the behavior of various quantities when small changes in density and temperature are considered. Indeed, the work of that reference provides some support for our treatment of the pion and kaon. It is shown that the Goldstone boson remains at zero mass in the chiral limit as long as the system remains in the Goldstone-Nambu mode of symmetry breaking. For finite current quark masses, we quote the result given in Eq. (5.6) of Ref. [62] for $T = 0$,

$$\frac{dm_\pi^2}{m_\pi^2} = \left(1 - 2m_u^2\langle r_S^2\rangle\right)\frac{d\langle\bar{u}u\rangle}{\langle\bar{u}u\rangle}\,. \tag{5.4.1}$$

Here, $r_S$ is the quasiparticle radius. That quantity is defined in terms of the form factor $F_S(\vec{p}-\vec{p}\,')$ that appears in the matrix element of the u-quark scalar density

$$\langle u(\vec{p}\,')|\,\bar{u}u(0)\,|\,u(\vec{p})\rangle = F_S(\vec{p}-\vec{p}\,')\bar{u}(p\,')u(p)\,. \tag{5.4.2}$$

In Eq. (5.4.2) $u(\vec{p})$ denotes the Dirac spinor of a constituent u quark with four-momentum $p$. The scalar mean-squared radius is then

$$\langle r_S^2\rangle = 6\frac{d}{dq^2}\ln F_S(q^2)\bigg|_{q^2=0}\,. \tag{5.4.3}$$

(See Eq. (A.7) of Ref. [62] for an explicit expression for $\langle r_S^2\rangle$ in terms of the parameters of the NJL model.) With the well-known relation [48]

$$\frac{d\langle\bar{u}u\rangle}{\langle\bar{u}u\rangle} = -\frac{\sigma_N\rho}{m_\pi^2 f_\pi^2}\,, \tag{5.4.4}$$

Eq. (5.4.1) becomes

$$dm_\pi^2 = -\left(1-2m_u^2\langle r_S^2\rangle\right)\frac{\sigma_N\rho}{f_\pi^2}\,. \tag{5.4.5}$$

If one ignores the quasiparticle size, one has $dm_\pi^2 = -(\sigma_N\rho/f_\pi^2)$ [63, 64], which implies pion condensation at a critical density $\rho_{crit} = f_\pi^2 m_\pi^2/\sigma_N = (0.148\,\mathrm{GeV})^3$, which is about 2.5 $\rho_{NM}$.

The second term in Eq. (5.4.5) works against condensation. With $m_u = 0.364$ GeV and $r_S = 0.40$ fm [62] one finds that $\delta m_\pi^2$ increases slowly with increasing density, as born out by the calculations reported in Ref. [62]. Our choice of $G_\pi(\rho) = G_\pi(0)[1-0.087\rho/\rho_{NM}]$ reproduces the almost constant value of $m_\pi$. We see that the density-dependent term in $G_\pi(\rho)$ plays a similar role in our model as that played by the second term in Eq. (5.4.5).

We have some confidence in our treatment of the pion and kaon at finite density. We recall that we were able to find satisfactory values of $G_\pi(0)$ and $G_K(0)$ using the values of $G_S$ and $G_D$ obtained in our study of the eta mesons [21]. Therefore, our work provides a unified approach for the nonet of pseudoscalar mesons in the presence of a model of confinement.

Since confinement is important for the $a_0(980)$ and $f_0(980)$ mesons, it is uncertain whether the results of Ref. [62] for the properties of these mesons can be trusted. These mesons are in the continuum of the NJL model without confinement and various assumptions need to be made as to how the formalism is to be applied. For a small increase in density, the mass of the $a_0$ in our model and in Ref. [62] are similar. For the larger values of density, the use of $G_{a_0}(\rho) = G_{a_0}(0)[1 - 0.045\rho/\rho_{NM}]$ in model leads to a rather small mass for the $a_0$ for $\rho \sim 2\rho_{NM}$. [See Fig. 5.3.]

Our treatment of the $a_0$ mesons is less satisfactory than that of $\pi$ and $K$ mesons, since coupled channel effects are important in the case of the scalar mesons. Using the values of $G_S$ and $G_D$ obtained in our study of the eta mesons [21], we found the lowest $a_0$ state at 1.13 GeV. To place the $a_0$ at 980 MeV, we increased the value of $G_{a_0}(0)$. That increase led to the possibility of an $a_0$ condensation, which was removed by reducing the coupling constant with increasing density. [See Fig. 5.3.] However, it might be preferable to accept the value of 1.13 GeV for the mass of the $a_0$ and, therefore, avoid the problem of $a_0$ condensation. Our difficulty in this case arises since we do not know the density dependence of the processes that move the $a_0$ mass from our predicted value to the experimental value of 980 MeV.

In our model we see some relation between the partial restoration of chiral symmetry and deconfinement. With reference to Fig. 2.5, we see that the up (or down) quark mass drops in a roughly linear manner with increasing density up to about 2 or 2.5 times nuclear matter density. With the reduction of the magnitude of the confining field, as seen in Fig. 2.3, the combined effect of the smaller confining field and

reduced quark mass values leads to deconfinement at about 1.8 $\rho_{NM}$. For the $K$ and $K_0^*$ mesons, the reduction of the mass of the quarks is less important, since these mesons have one strange quark. However, deconfinement still takes place at about $\rho = 1.8\rho_{NM}$ for these mesons.

In future work we will study the dependence of the deconfinement process on both temperature and density. In addition, it would be desirable to have some understanding of the mechanism by which the increased matter density modifies the confining interaction.

# Chapter 6

# Dense Matter

## 6.1 Introduction

### 6.1.1 Self-Energy

In recent years there has been a great deal of interest in understanding the properties of quark matter at relatively low temperature and high density [32, 33, 34, 35, 36]. Since it is difficult to study QCD at finite chemical potential using lattice simulations, the model of choice for such studies has been the Nambu–Jona-Lasinio model [12, 23, 22]. Of particular interest is the prediction of diquark condensates and color superconductivity at high densities. (Such studies may be relevant to the properties of neutron stars.) Calculations made for dense matter using the NJL model are carried out in Minkowski space. These calculations are limited in that they do not include a model of confinement and are, therefore, unable to provide a comprehensive description of the hadronic phase present at low density and temperature. However, it is generally believed that a good deal of information may be gained by studying quark matter, with a proper study of the hadronic phase deferred until some future time.

As is well known, the NJL model provides a microscopic dynamical description of chiral symmetry breaking with the generation of associated quark vacuum condensates and constituent masses. In the standard versions of the NJL model [12, 23, 22], the constituent quark mass that is generated in the model is a constant. However, it is known from lattice simulations of QCD that the constituent mass goes over to the current quark mass when the quark momentum, $p^2$, is less than about -2 GeV$^2$ [69]. It is our belief that, if we are to use the NJL model to study dense matter, it is desirable to make the model as realistic as possible. To that end, we have introduced a nonlocal version of the NJL model [83] that is able to reproduce the Euclidean-space behavior of the quark mass seen in lattice simulations of QCD [69]. To carry out that program we have introduced a momentum-dependent $q\bar{q}$ interaction in the calculation of the quark self-energy and have separated the regularization of the model from the specification of that interaction. (This procedure requires the introduction of additional parameters into the model.)

Recently, we have seen an attempt to obtain the quark self-energy in Minkowski space by analytic continuation of a Euclidean-space form based upon gluon exchange enhanced at small momentum transfers to simulate confinement [81]. The resulting Minkowski-space values exhibit resonant-like structures and very large values of the constituent mass. Such results do not appear to have any natural physical interpretation.

### 6.1.2 Quark Propagation

Another work we did is to research quark propagation in the quark-gluon plasma. The description of the quark-gluon plasma in terms of hydrodynamics has been advocated by the Stony Brook group [89, 90, 91]. That description appears to be in accord with the experimental data. In such a description the motion of the quarks is characterized

by an extremely short mean-free-path. The origin of that behavior is thought to be due to the relatively low-energy resonances in the $q\overline{q}$ system leading to very large scattering lengths. These resonances have been found in lattice studies of QCD which make use of the maximum entropy method (MEM) [9, 92, 93, 94, 95, 96]. Similar resonances are found in the scalar, pseudoscalar, vector and axial-vector $q\overline{q}$ channels [97]. Recently, an extensive exploration of charmonium studies in the confined and deconfined regions using lattice methods has been reported in Ref. [98]. In that work results are given for the dependence of the resonance excitation on the total momentum of the $q\overline{q}$ pair. We have studied that dependence for light quark systems in Ref. [99] and have found similar behavior to that reported in Ref. [98]. (We will make use of the results presented in Ref. [99] in the present work in which we calculate the imaginary part of the optical potential and the mean-free-path for a quark in the quark-gluon plasma.) We use a chiral model with rather large momentum cutoff. That model is meant to provide an approximate description of the instanton dynamics advocated by the Stony Brook group [89, 90, 91]. Earlier work using our model may be found in Refs. [100, 101, 102].

## 6.2 Quark and Nucleon Self-Energy in Dense Matter

### 6.2.1 the Quark Self-energy

We note that the quark self-energy may be written as Eq. 2.5.3 in vacuum. In matter there is another four-vector, $\eta^\mu$, that describes the motion of the matter rest frame. It is useful to put $\eta^2 = 1$ and to note that, if we work in the matter rest frame, we can put $\eta^\mu = [1, 0, 0, 0]$. In matter, we have

$$\Sigma(k^2, \eta\cdot k) = A(k^2, \eta\cdot k) + B(k^2, \eta\cdot k)\overline{\not{k}} + C(k^2, \eta\cdot k)\not{\eta}\,, \tag{6.2.1}$$

where we have found it useful to introduce the four-vector

$$\overline{k^\mu} = k^\mu - (k\cdot\eta)\eta^\mu\,. \tag{6.2.2}$$

Note that $\overline{k^0} = 0$ in the matter rest frame. In that frame, we may write

$$\Sigma(k^0, \vec{k}) = A(k^0, \vec{k}) - B(k^0, \vec{k})\vec{\gamma}\cdot\vec{k} + \gamma^0 C(k^0, \vec{k})\,. \tag{6.2.3}$$

As we will see, $A$ and $B$ satisfy coupled nonlinear equations, while $C$ may be calculated independently. (Note that $A$ and $C$ have the same dimension, while $B$ is dimensionless.)

We first discuss our results for the case in which we neglect the dependence of $A$, $B$, and $C$ on $k^0$. We anticipate that the dependence on $k^0$ will be relatively weak and justify that assumption later in this work. As a further simplification, we will at first neglect $B$ and study the behavior of $A(\vec{k}, \rho)$, where $\rho$ is the density of quark matter which is taken to contain equal numbers of up and down quarks. In this case, the

maximum value of $A(\vec{k},\rho)$ is found at $\vec{k}=0$, leading to a simpler presentation of our results. We then go on to the consideration of the coupled equations for $A(\vec{k},\rho)$ and $B(\vec{k},\rho)$. As usual, we may introduce a density and momentum-dependent mass defined by Eq. 2.5.4 We provide values of $A(\vec{k},\rho)$, $M(\vec{k},\rho)$ and $C(\vec{k},\rho)$ in the following sections.

We note that the inclusion of $C(\vec{k},\rho)$ precludes the passage to Euclidean space. The analogous problem arises when one introduces a finite chemical potential. As we will see, $C(\vec{k},\rho)$ is quite large at finite density and can only be neglected at very small densities. In vacuum, Lorentz invariance leads to a relation between $C(k^2)$ and $B(k^2)$. However, our formalism does not maintain Lorentz invariance. (For example, our regulator depends only upon $|\vec{k}|$.) Therefore, in the following we will only calculate the contribution to $C(\vec{k},\rho)$ from the matter, which takes the form of two Fermi seas of up and down positive-energy quarks with Fermi momentum $k_F$.

In our earlier work we obtained the quark self-energy from the solution of the equation depicted in Fig. 3.5 [83]. There, the open circle is a momentum-dependent quark interaction, obtained by the replacement

$$G_S \longrightarrow f(k-k')\, G_S f(k-k')\,, \tag{6.2.4}$$

where $k$ and $k'$ are the quark momenta entering (or leaving) the interaction. We have used

$$f(k-k') = \exp[-(k-k')^{2n}/2\beta] \tag{6.2.5}$$

with $n=4$ and $\beta = 20$ GeV$^8$ in Ref. [83]. The corresponding nonlocal Lagrangian is given in Ref. [83]. On the right-hand side of Fig. 3.5, the 't Hooft interaction (third term) and the confinement interaction (fourth term) are neglected for the purposes of

this work. In the second term we have contributions from the negative-energy states in vacuum as well as the positive-energy states at finite density, specified by the quark Fermi momentum, $k_F$, of the up and down quark Fermi seas.

In general, the quark propagator is

$$iS(k, k\cdot\eta) = \frac{i}{\not{k} - \Sigma(k^2, k\cdot\eta) + i\epsilon}\,, \tag{6.2.6}$$

which we will write as

$$iS(k^0, \vec{k}) = \frac{i}{(k^0 - C(k^0, \vec{k}))\gamma^0 - (1 - B(k^0, \vec{k}))\vec{\gamma}\cdot\vec{k} - A(k^0, \vec{k}) + i\epsilon}\,, \tag{6.2.7}$$

in the matter rest frame. In a first approximation we write

$$iS(k^0, \vec{k}) = \frac{i}{(k^0 - C(\vec{k}))\gamma^0 - (1 - B(\vec{k}))\vec{\gamma}\cdot\vec{k} - A(\vec{k}) + i\epsilon}\,, \tag{6.2.8}$$

with $A(\vec{k})$, $B(\vec{k})$ and $C(\vec{k})$ density-dependent, in general. (On occasion we will write $A(\vec{k}, \rho)$, etc.) We see that the presence of $C(\vec{k})$ precludes the passage to Euclidean space that was made in Ref. [83]. That is analogous to the problem created by the introduction of a chemical potential in the formalism. Note that

$$\begin{aligned}(k^0 - C(\vec{k}))^2 - (1 - B(\vec{k}))^2\vec{k}^2 - A^2(\vec{k}) + i\epsilon \\ = [k^0 - E^+(\vec{k}) + i\epsilon][k^0 - E^-(\vec{k}) - i\epsilon]\end{aligned} \tag{6.2.9}$$

with

$$E^+(\vec{k}) = C(\vec{k}) + \sqrt{\vec{k}^2(1 - B(\vec{k}))^2 + A^2(\vec{k}^2)} \tag{6.2.10}$$

and

$$E^-(\vec{k}) = C(\vec{k}) - \sqrt{\vec{k}^2(1-B(\vec{k}))^2 + A^2(\vec{k}^2)}\,. \tag{6.2.11}$$

Here $E^+(\vec{k})$ may be interpreted as the (on-mass-shell) energy of the positive-energy states, while $E^-(\vec{k})$ refers to the negative-energy states.

In order to simplify the notation somewhat, we write

$$iS(k^0,\vec{k}) = \frac{i}{\not{\Pi}(k^0,\vec{k}) - A(\vec{k}) + i\epsilon}\,, \tag{6.2.12}$$

where we have defined a four-component quantity

$$\Pi^\mu(k^0,\vec{k}) = [k^0 - C(\vec{k}), (1-B(\vec{k}))\vec{k}]\,. \tag{6.2.13}$$

We also introduce a scalar quantity

$$\rho_S(\vec{k}) = iN_c(-1)\int\frac{d^4k'}{(2\pi)^4}\,\frac{4A(\vec{k}')f^2(k-k')}{\Pi^2(k'^0,\vec{k}') - A^2(\vec{k}') + i\epsilon}\,, \tag{6.2.14}$$

where the minus sign is due to the closed Fermion loop in Fig. 3.5 and the factor of 4 comes from forming the trace associated with the closed loop. We see that $\rho_S(\vec{k})$ does not depend upon $k^0$, since we are making an on-shell approximation in the calculation of $f(k-k')$. In vacuum we have

$$-iA(\vec{k}) = -im^0 + (2G_S i)\rho_S(\vec{k})\,, \tag{6.2.15}$$

or

$$A(\vec{k}) = m^0 - 2G_S\rho_S(\vec{k})\,, \tag{6.2.16}$$

where $\rho_S(\vec{k})$ is real and negative. We remark when $f(k-k')=1$, $A(\vec{k}) \to m$ and $\rho_S(\vec{k}) \to \langle \bar{u}u \rangle$, so that we regain the usual result [12, 23, 22]

$$m_u = m_u^0 - 2G_S\langle \bar{u}u \rangle \,, \tag{6.2.17}$$

$$m_d = m_d^0 - 2G_S\langle \bar{d}d \rangle \,. \tag{6.2.18}$$

(Note that our $G_S$ is one-half of the $G_S$ defined in Ref. [23].)

The evaluation of $\rho_S(\vec{k})$ proceeds by closing to contour in the complex $k^0$ plane. In the vacuum we find

$$\rho_S(\vec{k}) = -2N_c \int \frac{d^3k'}{(2\pi)^3} \, \frac{f^2(k-k')A(\vec{k}')}{\sqrt{\vec{k}'^2(1-B(\vec{k}'))^2 + A^2(\vec{k}')}} \,. \tag{6.2.19}$$

We define

$$E(\vec{k}) = \sqrt{\vec{k}^2(1-B(\vec{k}))^2 + A^2(\vec{k})} \,, \tag{6.2.20}$$

and

$$(k-k')^2 = (E(\vec{k}) - E(\vec{k}'))^2 - (\vec{k}-\vec{k}')^2 \,, \tag{6.2.21}$$

so that $f(k-k')$ depends only upon $|\vec{k}|$, $|\vec{k}'|$ and the angle between $\vec{k}$ and $\vec{k}'$.

Integrals such as that in Eq. (6.2.19) require regularization. For our calculations we insert a factor $\exp[-\vec{k}'^2/\,\alpha^2]$ with $\alpha = 0.60$ GeV. (We have used the same Gaussian regulator in our calculations of meson spectra, where we have used $\alpha = 0.605$ GeV [21, 20, 84]. However, those calculations included a model of confinement, so that we can not directly take over the parameters $G_S$, $G_V$ and $G_D$ used in those works.)

We remark that an expression for the density-dependent condensate $\langle \bar{u}u \rangle_\rho$ may be obtained by using Eq. (6.2.19) with $f(k-k')=1$.

In the presence of matter it is useful to separate the propagator into two parts, one of which will give rise to the explicitly density-dependent terms. In this regard, it is useful to generalize Eq. (5.8) of Ref. [12]. We define

$$\Lambda^{(+)}(\vec{k}) = \frac{E(\vec{k})\gamma^0 - \vec{\gamma}\cdot\vec{k}(1-B(\vec{k})) + A(\vec{k})}{2A(\vec{k})}\,, \tag{6.2.22}$$

$$\Lambda^{(-)}(-\vec{k}) = \frac{-E(\vec{k})\gamma^0 - \vec{\gamma}\cdot\vec{k}(1-B(\vec{k})) + A(\vec{k})}{2A(\vec{k})}\,, \tag{6.2.23}$$

where $E(\vec{k}) = [\vec{k}^2(1-B(\vec{k}))^2 + A^2(\vec{k})]^{1/2}$. Then

$$\begin{aligned} S(k) = \quad & \frac{A(\vec{k})}{E(\vec{k})}\left[\frac{\Lambda^{(+)}(\vec{k})}{k^0 - E^+(\vec{k})} - \frac{\Lambda^{(-)}(-\vec{k})}{k^0 - E^-(\vec{k})}\right] \\ + \quad & 2\pi i \frac{A(\vec{k})}{E(\vec{k})}\Lambda^{(+)}(\vec{k})\,\theta(k_F - |\vec{k}|)\,\delta(k^0 - E^+(\vec{k})) \end{aligned} \tag{6.2.24}$$

In the limit that $A(\vec{k}) \to m^*$ and $B(\vec{k}) = C(\vec{k}) = 0$, we have, with

$$E^*(\vec{k}) = \sqrt{\vec{k}^2 + m^{*2}}\,, \tag{6.2.25}$$

$$\begin{aligned} S(k) &= \frac{m^*}{E^*(\vec{k})}\left[\frac{\Lambda^{(+)}(\vec{k})}{k^0 - E^*(\vec{k})} - \frac{\Lambda^{(-)}(-\vec{k})}{k^0 + E^*(\vec{k})}\right] && (6.2.26) \\ &+ 2\pi i \frac{m^*}{E^*(\vec{k})}\Lambda^{(+)}(\vec{k})\,\theta(k_F - |\vec{k}|)\,\delta(k^0 - E^*(\vec{k})) \\ &= \frac{\not{k} + m^*}{k^2 - m^{*2}} + \frac{i\pi}{E^*(\vec{k})}(\not{k} + m^*)\,\theta(k_F - |\vec{k}|)\,\delta(k^0 - E^*(\vec{k}))\,, && (6.2.27) \end{aligned}$$

which agrees with Eq. (5.8) of Ref. [12].

In the presence of matter, we have

$$A(\vec{k},\rho) = m^0 - 2G_S[\rho_S^{\rm vac}(\vec{k}) - \rho_S^{\rm mat}(\vec{k})]\,, \tag{6.2.28}$$

where $\rho_S^{\rm mat}(\vec{k})$ is calculated in the same manner as $\rho_S^{\rm vac}(\vec{k})$, except that the upper limit of the integral over $|\vec{k}'|$ is $k_F$. Equation 6.2.24 is a generalization of a corresponding equation that may be found in Klevansky's review. (See Eqs. (5.18) of Ref. [12].)

If we neglect $B(\vec{k})$, Eqs. (6.2.14) and (6.2.19) provide a nonlinear equation for $A(\vec{k})$ which may be solved by iteration. The results of such a calculation are reported in Table 6.1 where, for nuclear matter, we put $k_F = 0.268$ GeV. In Figs. 6.1 and 6.2 we show values of the condensate $\langle\bar{u}u\rangle$ and $A(0,\rho)$ as a function of the density. These results may be usefully discussed in terms of the relation [48] as Eq. 2.4.10 Where $\sigma_N$ is the pion-nucleon sigma term and $\rho_N$ is the density of nucleons. If we put $\sigma_N = 0.050$ GeV, $\rho_N = (0.109\,\text{GeV})^3$, $f_\pi = 0.0942$ GeV and $m_\pi = 0.138$ GeV, we find a 38% reduction of the condensate at nuclear matter density, which agrees with our results given in Table 6.1 and Fig. 6.1. It is of interest to note that the linear dependence on the density implied by Eq. (2.4.10) appears to be valid up to about twice nuclear matter density. However, one may be concerned that, since we study quark matter rather than nuclear matter, Eq. (2.4.10) may not be appropriate. Consider, however, the relation

$$\langle\bar{u}u\rangle_\rho = \langle\bar{u}u\rangle_0 \left(1 - \frac{\sigma_q\rho_q}{f_\pi^2 m_\pi^2} + \cdots\right)\,, \tag{6.2.29}$$

where $\sigma_q$ is the quark sigma term and $\rho_q$ is the number density of the quarks, which we may put equal to $3\rho_N$. Thus, if $3\sigma_q = \sigma_N$, we may use Eq. (2.4.10). The fact that $\sigma_q \simeq 15$ MeV has been discussed by Vogl and Weise [23]. We have also discussed this matter in great detail in Ref. [51], where we calculated similar values of $\sigma_q$ using the standard version of the NJL model. We conclude that the use of Eq. (2.4.10), or Eq.

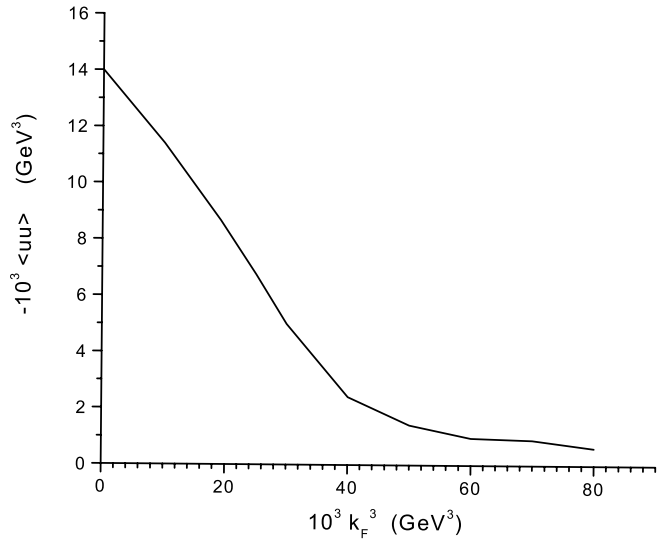


Figure 6.1: Values of the condensate $\langle \bar{u}u \rangle$ are given as a function of $10^3 k_F^3$. For nuclear matter $10^3 k_F^3 = 19.2$ GeV$^3$. [See Table 6.1.] Here $G_S = 13.0$ GeV$^{-2}$ and $B(\vec{k}, \rho)$ is put equal to zero.

(6.2.29), with an appropriate value of $\sigma_q$, is satisfactory. For example, if $\sigma_q = \sigma_N/3$, as suggested in Ref. [23], the two relations imply the same density dependence of the condensate.

In Fig. 6.2 we show $A(0, \rho)$ which is the density-dependent mass parameter of the theory when $B(\vec{k}, \rho) = 0$. We see that $A(0, \rho)$ follows the trend seen in Fig. 6.1 for the density dependence of the condensate.

### 6.2.2 Lorentz-vector Terms of the Quark Self-energy

We now write $\Sigma(\vec{k}) = \Sigma_S(\vec{k}) + \Sigma_V(\vec{k})$ where

$$\Sigma_V(\vec{k}) = -\vec{\gamma} \cdot \vec{k} B(\vec{k}) + \gamma^0 C(\vec{k}) \,. \tag{6.2.30}$$

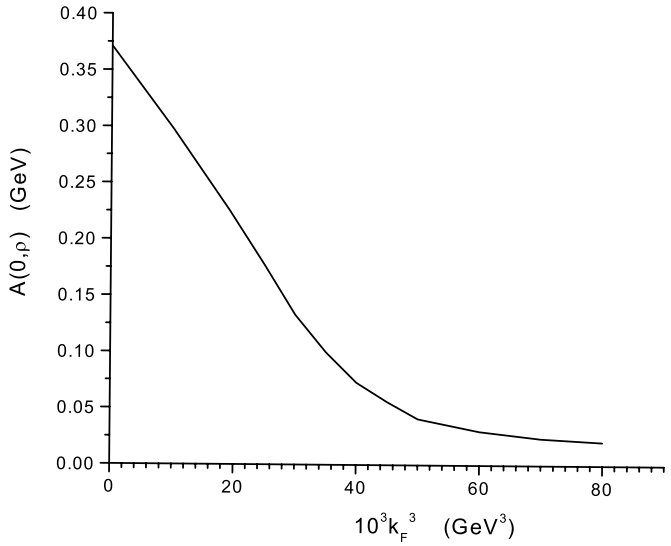


Figure 6.2: Values of $A(0,\rho)$ are given as a function of $10^3 k_F^3$. [See Table 6.1 and the caption of Fig. 6.1.]

| $10^3 k_F^3$ ( GeV$^3$) | $-\langle\bar{u}u\rangle^{1/3}$ (GeV) | $-10^3\langle\bar{u}u\rangle$ ( GeV$^3$) | $A(0,\rho)$ (GeV) |
|---|---|---|---|
| 0 | 0.241 | 14.0 | 0.371 |
| 10 | 0.225 | 11.4 | 0.298 |
| 19.2(nm) | 0.205 | 8.67 | 0.226 |
| 25 | 0.189 | 6.75 | 0.177 |
| 30 | 0.171 | 5.00 | 0.133 |
| 40 | 0.134 | 2.46 | 0.077 |
| 50 | 0.113 | 1.44 | 0.041 |
| 60 | 0.0990 | 0.967 | 0.030 |
| 70 | 0.0915 | 0.898 | 0.024 |
| 80 | 0.0853 | 0.620 | 0.021 |
| 90 | 0.0805 | 0.522 | 0.018 |

Table 6.1: Values of the condensate and $A(0,\rho)$ are given for $G_S = G_V = 13.0$ GeV$^{-2}$ and $m_u^0 = m_d^0 = 0.005$ GeV. Here $k_F = 0.268$ GeV for nuclear matter. We note the reduction of the condensate of 38% and a 40% reduction of $A(0,\rho)$ at nuclear matter density [$10^3 k_F^3 = 19.2$ GeV$^3$]. Here $\alpha = 0.60$ GeV is used in the Gaussian regulator $\exp[-\vec{k}^2/\alpha^2]$.

For the calculation of $C(\vec{k})$ we obtain the contribution from the last term in Eq. (6.2.24), with the result that

$$C(\vec{k}) = 2G_V \rho_2^V(\vec{k}) \tag{6.2.31}$$

with

$$\rho_2^V(\vec{k}) = 2N_c \int^{k_F} \frac{d^3k'}{(2\pi)^3} f^2(k-k')\,. \tag{6.2.32}$$

An expression for $B(\vec{k})$ may be found from the relation

$$-i[-\vec{\gamma}\cdot\vec{k}B(\vec{k})] = (-2G_V i)(-1)i\int\frac{d^4k'}{(2\pi)^4}\,S(k')f^2(k-k') \tag{6.2.33}$$

if we only keep the term proportional to $\vec{\gamma}\cdot\vec{k}'$ in the expression for the quark propagator. In vacuum we may compare corresponding terms in Eq. (6.2.33)

$$-\vec{\gamma}\cdot\vec{k}B(\vec{k}) = -2G_V\int\frac{d^4k'}{(2\pi)^4}\,\frac{-\vec{\gamma}\cdot\vec{k}'[1-B(\vec{k}')]f^2(k-k')}{[k_0'-E^+(\vec{k}')+i\epsilon][k_0'-E^-(\vec{k}')-i\epsilon]}\,. \tag{6.2.34}$$

Thus,

$$B^{\rm vac}(\vec{k}) = 2G_V\rho_1^{\rm vac}(\vec{k})\,, \tag{6.2.35}$$

with

$$|\vec{k}|\rho_1^{\rm vac}(\vec{k}) = 2N_c\int\frac{d^3k'}{(2\pi)^3}\,\frac{|\vec{k}'|(\hat{k}\cdot\hat{k}')f^2(k-k')[1-B(\vec{k}')]}{\sqrt{\vec{k}'^2[1-B(\vec{k}')]^2+A^2(\vec{k}')}}\,. \tag{6.2.36}$$

Here, $\hat{k}$ and $\hat{k}'$ are unit vectors. As in the calculation of $A(\vec{k})$, Eq. (6.2.35) is generalized to read

$$B(\vec{k}) = 2G_V[\rho_1^{\rm vac}(\vec{k}) - \rho_1^{\rm mat}(\vec{k})]\,, \tag{6.2.37}$$

where $\rho_1^{\rm mat}(\vec{k})$ is calculated using Eq. (6.2.36) with an upper limit on $|\vec{k}'|$ of $k_F$.

In Table 6.2 we present results of our calculation of the condensate, $A(0,\rho)$, $A(0,\rho)/[1-B(0,\rho)]$, $C(0,\rho)$, $B(0,\rho)$ and $A(0,\rho)-A(0,0)$. We also define

$$U_S(\vec{k},\rho) = A(\vec{k},\rho) - A(\vec{k},0)\,, \tag{6.2.38}$$

where $U_S(\vec{k},\rho)$ is the density-dependent modification of $A(\vec{k},0)$ in matter.

It may be seen from the values given in Table 6.2 that there is a thirty percent reduction of the condensate at the density of nuclear matter, while the value of $A(0)$ is reduced by thirty-nine percent. We would obtain a thirty percent reduction of the condensate if $\sigma_N = 39$ MeV.

In Figs. 6.3 and 6.4 we exhibit values of $A(\vec{k},\rho)$ and $A(\vec{k},\rho)/[1-B(\vec{k},\rho)]$ for various densities and in Fig. 6.5 we present values of $C(\vec{k},\rho)$. Figure 7 shows the values of $U_S(\vec{k},\rho_{NM})$ and $C(\vec{k},\rho_{NM})$.

### 6.2.3 Off-mass-shell Effects

In our calculations we have neglected the $k_0$ dependence of $A$, $B$ and $C$. In this Section we provide some justification of that approximation. We can combine Eqs. (6.2.12) and (6.2.14) to yield a nonlinear equation for $A(k^0,\vec{k})$ in vacuum

$$A(k^0,\vec{k}) = -(2G_S i)N_c(-1)\int\frac{d^4k'}{(2\pi)^4}\,\frac{4A(k'^0,\vec{k}')f^2(k-k')}{\not{k}' - A(k'^0,\vec{k}') + i\epsilon}\,. \tag{6.2.39}$$

| $10^3 k_F^3$ ( GeV$^3$) | $-\langle\bar{u}u\rangle^{1/3}$ (GeV) | $-10^3\langle\bar{u}u\rangle$ ( GeV$^3$) | $A(0,\rho)$ (GeV) | $\frac{A(0,\rho)}{1-B(0,\rho)}$ (GeV) | $U_S(0,\rho)$ (GeV) | $C(0,\rho)$ (GeV) | $B(0,\rho)$ |
|---|---|---|---|---|---|---|---|
| 0 | 0.2401 | 13.85 | 0.365 | 0.347 | 0 | 0 | -0.0544 |
| 10 | 0.2279 | 11.84 | 0.292 | 0.272 | -0.073 | 0.0794 | -0.0736 |
| 19.2 | 0.2128 | 9.64 | 0.223 | 0.203 | -0.142 | 0.0988 | -0.1019 |
| 30 | 0.1755 | 5.36 | 0.114 | 0.0942 | -0.252 | 0.115 | -0.210 |
| 40 | 0.1441 | 2.99 | 0.0606 | 0.0435 | -0.304 | 0.126 | -0.394 |
| 50 | 0.1291 | 2.15 | 0.0432 | 0.0279 | -0.322 | 0.136 | -0.545 |

Table 6.2: Various values are given for the case $G_S = 13.5$ GeV$^{-2}$, $G_V = 10.0$ GeV$^{-2}$, $m_u^0 = m_d^0 = 0.005$ GeV and $\alpha = 0.60$ GeV. Note a reduction of 30% for the condensate and 39% for $A(0,\rho)$ at nuclear matter density, where $k_F = 0.268$ GeV and $10^3 k_F^3 = 19.2$ GeV$^3$.

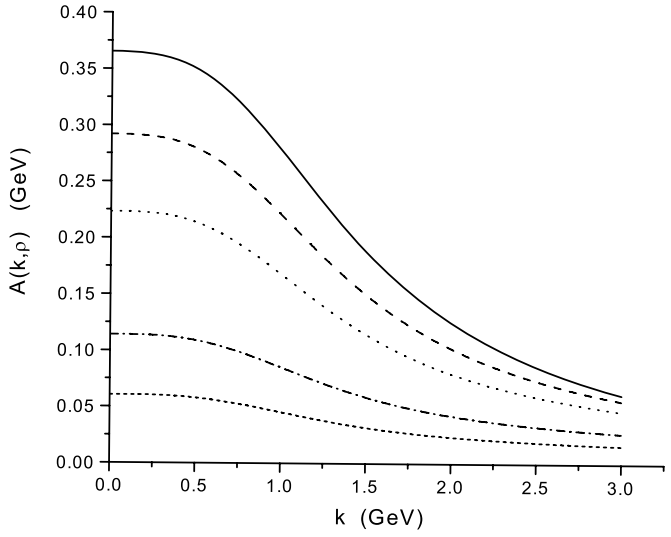


Figure 6.3: Values of $A(\vec{k},\rho)$ are given as a function of $|\vec{k}|$ for various densities: a) $10^3 k_F^3 = 0$ [solid line]; b) $10^3 k_F^3 = 10.0$ GeV$^3$ [dashed line]; c) $10^3 k_F^3 = 19.2$ GeV$^3$ [dotted line]; d) $10^3 k_F^3 = 30.0$ GeV$^3$ [dot-dash line] and e) $10^3 k_F^3 = 40.0$ GeV$^3$ [short dash]. Here $G_S = 13.5$ GeV$^{-2}$, $G_V = 10.0$ GeV$^{-2}$, $m^0 = 0.005$ GeV and $\alpha = 0.60$ GeV. [See Table 6.2.]

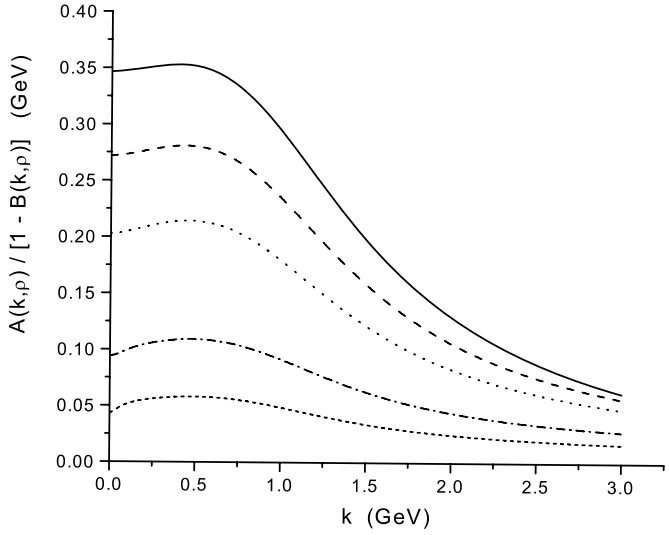


Figure 6.4: The quantity $A(\vec{k},\rho)/[1-B(\vec{k},\rho)]$, which plays the role of a momentum- and density-dependent mass parameter, is shown. [See Table 6.2 and the caption of Fig. 6.3.]

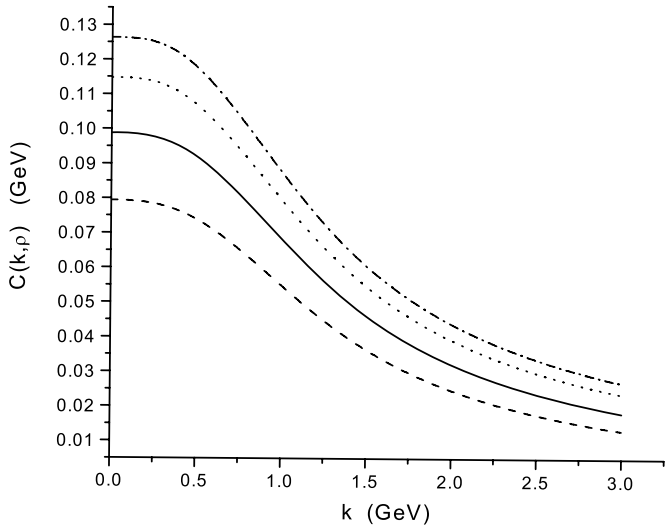


Figure 6.5: Values of $C(\vec{k},\rho)$ are shown for various densities: a) $10^3 k_F^3 = 10.0$ GeV$^3$ [dashed line]; b) $10^3 k_F^3 = 19.2$ GeV$^3$ [solid line]; c) $10^3 k_F^3 = 30.0$ GeV$^3$ [dotted line] and d) $10^3 k_F^3 = 40.0$ GeV$^3$ [dash-dot line]. Here $G_S = 13.5$ GeV$^{-2}$, $G_V = 10.0$ GeV$^{-2}$, $m^0 = 0.005$ GeV and $\alpha = 0.60$ GeV.

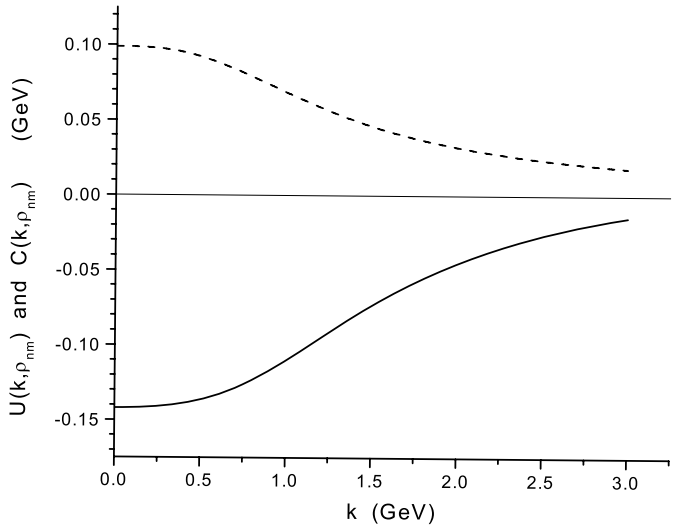


Figure 6.6: The values of $U(\vec{k}, \rho_{NM}) = A(\vec{k}, \rho_{NM}) - A(\vec{k}, 0)$ [solid line] and $C(\vec{k}, \rho_{NM})$ [dashed line] are shown. $U(\vec{k}, \rho_{NM})$ represents the density-dependent correction to the vacuum value of the scalar term of the quark self-energy.

Here we have neglected $m^0$ and $B(k^0, \vec{k})$. We see that $k^0$ dependence arises from $f^{\,2}(k - k')$ which is given by

$$f^{\,2}(k - k') = \exp[-(k - k')^{\,2n}/\beta]\,, \tag{6.2.40}$$

with

$$(k - k')^2 = (k^0 - k'^0)^2 - (\vec{k} - \vec{k}')^2\,, \tag{6.2.41}$$

which differs from the on-mass-shell version given in Eq. (6.2.21).

The solution of Eq. (6.2.39) for $A(k^0, \vec{k})$ is shown in Fig. 6.7 for various values of $k^0$. It is seen that the dependence on $k^0$ is weak as was assumed in this work.

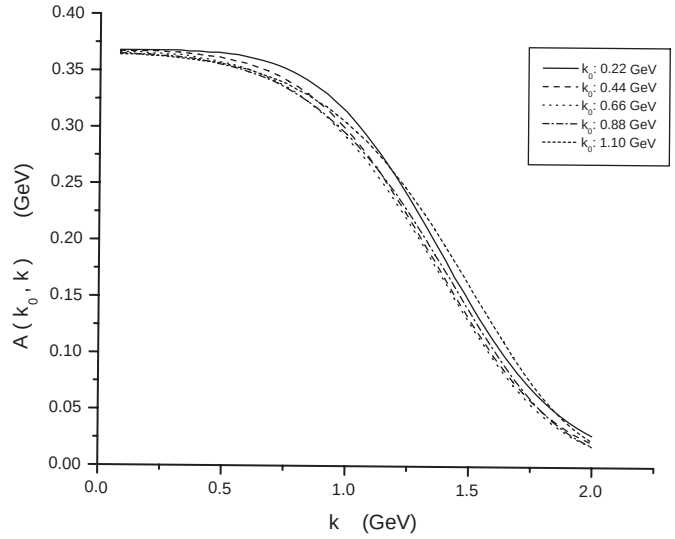


Figure 6.7: Values of $A(k^0, \vec{k})$ are shown as a function of $|\vec{k}|$ for various values of $k^0$.

### 6.2.4 The Nucleon Self-energy in Matter

If one uses the Dirac equation to describe the interaction of a nucleon with a nucleus, or with nuclear matter, it is found that a strong scalar attraction is needed as well as a strong vector repulsion [49, 50]. The scalar field is of the order of -400 MeV and the vector field is about 300 MeV. It is of interest to see if the nucleon self-energy, $\Sigma_N = V_S + \gamma^0 V_V$, can be calculated in terms of the quark self-energy obtained in this work. To carry out this program we use a simple model of the nucleon in which a quark is coupled to a scalar diquark. The full complexity of the wave function, including vector diquarks and various relativistic effects, is discussed in Ref. [85].

We can calculate the nucleon self-energy in nuclear matter using a triangle diagram in which one of the lower two vertices of the triangle represents a vertex function for a zero-momentum nucleon to emit a quark of momentum $\vec{k}$ leaving a spectator (on-mass-shell) diquark of momentum $-\vec{k}$. The other lower vertex represents the inverse process. At the upper vertex we insert the quark self-energy, $\Sigma(\vec{k}) = U_S(\vec{k}) + \gamma^0 C(\vec{k})$

calculated in this work and integrate over $\vec{k}$. We make use of Fig. 4 of Ref. [85] and parametrize the product of the vertex function and the quark Greens function by the quark-diquark wave function

$$\psi(\vec{k}) = \frac{1}{\sqrt{N}}\, e^{-\vec{k}^2/\lambda^2} u(\vec{k}, s)\,, \tag{6.2.42}$$

where $u(\vec{k}, s)$ is a spinor for a quark of momentum $\vec{k}$ and spin projection $s$ [85].

The normalization for a single quark is obtained from the relation

$$\frac{1}{N}\int \frac{d^3k}{(2\pi)^3}\, e^{-2\vec{k}^2/\lambda^2} \left(1 + \frac{\vec{k}^2}{[E_q(\vec{k}) + m_q]^2}\right) = 1\,, \tag{6.2.43}$$

where we put $\lambda = 0.18$ GeV to correspond to the results of Ref. [85]. We may then relate the nucleon self-energy to the quark self-energy. For a nucleon of momentum $\vec{P} = 0$, we have, with $E_q(\vec{k}) = [\vec{k}^2 + m_q^2]^{1/2}$, and $m_q = 0.364$ GeV,

$$V_V = \frac{3}{N}\int \frac{d^3k}{(2\pi)^3}\, C(\vec{k})\, e^{-2\vec{k}^2/\lambda^2} \left(1 + \frac{\vec{k}^2}{[E_q(\vec{k}) + m_q]^2}\right)\,, \tag{6.2.44}$$

and

$$V_S = \frac{3}{N}\int \frac{d^3k}{(2\pi)^3}\, U_S(\vec{k})\, e^{-2\vec{k}^2/\lambda^2} \left(1 - \frac{\vec{k}^2}{[E_q(\vec{k}) + m_q]^2}\right)\,. \tag{6.2.45}$$

The difference of sign in the brackets appearing in Eqs. (6.2.44) and (6.2.45) is due to the different behavior of the Dirac matrices, $\mathbf{1}$ and $\gamma^0$, at the upper vertex of the triangle.

Since the momentum content of the quark-diquark wave function is small [85], we expect that $V_S \simeq 3U_S(0)$ and $V_V \simeq 3C(0)$, so that $V_V \simeq 296$ MeV and $V_S \simeq -426$ MeV. A more careful evaluation of the integrals in Eqs. (6.2.44) and (6.2.45) yields $V_V = 295$ MeV and $V_S = -392$ MeV, which is in general accord with the values given

in Refs. [49, 50].

### 6.2.5 Discussion

The behavior of matter at high density and low temperature has received a good deal of attention in the last few years [32, 33, 34, 35, 36]. A large part of the work in this area has made use of the NJL model. In our work we have attempted to modify the NJL model so that its predictions are in greater accord with QCD. As a first step, in Ref. [83] we introduced a momentum-dependent $q\bar{q}$ interaction which allowed us to reproduce the Euclidean-space behavior for the constituent quark mass obtained in lattice simulation of QCD [69]. In the present study we have considered the important vector interactions of an extended NJL model. Of particular interest is the behavior of the quark condensate at finite density. We find that the linear behavior in the density exhibited in Eq. (2.4.10) holds in our model up to about twice nuclear matter density. Also, we note that the use of a nonzero current quark mass is important for that result, since in the absence of an explicit chiral symmetry breaking term, the model exhibits a first-order phase transition at about 1.25 times nuclear matter density.

Another point of interest are the results shown in Fig. 6.6. The quark self-energy is similar to that found in relativistic nuclear physics, with strong scalar attraction and strong vector repulsion. The simple calculation reported in Section 6.2.4 suggests that the quark self-energy, when multiplied by 3, provides a satisfactory estimate of the nucleon self-energy which is in accord with results of relativistic nuclear physics [49, 50].

There is a body of work based upon the solutions of the Schwinger-Dyson and Bethe-Salpeter equations with a phenomenological form for the gluon propagator [86, 87, 6, 88]. This body of work is reviewed in Ref. [52]. In contrast to the results of

our work, it is found that the quark condensate *increases* with increasing chemical potential. The authors of Ref. [86] argue that the baryon density is zero up to the critical chemical potential, $\mu_c$, for deconfinement. They state that "This result is an expected consequence of confinement which entails that each additional quark must be locally paired with an antiquark thereby increasing the density of condensate pairs as $\mu$ is increased. For this reason, as long as $\mu < \mu_c$, there is no excess of particles over antiparticles in the vacuum and hence the baryon number density remains zero." We note, however, that the baryon density usually considered in such calculations is due to the presence of *nucleons*, which have a finite baryon density. As noted earlier, in our work the baryon density is due to the presence of Fermi seas of up and down quarks, which serve to provide a model of the baryon density that would arise due to the presence of nucleons. We suggest that the conclusions presented in Ref. [86] do not refer to the situation of physical interest in which one studies the value of the quark condensate in nuclei or in nuclear matter.

## 6.3 Quark Propagation in the Quark-Gluon Plasma

### 6.3.1 Calculation of the Quark Optical Potential

In the study of hadronic current correlators [100, 101, 102] it is important to use a model which respects chiral symmetry when $m^0 = 0$. Therefore, we make use of the Lagrangian of Eq. (2.1.1), while neglecting the 't Hooft interaction and $\mathcal{L}_{conf}$. In order to make contact with the results of lattice simulations we use the model with the number of flavors $N_f = 1$. Therefore, the $\lambda^i$ matrices in Eq. (2.1.1) may be replaced by unity. We then use

$$\begin{aligned} \mathcal{L} &= \overline{q}(i\not{\partial} - m^0)q + \frac{G_S}{2}[(\overline{q}q)^2 + (\overline{q}i\gamma_5 q)^2] \\ &- \frac{G_V}{2}[(\overline{q}\gamma_\mu q)^2 + (\overline{q}\gamma_5\gamma_\mu q)^2] \end{aligned} \tag{6.3.1}$$

in order to calculate the hadronic current correlation functions. Thus, there are essentially three parameters to consider, $G_S$, $G_V$ and a Gaussian cutoff parameter $\alpha$, which restricts the momentum integrals through a factor $\exp[-\overrightarrow{k}^2/\alpha^2]$. As suggested by the Stony Brook group, we consider the NJL model and the associated chiral Lagrangian of Eq. (6.3.1) as providing a simplified representation of the instanton dynamics important for the problems considered in this work. Since the results obtained for the hadronic current correlation functions are similar in the scalar, pseudoscalar, vector and axial-vector channels, we carry out our calculations for the scalar $q\overline{q}$ states and multiple our results for the optical potential by 4. The parameters $G$ and $\alpha$ were fixed in our earlier studies [99]. We take $G$ =1.0 GeV$^{-2}$ and $\alpha$ = 4.4 GeV. These values provide good fits [99] to the hadronic current correlation functions found in the lattice studies [97]. In order to calculate the optical potential for a quark we consider the quark moving in an antiquark distribution characterized by a temperature-dependent occupation factor $n(\overrightarrow{p_1})$ which depends upon the chemical potential $\mu$. The energy

of a quark is given by $E(\overrightarrow{p}) = [\overrightarrow{p}^2 + m^2]^{1/2}$. We follow the work of Shuryak [89], for example, and put $m = 1$ GeV. In Shuryak's work this mass is not the current quark mass, but is called the "chiral mass". (We would prefer to call the 1 GeV mass, the "thermal mass", however, the terminology used is not important for this work.) The quark thermal mass is given in Ref. [39], with $C_F = 4/3$, as

$$m^2 = \frac{1}{8} g^2 C_F (T^2 + \frac{\mu^2}{\pi^2}), \tag{6.3.2}$$

for the case of a finite chemical potential. The thermal gluon mass is

$$m_g^2 = \frac{1}{6} g^2 T^2 (C_A + \frac{1}{2} N_f). \tag{6.3.3}$$

(The relation between thermal masses in QED and QCD is given on p.146 of Ref. [39].) In studies of baryon matter, the chemical potentials used are often about 300 MeV or less. However, once we introduce a thermal mass of about 1 GeV, we need to determine the chemical potential for the quarks. In this work we will consider a chemical potential of about 1 GeV, although the calculations are easily made for other values. Once we put $m = 1$ GeV, the chemical potential is the only parameter which is varied in our study.

It is useful to contrast the calculation of the quark optical potential with the calculation of the nucleon optical potential that is to be used in the Dirac equation. The latter calculation is discussed in detail in Ref. [50]. In that calculation of the nucleon-nucleus potential one calculates the $T$-matrix for nucleon-nucleon scattering using the one-boson-exchange (OBE) model. In that case the mesons of the OBE model undergo $t$-channel and $u$-channel exchange between the nucleons. The result is that the imaginary part of the optical potential has a magnitude of about 10 MeV [50]. That in turn leads to a mean-free-path of about 10 fm for a 500 MeV nucleon. Many years ago, the relatively large value for the nucleon mean-free-path lead to the

characterization of the optical model for nucleon-nucleus scattering as the "cloudy crystal ball" model. When we study quark propagation in the quark-gluon plasma we may consider a similar calculation of the optical potential at finite temperature. In the case of the quark-antiquark interaction the $T$ matrix is dominated by $s$-channel resonances of the type found in the MEM studies. As we will see, the interaction in this case is quite strong, leading to a small mean-free-path. The resulting model is called the "sticky molasses" model [89, 90, 91] as opposed to the "cloudy crystal ball" model used to describe nucleon-nucleus scattering. We now consider the potential seen by a quark of momentum $\overrightarrow{p_2}$ and average over the quark spin $s_2$. (We will consider quarks of a single flavor, since that was done in the MEM studies that we have used to fix the parameters of our model.) In Ref. [50] the relativistic optical potential was denoted as $\Sigma(\overrightarrow{p}, s)$ and, for this work, we consider

$$\Sigma^{++}(\overrightarrow{p_2}) = \frac{1}{2}\sum_{s_2} \overline{u}(\overrightarrow{p_2}, s_2)\Sigma(\overrightarrow{p_2}, s_2)u(\overrightarrow{p_2}, s_2). \tag{6.3.4}$$

It is useful to introduce [101]

$$U(\overrightarrow{p_2}) = N\sqrt{\frac{m}{E(\overrightarrow{p_2})}}\Sigma^{++}(\overrightarrow{p_2})\sqrt{\frac{m}{E(\overrightarrow{p_2})}}. \tag{6.3.5}$$

Here the factor of $N = 4$ takes into account the sum of the interactions in the scalar, pseudoscalar, vector and axial-vector channels which are taken to be equal for the purposes of this work. The approximate equality of the interactions in these channels may be seen in Ref. [97]. (Note that values of $U(\overrightarrow{p})$ are given in Ref. [50] for the case of nucleon-nucleus scattering.)

If $p_1$ is the momentum of the antiquark in the medium, we may introduce the four-

vector

$$P^\mu = (p_1 + p_2)^\mu. \tag{6.3.6}$$

Now

$$\begin{aligned} P^2 &= P_0^2 - \overrightarrow{P}^2 && (6.3.7)\\ &= (E(\overrightarrow{p_1}) + E(\overrightarrow{p_2}))^2 - (\overrightarrow{p_1}^2 + \overrightarrow{p_2}^2 + 2p_1p_2\cos\theta). && (6.3.8) \end{aligned}$$

Here, we take $\overrightarrow{p_2}$ along the $z$ axis. We define

$$t(\overrightarrow{p_1}, \overrightarrow{p_2}) = \frac{1}{\pi P^2}\left[\frac{G}{1 - GJ(\overrightarrow{p_1}, \overrightarrow{p_2})}\right], \tag{6.3.9}$$

where $J(\overrightarrow{p_1}, \overrightarrow{p_2})$ is the $q\overline{q}$ vacuum polarization function defined in Appendix B. (We remark that we may also use the notation $t(P^2, p_2)$ for the quantity defined in Eq. (6.3.9).)

It is also useful to introduce the occupation factor $n(\overrightarrow{p_1})$:

$$n(\overrightarrow{p_1}) = \frac{1}{\exp\beta[E(\overrightarrow{p_1}) - \mu] + 1}, \tag{6.3.10}$$

with $\beta = 1/T$ and $E(\overrightarrow{p_1}) = \left[\overrightarrow{p_1}^2 + m^2\right]^{1/2}$. We recall

$$\sum_{s_2} u(p_2, s_2)\overline{u}(p_2, s_2) = \left(\frac{\not{p}_2 + m}{2m}\right), \tag{6.3.11}$$

$$\sum_{s_1} v(p_1, s_1)\overline{v}(p_1, s_1) = \left(\frac{\not{p}_1 - m}{2m}\right), \tag{6.3.12}$$

and note that

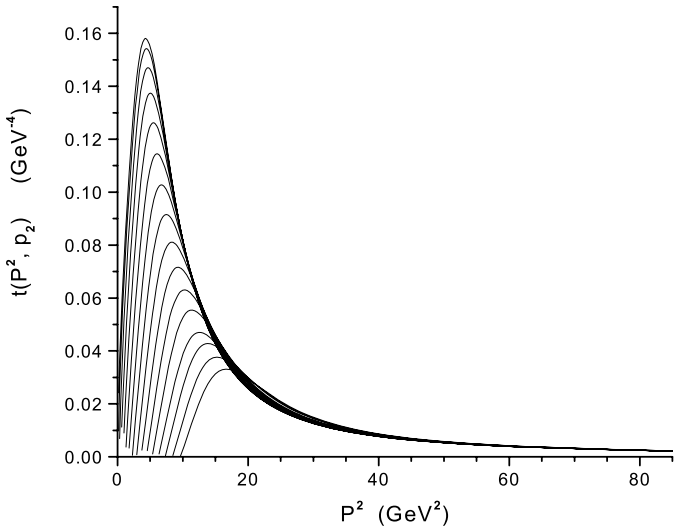


Figure 6.8: Values of $t(P^2, p_2)$ are shown for various values of the quark momentum $|\vec{p}_2|$. Starting with the uppermost curve, the $|\vec{p}_2|$ values in GeV units are 0.01, 0.03, 0.05, 0.07, 0.09, 0.11, 0.13, 0.15, 0.17, 0.19, 0.21, 0.23, 0.25, 0.27, 0.29 and 0.31. (For large $P^2$, we have $t(P^2, p_2) \simeq (1/\pi P^2)G$.) Here $P^2 = (p_1 + p_2)^2$, where $p_1$ is the antiquark momentum.

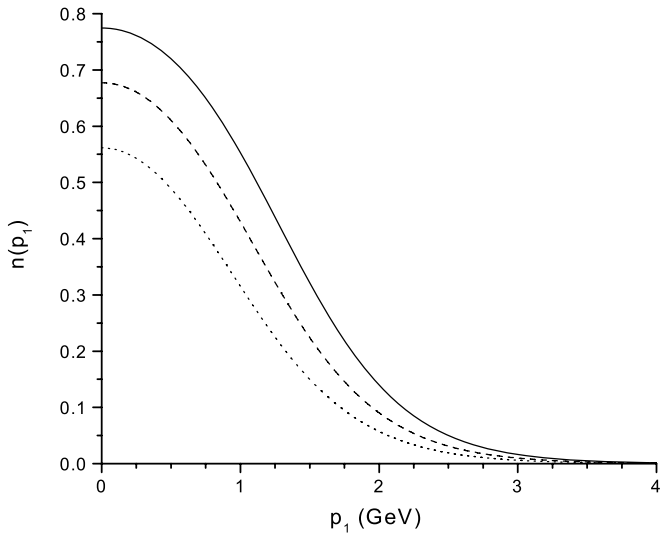


Figure 6.9: Values of $n(p_1)$ are shown for $\mu = 1.1\,\mathrm{GeV}$ (dotted curve), $\mu = 1.3\,\mathrm{GeV}$ (dashed curve) and $\mu = 1.5\,\mathrm{GeV}$ (solid curve). Here $T = 1.5\,T_c$ with $T_c = 270\,\mathrm{MeV}$.

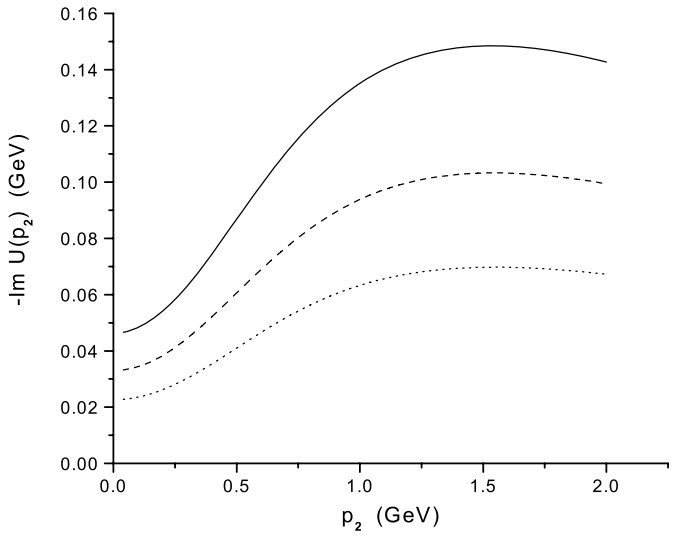


Figure 6.10: The imaginary part of the quark optical potential is shown for $\mu = 1.1\,\mathrm{GeV}$ (dotted curve), $\mu = 1.3\,\mathrm{GeV}$ (dashed curve) and $\mu = 1.5\,\mathrm{GeV}$ (solid curve). (We recall that the nucleon-nucleus imaginary optical potential is about $0.01\,\mathrm{GeV}$ in magnitude [50].)

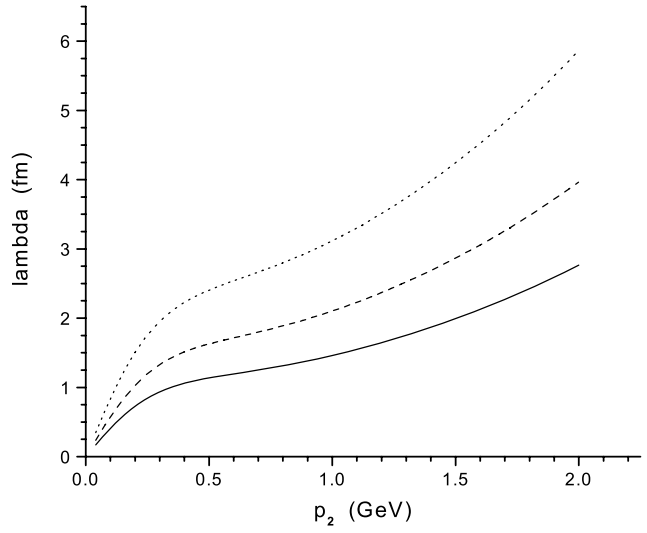


Figure 6.11: Values of $\lambda(p_2)$ are shown for $\mu = 1.1\,\mathrm{GeV}$ (dotted curve), $\mu = 1.3\,\mathrm{GeV}$ (dashed curve) and $\mu = 1.5\,\mathrm{GeV}$ (solid curve).

$$\mathrm{Tr}\left(\frac{\not{p}_2+m}{2m}\right)\left(\frac{\not{p}_1-m}{2m}\right)=\left[\frac{(E_1E_2-\overrightarrow{p_1}\cdot\overrightarrow{p_2})-m^2}{m^2}\right]. \tag{6.3.13}$$

Thus,

$$\mathrm{Im}\Sigma^{++}(p_2)=-\frac{1}{2}\int\frac{d\overrightarrow{p_1}}{(2\pi)^3}\frac{m}{E(\overrightarrow{p_1})}\mathrm{Im}\left[\frac{G}{1-GJ(\overrightarrow{p_1},\overrightarrow{p_2})}\right] \times\left[\frac{E_1E_2-\overrightarrow{p_1}\cdot\overrightarrow{p_2}-m^2}{m^2}\right]n(\overrightarrow{p_1}), \tag{6.3.14}$$

and

$$U(\overrightarrow{p_2})=-\frac{N}{2}\frac{m}{E(\overrightarrow{p_2})}\int\frac{d\overrightarrow{p_1}}{(2\pi)^3}\frac{m}{E(\overrightarrow{p_1})}\pi P^2t(\overrightarrow{p_1},\overrightarrow{p_2}) \times\left[\frac{E_1E_2-\overrightarrow{p_1}\cdot\overrightarrow{p_2}-m^2}{m^2}\right]n(\overrightarrow{p_1}). \tag{6.3.15}$$

Here $E_1=E(\overrightarrow{p_1})$, $E_2=E(\overrightarrow{p_2})$ and we have made use of Eqs. 6.3.5 and 6.3.9. Values of $t(P^2,p_2)$ are shown in Fig. 6.8 for values of $|\overrightarrow{p_2}|$ ranging from 0.01 GeV to 0.31 GeV. In Fig. 6.9 we show the values of $n(\overrightarrow{p_1})$ for the three values of $\mu$ considered here and in Fig. 6.10 we present values of $\mathrm{Im}U(\overrightarrow{p_2})$ for those values of $\mu$. In Fig. 6.11 we show the values for the mean-free-path

$$\lambda=\frac{|\overrightarrow{p_2}|}{m}\frac{1}{\mathrm{Im}U(\overrightarrow{p_2})}. \tag{6.3.16}$$

### 6.3.2 Discussion

Information is available concerning the *baryon* chemical potential. That chemical potential is parameterized in Ref. [103] as

$$\mu_B = \frac{1270\,\mathrm{MeV}}{(1+\frac{\sqrt{S_{NN}}}{4.3})}, \tag{6.3.17}$$

and varies strongly with $\sqrt{S_{NN}}$, which is in GeV units in Eq. (6.3.17). For $\sqrt{S_{NN}} =$ 200 GeV, we have $\mu_B = 26.7$ MeV.

Of particular significance for our results is the choice of the chemical potential for the quarks. We have taken $\mu \sim 1$ GeV. In the case of the quarks, the choice of $\mu \simeq$ 1 GeV leads to small mean-free-paths consistent with the suggestion of Shuryak that the resonances seen in the MEM analysis of the lattice results are responsible for the small mean-free-paths of the "sticky molasses" model.

We remark that in nuclear matter the baryon density is 0.17 fm$^{-3}$ or 0.51 quarks/fm$^3$ if we consider the nucleon to be composed of three quarks. For the values of $n(\overrightarrow{p_1})$ shown in Fig. 6.9 for the case $\mu = 1.3$ GeV, we may calculate the density of antiquarks to be 5.91 fm$^{-3}$, so that the density of quarks and antiquarks is about 12 fm$^{-3}$ in our model. We remark that the energy density at RHIC for $\sqrt{S_{NN}} = 200$ GeV is 4.1 GeV/fm$^3$ [103], which is about 26 times the energy density of nuclear matter, which is approximately 0.16 GeV/fm$^3$.

In this work we have attempted to provide a quantitative analysis of the suggestion [89] that the large $q\overline{q}$ resonant scattering cross sections are responsible for the small quark mean-free-paths, with the associated relevance of the hydrodynamic description of the system that is created in high-energy nucleus-nucleus collisions. We have considered the interaction in the scalar, pseudoscalar, vector and axial-vector channels of the $q\overline{q}$ system. It is possible that there are important resonances of $qq$ character,

as well as the $q\overline{q}$ resonances considered here. Such $qq$ states are depicted in Fig. 8a of Ref. [89]. It would be of interest to see if such states are found in lattice studies using the MEM scheme.

# Appendix A

# Hadronic Current Correlators

For ease of reference, we present a discussion of our calculation of hadronic current correlators taken from Ref.[102]. The procedure we adopt is based upon the real-time finite-temperature formalism, in which the imaginary part of the polarization function may be calculated. Then, the real part of the function is obtained using a dispersion relation. The result we need for this work has been already given in the work of Kobes and Semenoff [15]. (In Ref. [15] the quark momentum is $k^\mu$ and the antiquark momentum is $k^\mu - P^\mu$. We will adopt that notation in this section for ease of reference to the results presented in Ref. [15].)

With reference to Eq. (5.4) of Ref. [15], we write the imaginary part of the scalar polarization function as Eq. 4.2.1. Relative to Eq. (5.4) of Ref. [15], we have changed the sign, removed a factor of $g^2$ and have included a statistical factor of $N_c$. In addition, we have included a Gaussian regulator, $\exp[\,-\vec{k}^{\,2}/\alpha^2\,]$. The value $\alpha = 0.605$ GeV was used in our applications of the NJL model in the calculation of meson properties at $T = 0$. We also note Eqs. 4.2.2 and 4.2.3. For the calculation of the imaginary part of the polarization function, we may put $k^2 = m_1^2(T)$ and $(k - P)^2 = m_2^2(T)$, since in that calculation the quark and antiquark are on-mass-shell. In Eq. (4.2.1) the factor $\beta_S$ arises from a trace involving Dirac matrices, such that

4.2.4-4.2.5 where $m_1$ and $m_2$ depend upon temperature. In the frame where $\vec{P} = 0$, and in the case $m_1 = m_2$, we have $\beta_S = 2P_0^2(1 - 4m^2/P_0^2)$. For the scalar case, with $m_1 = m_2$, we find Eq. 4.2.6.

For pseudoscalar mesons, we replace $\beta_S$ by Eq. 4.2.8 and 4.2.9 which for $m_1 = m_2$ is $\beta_P = 2P_0^2$ in the frame where $\vec{P} = 0$. We find Eq. 4.2.10 for the $\pi$ mesons, where $\vec{k}^{\,2} = P_0^2/4 - m_u^2(T)$, as above. Thus, we see that the phase space factor has an exponent of 1/2 corresponding to a $s$-wave amplitude. For the scalars, the exponent of the phase-space factor is 3/2, as seen in Eq. (4.2.6).

For a study of vector mesons we consider 4.2.11 and calculate 4.2.12 which, in the equal-mass case, is equal to $4P_0^2+8m^2(T)$, when $\vec{P} = 0$. This result is needed when we calculate the correlator of vector currents. Note that, for the elevated temperatures considered in this work, $m_u(T) = m_d(T)$ is quite small, so that $4P_0^2 + 8m_u^2(T)$ can be approximated by $4P_0^2$, when we consider the vector current correlation functions. In that case, we have

$$\mathrm{Im}\, J_V(P^2, T) \simeq \frac{2}{3}\mathrm{Im}\, J_P(P^2, T)\,. \tag{A1}$$

At this point it is useful to define functions that do not contain that Gaussian regulator:

$$\mathrm{Im}\, \tilde{J}_P(P^2, T) = \frac{N_c P_0^2}{8\pi}\left(1 - \frac{4m^2(T)}{P_0^2}\right)^{1/2}[\,1 - 2n_1(k)\,]\,, \tag{A2}$$

and

$$\mathrm{Im}\, \tilde{J}_V(P^2, T) = \frac{2}{3}\frac{N_c P_0^2}{8\pi}\left(1 - \frac{4m^2(T)}{P_0^2}\right)^{1/2}[\,1 - 2n_1(k)\,]\,, \tag{A3}$$

For the functions defined in Eq. (A2) and (A3) we need to use a twice-subtracted

dispersion relation to obtain $\mathrm{Re}\,\tilde{J}_P(P^2,T)$, or $\mathrm{Re}\,\tilde{J}_V(P^2,T)$. For example,

$$\mathrm{Re}\,\tilde{J}_P(P^2,T) = \mathrm{Re}\,\tilde{J}_P(0,T) + \frac{P^2}{P_0^2}[\,\mathrm{Re}\,\tilde{J}_P(P_0^2,T) - \mathrm{Re}\,\tilde{J}_P(0,T)\,] + \frac{P^2(P^2-P_0^2)}{\pi}\int_{4m^2(T)}^{\tilde{\Lambda}^2} ds \frac{\mathrm{Im}\,\tilde{J}_P(s,T)}{s(P^2-s)(P_0^2-s)}\,, \tag{A4}$$

where $\tilde{\Lambda}^2$ can be quite large, since the integral over the imaginary part of the polarization function is now convergent. We may introduce $\tilde{J}_P(P^2,T)$ and $\tilde{J}_V(P^2,T)$ as complex functions, since we now have both the real and imaginary parts of these functions. We note that the construction of either $\mathrm{Re}\,J_P(P^2,T)$, or $\mathrm{Re}\,J_V(P^2,T)$, by means of a dispersion relation does not require a subtraction. We use these functions to define the complex functions $J_P(P^2,T)$ and $J_V(P^2,T)$.

In order to make use of Eq. (A4), we need to specify $\tilde{J}_P(0)$ and $\tilde{J}_P(P_0^2)$. We found it useful to take $P_0^2 = -1.0$ GeV$^2$ and to put $\tilde{J}_P(0) = J_P(0)$ and $\tilde{J}_P(P_0^2) = J_P(P_0^2)$. The quantities $\tilde{J}_V(0)$ and $\tilde{J}_V(P_0^2)$ are determined in an analogous function. This procedure in which we fix the behavior of a function such as $\mathrm{Re}\tilde{J}_V(P^2)$ or $\mathrm{Re}\tilde{J}_V(P^2)$ is quite analogous to the procedure used in Ref.[104]. In that work we made use of dispersion relations to construct a continuous vector-isovector current correlation function which had the correct perturbative behavior for large $P^2 \to -\infty$ and also described the low-energy resonance present in the correlator due to the excitation of the $\rho$ meson. In Ref.[104] the NJL model was shown to provide a quite satisfactory description of the low-energy resonant behavior of the vector-isovector correlation function.

We now consider the calculation of temperature-dependent hadronic current correlation functions. The general form of the correlator is a transform of a time-ordered product of currents as Eq. 4.2.13 where the double bracket is a reminder that we are considering the finite temperature case.

For the study of pseudoscalar states, we may consider currents of the form $j_{P,i}(x) =$

$\tilde{q}(x)i\gamma_5\lambda^i q(x)$, where, in the case of the $\pi$ mesons, $i = 1, 2$ and 3. For the study of scalar-isoscalar mesons, we introduce $j_{S,i}(x) = \tilde{q}(x)\lambda^i q(x)$, where $i = 0$ for the flavor-singlet current and $i = 8$ for the flavor-octet current.

In the case of the pseudoscalar-isovector mesons, the correlator may be expressed in terms of the basic vacuum polarization function of the NJL model, $J_P(P^2, T)$. Thus,

$$C_P(P^2, T) = J_P(P^2, T)\frac{1}{1 - G_P(T)J_P(P^2, T)}\,, \tag{A5}$$

where $G_P(T)$ is the coupling constant appropriate for our study of $\pi$ mesons. We have found $G_P(T) = 13.49$ GeV$^{-2}$ by fitting the pion mass in a calculation made at $T = 0$, with $m_u = m_d = 0.364$ GeV. The result given in Eq. (A5) is only expected to be useful for small $P^2$, since the Gaussian regulator strongly modifies the large $P^2$ behavior. Therefore, we suggest that the following form is useful, if we are to consider the larger values of $P^2$.

$$\frac{C_P(P^2, T)}{P^2} = \left[\frac{\tilde{J}_P(P^2, T)}{P^2}\right]\frac{1}{1 - G_P(T)J_P(P^2, T)}\,. \tag{A6}$$

(As usual, we put $\vec{P} = 0$.) This form has two important features. At large $P_0^2$, $\mathrm{Im}\, C_P(P_0, T)/P_0^2$ is a constant, since $\mathrm{Im}\,\tilde{J}_P(P_0^2, T)$ is proportional to $P_0^2$. Further, the denominator of Eq. (A6) goes to 1 for large $P_0^2$. On the other hand, at small $P_0^2$, the denominator is capable of describing resonant enhancement of the correlation function. As we have seen, the results obtained when Eq. (A6) is used appear quite satisfactory. ( We may again refer to Ref.[104], in which a similar approximation is described.)

For a study of the vector-isovector correlators, we introduce conserved vector currents $j_{\mu,i}(x) = \tilde{q}(x)\gamma_\mu\lambda_i q(x)$ with i=1, 2 and 3. In this case we define

$$J_V^{\mu\nu}(P^2, T) = \left(g^{\,\mu\nu} - \frac{P^{\,\mu}P^{\,\nu}}{P^2}\right)J_V(P^2, T) \tag{A7}$$

and

$$C_V^{\mu\nu}(P^2,T) = \left(g^{\,\mu\nu} - \frac{P^{\,\mu}P^{\,\nu}}{P^2}\right) C_V(P^2,T)\,, \tag{A8}$$

taking into account the fact that the current $j_{\mu,\,i}(x)$ is conserved. We may then use the fact that

$$J_V(P^2,T) = \frac{1}{3} g_{\mu\nu} J_V^{\mu\nu}(P^2,T) \tag{A9}$$

and

$$\begin{aligned} \mathrm{Im}\, J_V(P^2,T) &= \frac{2}{3}\left[\frac{P_0^2 + 2m_u^2(T)}{8\pi}\right]\left(1 - \frac{4m_u^2(T)}{P_0^2}\right)^{1/2} e^{-\vec{k}^{\,2}/\alpha^2}[\,1 - 2n_1(k)\,] \qquad \text{(A10)} \\ &\simeq \frac{2}{3}\mathrm{Im}J_P(P^2,T)\,. \qquad \text{(A11)} \end{aligned}$$

(See Eq. (4.2.7) for the specification of $k = |\vec{k}|$.) We then have

$$C_V(P^2,T) = \tilde{J}_V(P^2,T)\frac{1}{1 - G_V(T)J_V(P^2,T)}\,, \tag{A12}$$

where we have introduced

$$\begin{aligned} \mathrm{Im}\tilde{J}_V(P^2,T) &= \frac{2}{3}\left[\frac{P_0^2 + 2m_u^2(T)}{8\pi}\right]\left(1 - \frac{4m_u^2(T)}{P_0^2}\right)^{1/2} [\,1 - 2n_1(k)\,] \qquad \text{(A13)} \\ &\simeq \frac{2}{3}\mathrm{Im}\tilde{J}_P(P^2,T)\,. \qquad \text{(A14)} \end{aligned}$$

In the literature, $\omega$ is used instead of $P_0$ [9, 92, 93]. We may define the spectral

functions

$$\sigma_V(\omega, T) = \frac{1}{\pi} \operatorname{Im} C_V(\omega, T)\,, \tag{A15}$$

and

$$\sigma_P(\omega, T) = \frac{1}{\pi} \operatorname{Im} C_P(\omega, T)\,, \tag{A16}$$

Since different conventions are used in the literature [9, 92, 93], we may use the notation $\overline{\sigma}_P(\omega, T)$ and $\overline{\sigma}_V(\omega, T)$ for the spectral functions given there. We have the following relations:

$$\overline{\sigma}_P(\omega, T) = \sigma_P(\omega, T)\,, \tag{A17}$$

and

$$\frac{\overline{\sigma}_V(\omega, T)}{2} = \frac{3}{4}\sigma_V(\omega, T)\,, \tag{A18}$$

where the factor $3/4$ arises because, in Refs. [9, 92, 93], there is a division by 4, while we have divided by 3, as in Eq. (A9).

# Appendix B

# Further

Here we extend the work of Appendix A to consider case of finite three-momentum, $\vec{P}$. We consider the calculation of $\mathrm{Im}J_P(P^0, \vec{P}, T)$. The momenta $P^0$ and $\vec{P}$ are the values external to the loop diagram. Internal to the diagram, we have a quark of momentum $k^\mu + P^\mu/2$ leaving the left-hand vertex and an antiquark of momentum $k^\mu - P^\mu/2$ entering the left-hand vertex. It is useful to define

$$E_1(k) = \left|\vec{k} + \vec{P}/2\right| \tag{B1}$$

$$= \left(k^2 + \frac{P^2}{4} + kP\cos\theta\right)^{1/2} \tag{B2}$$

and

$$E_2(k) = \left|\vec{k} - \vec{P}/2\right| \tag{B3}$$

$$= \left(k^2 + \frac{P^2}{4} - kP\cos\theta\right)^{1/2}. \tag{B4}$$

Here $k = |\vec{k}|$ and $P = |\vec{P}|$.

We have

$$\begin{aligned}\mathrm{Im}\, J_P(P^0,\vec{P},T) = \frac{1}{2}N_c\beta_P\,\epsilon(P^0)\int\frac{d^3k}{(2\pi)^3}\,e^{-\vec{k}^{\,2}/\alpha^2}\left(\frac{2\pi}{2E_1(k)2E_2(k)}\right) \\ \times\{[1-n_1(k)-n_2(k)]\delta(P^{\,0}-E_1(k)-E_2(k)) \\ -[n_1(k)-n_2(k)]\delta(P^{\,0}+E_1(k)-E_2(k)) \\ -[n_2(k)-n_1(k)]\delta(P^{\,0}-E_1(k)+E_2(k)) \\ -[1-n_1(k)-n_2(k)]\delta(P^{\,0}+E_1(k)+E_2(k))\}\,.\end{aligned} \tag{B5}$$

Here,

$$n_1(k) = \frac{1}{e^{\,\beta E_1(k)}+1}\,, \tag{B6}$$

and

$$n_2(k) = \frac{1}{e^{\,\beta E_2(k)}+1}\,. \tag{B7}$$

In Eq. (B5), the second and third terms cancel and the fourth term does not contribute. It is useful to rewrite $\delta(P^0-E_1(k)-E_2(k))$ using

$$\delta[f(\cos\theta)] = \frac{2}{\left|\frac{\partial f}{\partial\cos\theta}\right|_x}\delta(\cos\theta - x)\,, \tag{B8}$$

where

$$\begin{aligned}x^2 &= \cos^2\theta \\ &= \frac{4P_0^2(k^2+P^2/4)-P_0^4}{4k^2P^2}\,.\end{aligned} \tag{B9}$$

We find

$$\left|\frac{\partial f}{\partial \cos\theta}\right| = \frac{1}{2}kP\left|\frac{E_1(k)-E_2(k)}{E_1(k)E_2(k)}\right|, \tag{B10}$$

and obtain

$$\begin{aligned}\mathrm{Im}\, J_P(P^0,\vec{P},T) = \frac{1}{2}N_c\beta_P\,\epsilon(P^0)(2\pi)^2\int\frac{k^2dk}{(2\pi)^3}e^{-k^2/\alpha^2} \\ \int\frac{1}{2E_1(k)E_2(k)}[1-n_1(k)-n_2(k)]\left|\frac{\partial f(\cos\theta)}{\partial\cos\theta}\right| \\ \times\delta(\cos\theta-x)d(\cos\theta)\,.\end{aligned} \tag{B11}$$

We note there is a singularity when $E_1(k) = E_2(k)$. That occurs when $\cos\theta = 0$ or $\theta = \pi/2$. For our calculations we eliminate the point with $\theta = \pi/2$ when evaluating the angular integral over $d(\cos\theta)\delta(\cos\theta - x)$ in the last expression. We obtain

$$\begin{aligned}\mathrm{Im}\, J_P(P^0,\vec{P},T) = N_c\beta_P\,\epsilon(P^0)\frac{4\pi^2}{(2\pi)^3}\int^{k_{max}}k^2dk\,e^{-k^2/\alpha^2} \\ \times\left.\frac{[1-n_1(k)-n_2(k)]}{kP|E_1(k)-E_2(k)|}\right|_x,\end{aligned} \tag{B12}$$

where $x$ is obtained from Eq. (B10),

$$x = \frac{P^0}{kP}\left[k^2+\frac{P^2}{4}-\frac{P_0^2}{4}\right]^{1/2} \tag{B13}$$

For the calculations reported in this work we have $P^0 = E(\overrightarrow{p_1}) + E(\overrightarrow{p_2})$ and $\overrightarrow{P} = \overrightarrow{p_1}+\overrightarrow{p_2}$, where $\overrightarrow{p_2}$ is the quark momentum and $\overrightarrow{p_1}$ is the antiquark momentum. Thus, we may also use the notation $J(\overrightarrow{p_1},\overrightarrow{p_2})$ as we have done in the main text.

# Bibliography


[1] C. DeTar, Phys. Rev. D **32**, 276 (1985).

[2] T. Hatsuda and T. Kunihiro, Phys. Rev. Lett. **55**, 158 (1985).

[3] Y. Nambu and G. Jona-Lasinio, Phys. Rev. **123**, 345 (1961); **124**, 246 (1961).

[4] T. Matsubara, Prog. Theor. Phys. **14**, 351 (1955).

[5] A. L. Fetter and J. D. Walecka, *Quantum Theory of Many-Particle Systems*, (Mc Graw-Hill, New York, 1971).

[6] P. Maris, C. D. Roberts, S. M. Schmidt, and P. C. Tandy, Phys. Rev. C **63**, 025202 (2001).

[7] M. Asakawa, T. Hatsuda and Y. Nakahara, hep-lat/0208059.

[8] F. Karsch, S. Datta, E. Laermann, P. Petreczky, S. Stickan, and I. Wetzorke, hep-ph/0209028.

[9] I. Wetzorke, F. Karsch, E. Laermann, P. Petreczky, and S. Stickan, Nucl. Phys. B (Proc. Suppl.) **106**, 510 (2002).

[10] M. Asakawa, Y. Nakahara and T. Hatsuda, Prog. Part. Nucl. Phys. **46**, 459 (2001).

[11] Hu Li and C. M. Shakin, Chiral symmetry restoration and deconfinement of light mesons at finite temperature, hep-ph/0209136.

[12] S. P. Klevansky, Rev. Mod. Phys. **64** , 649 (1992).

[13] Bing He, Hu Li, Qing Sun, and C. M. Shakin, nucl-th/0203010.

[14] C. DeTar, O. Kaczmarek, F. Karsch, and E. Laermann, Phys. ReV. D **59** , 031501 (1998).

[15] R. L. Kobes and G. W. Semenoff, Nucl. Phys. B **260**, 714 (1985).

[16] C. M. Shakin and Huangsheng Wang, Phys. Rev. D **63** , 014019 (2000).

[17] L. S. Celenza, Huangsheng Wang, and C. M. Shakin, Phys. Rev. C **63** , 025209 (2001).

[18] C. M. Shakin and Huangsheng Wang, Phys. Rev. D **63** , 074017 (2001).

[19] C. M. Shakin and Huangsheng Wang, Phys. Rev. D **63** , 114007 (2001).

[20] C. M. Shakin and Huangsheng Wang, Phys. Rev. D **64** , 094020 (2001).

[21] C. M. Shakin and Huangsheng Wang, Phys. Rev. D **65** , 094003 (2002).

[22] T. Hatsuda and T. Kunihiro, Phys. Rep. **247** , 221 (1994).

[23] U. Vogl and W. Weise, Prog. Part. Nucl. Phys. **27** , 195 (1991).

[24] D. Zschiesche, S. Schramm, J. Schaffner-Bielich, H. Stöcker, and W. Greiner, nucl-th/0209022.

[25] H. D. Trottier, Phys. Rev. D **60** , 034506 (1999).

[26] O. Kaczmarek, F. Karsch, and E. Laermann and M. Lütgemeier, Phys. Rev. D **62** , 034021 (2000).

[27] B. Bolder *et al.*, Phys. Rev. D **63** , 074504 (2001).

[28] C. Bernard *et al.*, Phys. Rev. D **64** , 074509 (2001).

[29] A. Duncan, E. Eichten, and H. Thacker, Phys. Rev. D **63** , 111501(R) (2001).

[30] Hu Li and C. M. Shakin, Phys. Rev. D **66**, 074016 (2002).

[31] Bing He, Hu Li, Qing Sun, and C. M. Shakin, nucl-th/0203010.

[32] For reviews, see K. Rajagopal and F. Wilcek, in B. L. Ioffe Festscrift; *At the Frontier of Particle Physics/Handbook of QCD*, M. Shifman ed. (World Scientific, Singapore 2001); M. Alford, Annu. Rev. Nucl. Part. Sci. **51**, 131 (2001).

[33] M. Alford, R. Rajagopal and F. Wilcek, Phys. Lett. B **422** , 247 (1998).

[34] R. Rapp, T. Schäfer, E. V. Shuryak and M. Velkovsky, Phys. Rev. Lett. **81** , 53 (1998).

[35] M. Alford, J. Berges and K. Rajagopal, Nucl. Phys. B **558** , 219 (1999).

[36] J. Kundu and K. Rajagopal, Phys. Rev. D **65**, 094022 (2002).

[37] S. Datta, F. Karsck, P. Petreczky and I. Wetzorke, hep-lat/0208012.

[38] S. Digal, P. Petreczky, and H. Satz, Phys. Rev. D **64** , 094015 (2001).

[39] M. Le Bellac, *Thermal Field Theory*, (Cambridge Univ. Press, Cambridge, U.K., 1996).

[40] R. L. Kobes and G. W. Semenoff, Nucl. Phys. B **260**, 714 (1985).

[41] C. R. Allton, S. Ejiri, S. J. Hands, O. Kaczmarek, F. Karsch, E. Laermann, Ch. Schmidt and L. Scorzato, hep-lat /0204010

[42] S. Ejiri, C. R. Allton, S. J. Hands, O. Kaczmarek, F. Karsch, E. Laermann and L. Scorzato, Nucl. Phys. Proc. Suppl. **106**, 459 (2002).

[43] F. Karsch, Lect. Notes. Phys. **583**, 209 (2002).

[44] F. Karsch, Nucl. Phys. Proc. Suppl. **83**, 14 (2000).

[45] J. Engels, O. Kaczmarek, F. Karsch and E. Laermann, Nucl. Phys. B **558**, 307 (1999).

[46] Z. Fodor and S. D. Katz, hep-lat /0204029; Nucl. Phys. Proc. Suppl. **106**, 441 (2002); Phys. Lett. B **534**, 87 (2002).

[47] L. S. Celenza, Bing He, Hu Li, Qing Sun, and C. M. Shakin, nucl-th/0203010.

[48] E. G. Drukarev and E. M. Levin, Prog. Part. Nucl, Phys. **27** , 77 (1991).

[49] B. D. Serot and J. D. Walecka, in Advances in Nuclear Physics, Vol. 16, edited by J. W. Negele and E. Vogt (Plenum, New York, 1986).

[50] L. S. Celenza and C. M. Shakin, *Relativistic Nuclear Physics: Theories of Structure and Scattering* (World Scientific, Singapore, 1986).

[51] Nan-Wei Cao, C. M. Shakin and Wei-Dong Sun, Phys. Rev. C **46** , 2535 (1992).

[52] C. D. Roberts and S. M. Schmidt, Porg. Part. Nucl. Phys. **45** , S1 (2000).

[53] C. Shakin, Ann. Phys. (NY) **192** , 254 (1989).

[54] L. S. Celenza, Hui-Wen Wang and Xin-Hua Yang, Intl. J. Mod. Phys. A **4** , 3807 (1989).

[55] V. M. Bannur, L. S. Celenza, Huang-he Chen, Shun-fu Gao and C. M. Shakin, Intl. J. Mod. Phys. A **5** , 1479 (1990).

[56] V. M. Bannur, L. S. Celenza, C. M. Shakin, and Hui-Wen Wang, Description of the QCD Vacuum as a Random Medium, Brookly College Report: BCCNT89/032/189—unpublished.

[57] A. B. Migdal, Soviet Phys., JETP **34** , 1184 (1972).

[58] T. Ericson and W. Weise, *Pions and Nuclei* (Oxford Univ. Press, Oxford, 1988).

[59] L. S. Celenza, Shun-fu Gao, Bo Huang, Huangsheng Wang, and C. M. Shakin, Phys. Rev. C **61** , 035201 (2000).

[60] C. M. Shakin, Phys. Rev. D **65** , 114011 (2002).

[61] D. J. Rowe, *Nuclear Collective Motion*, (Methuen, London, 1970).

[62] M. Lutz, S. Klimt, and W. Weise, Nucl. Phys. A **541** , 521 (1992).

[63] D. B. Kaplan and A. E. Nelson, Phys. Letter. B **175** , 57 (1986).

[64] A. E. Nelson and D. B. Kaplan, Phys. Letter. B **192** , 193 (1987).
J. Kundu and K. Rajagopal, hep-ph/0112206 (2002).

[65] C. Gocke, D. Blaschke, A. Khalatyan and H. Grigoria, hep-ph/0104183-v2 (2002).

[66] I. A. Shovkovy, hep-ph/0110352 (2002).

[67] D. T. Son, Phys. Rev. D **59** , 094019 (1999).

[68] T. Shäfer, E. V. Shuryak and M. Velkovsky, Phys. Rev. Lett. **81** , 53 (1998).

[69] J. Skullerud, D. B. Leinweber, and A. G. Williams, Phys. Rev. D **64** , 074508 (2001).

[70] H. Ito, W. W. Buck and F. Gross, Phys. Rev. C **43** , 2483 (1991); C **45** , 1918 (1992).

[71] S. Schmidt, D. Blaschke, Y. L. Kalinovsky, Phys. Rev. C **50** , 435 (1994).

[72] R. S. Plant and M. C. Birse, Nucl. Phys. A **628** , 607 (1998).

[73] R. D. Bowler and M. C. Birse, Nucl. Phys. A **582** , 655 (1995).

[74] R. S. Plant and M. C. Birse, hep-ph/0007340 and references therein.

[75] L. S. Celenza, Xiang-Dong Li, and C. M. Shakin, Phys. Rev. C **55** , 1492 (1997). In this reference a negative value of $\kappa$ was used. Therefore, the sign on the right-hand sides of Eqs. (2.4) and (2.5), appearing in this reference, should be corrected to be positive.

[76] G. Amoros, J. Bijnens, and P. Talavera, Nucl. Phys. B **602** , 87 (2001).

[77] M. Asakawa and K. Yazaki, Nucl. Phys. A **504** , 668 (1989).

[78] V. Bernard, Ulf-G. Meissner, and I. Zahed, Phys. Rev. D **36** , 819 (1987).

[79] F. Gastineau, R. Nebauer, and J. Aichelin, hep-ph/0101289 (2001).

[80] M. Shifman, A. Vainstein and V. Zakarov, Nucl. Phys. B **147** , 385 (1979); 448 (1979);
L. Reinders, H. Rubinstein and Y. Yazaki, Phys. Rep. **127** , 2 (1985).

[81] R. Alkofer, P. Watson and H. Weigel, hep-ph/0202053 (2002).

[82] P. Maris and P. C. Tandy, Phys. Rev. C **60** , 055214 (1999).

[83] Bing He, Hu Li, Qing Sun, and C. M. Shakin, nucl-th/0203010.

[84] L. S. Celenza, Shun-fu Gao, Bo Huang, Huangsheng Wang, and C. M. Shakin, Phys. Rev. C **61** , 035201 (2000).

[85] J. Szweda, L. S. Celenza, C. M. Shakin and W.-D. Sun, Few-Body Systems **20** , 93 (1996).

[86] A. Bender, G. I. Poulis, C. D. Roberts, S. Schmidt and A. W. Thomas, Phys. Lett. B **431**, 263 (1998).

[87] D. Blaschke, C. D. Roberts, and S. Schmidt, Phys. Lett. B **425**, 232 (1998).

[88] P. Maris, C. D. Roberts and S. Schmidt, Phys. Rev. C **57**, R2821 (1998).

[89] E. Shuryak, hep-ph/0312227.

[90] G. E. Brown, C. H. Lee, M. Rho, and E. Shuryak, hep-ph/0312175

[91] G. E. Brown, C. H. Lee, M. Rho, and E. Shuryak, hep-ph/0202068; G. E. Brown, C. H. Lee, and M. Rho, hep-ph/0402207

[92] F. Karsch, S. Datta, E. Laermann, P. Petreczky, and S. Stickan, and I. Wetzorke, Nucl. Phys. A **715**, 701c (2003)

[93] F. Karsch, E.Laermann, P. Petreczky, S. Stickan, and I. Wetzorke, Phys. Lett. B **530**, 147 (2002).

[94] M. Asakawa, T. Hatsuda and Y. Nakahara, Nucl. Phys. A **715**, 863 (2003)

[95] T. Umeda, K. Nomura and H. Matsufuru, hep-ph/0211003.

[96] I. Wetzorke, hep-ph/0305012. (Invited talk at the 'Seventh Workshop on Quantum Chromodunamics', Villefranche-sur-mer, France, Jan. 6-10, 2003)

[97] P. Petreczky, hep-ph/0305189.

[98] S. Datta, F. Karsch, P. Petreczky and I. Wetzorke, hep-lat/0312037.

[99] Xiangdong Li, Hu Li, C.M. Shakin, Qing Sun, and Huangsheng Wang, hep-ph/0402073.

[100] Bing He, Hu Li, C. M. Shakin, and Qing Sun, Phys. Rev. D **67**, 014022 (2003).

[101] Bing He, Hu Li, C. M. Shakin, and Qing Sun, Phys. Rev. D **67**, 114012 (2003).

[102] Bing He, Hu Li, C. M. Shakin, and Qing Sun, Phys. Rev. C **67**, 065203 (2003).

[103] A. Andronic and P. Braun-Munzinger, hep-ph/0402291.

[104] C. M. Shakin, Wei-Dong Sun, and J. Szweda, Ann. of Phys. (NY) **241**, 37 (1995).